ABSTRACT

A SURVEY OF THE (^{3}He,^{7}Be) REACTION AT 70 MeV

By

William Frederick Steele

Using the 70 MeV ^{3}He beam of the Michigan State University cyclotron, a study of the (^{3}He,^{7}Be) reaction has been undertaken. By surveying a wide range of target nuclides, namely ^{12,13}C, ^{16}O, ^{24,26}Mg, ^{40,48}Ca, ^{58,60,62,64}Ni, ^{90}Zr, ^{120,124}Sn, ^{144}Sm, and ^{206}Pb, systematics of the α clustering phenomenon are investigated. In addition, masses and energy levels of ^{44}Ar, ^{60}Fe, and ^{120}Cd are measured. In order to assure adequate resolution for a large acceptance solid angle, an Enge split pole magnetic spectrograph is used to analyze momenta of the reaction products. A single wire gas filled proportional counter measures the relative positions of the ions as they cross the magnet's focal plane. Taking advantage of the well defined time structure of the cyclotron beam, charged particle time of flight, together with the proportional counter energy signal, is used for particle identification. Despite the relatively low yield, excellent particle identification is achieved. Differential cross sections as low as 200 nb/str are successfully measured.

The finite range DWBA program LOLA of R. M. DeVries has been used to calculate reaction differential cross sections for comparison to data, assuming the reaction to proceed by a direct α transfer mechanism. α spectroscopic factors are

extracted. Despite the sharp decline of peak differential cross section with increasing target mass, the corresponding spectroscopic factors remain nearly constant. Since the α spectroscopic factor may be taken as a measure of surface α cluster probability, α clustering appears to remain important for heavy nuclides.

A SURVEY OF THE (^{3}He,^{7}Be) REACTION AT 70 MeV

By

William Frederick Steele

A DISSERTATION

Submitted to

Michigan State University

in partial fulfillment of the requirements

for the degree of

DOCTOR OF PHILOSOPHY

Department of Physics

1974

ACKNOWLEDGMENTS

I would like to thank the laboratory staff for providing a good environment in which to work. For his guidance and unceasing encouragement, I wish to thank my advisor, Dr. G. M. Crawley. For helping with data collection and analysis, I would like to thank Paul Smith. I am particularly indebted to Joseph Finck who, in addition to helping gather and analyze data, has spent many hours preparing the figures and performing the DWBA calculations presented in this work.

TABLE OF CONTENTS

LIST OF TABLES

LIST OF FIGURES

I. INTRODUCTION

Probably the most obvious and well understood nuclear phenomenon is natural radioactive decay. α, β, and γ radiations emanating from a variety of nuclides have been studied for decades. γ radiation is understood in terms of electromagnetic transitions within the nucleus. β decay, before the discovery of the neutron, was thought to be the ejection from the nucleus of a free electron. Now, however, β decay is known to be a manifestation of the weak interaction; a neutron within the nucleus splits into a proton, electron, and an antineutrino. α decay is an example of quantum mechanical barrier penetration. In contrast to β and γ decay, however, the source of α particles within the nucleus is not clearly established. That is, where do the α particles form, how long do they exist, and to what extent does the nuclear matter condense into α particles? Because of the quantitative uncertainty in the penetrability of the large Coulomb barrier, Wilkinson[1] points out that α decay, by itself, is an inadequate tool to answer these questions. He discusses two, nore direct, methods for determining the degree of α clustering: α knockout reactions and K^- meson capture studies. Igo[2], for example, has investigated the $(\alpha,2\alpha)$ reaction at 915 MeV. The two α particles are detected in coincidence at a relative angle of 87.5°, the angle for a 915 MeV α particle elastically scattered from a free α particle at rest. Because of the strong absorption of α

particles in nuclear matter, only the pole caps of the target nucleus where the nuclear density is 5% of the central density may be probed. The number of elastic α-α events observed indicates that all of the nuclear matter in these polar regions is clustered into α particles.

More recently, α particle transfer reactions have been used to estimate α clustering. If such a reaction is, in fact, dominated by an α transfer mechanism and is direct, reaction calculations may allow extraction of α spectroscopic factors which may be taken as an indication of α clustering. α spectroscopic factors have been obtained, for example, by Martin[3], et. al. using the (d,^{6}Li) reaction at 28 MeV. The direct character of the (d,^{6}Li) reaction is questionable however. Comfort[4], et. al. find that complex multistep processes are significant for the reaction, probably at all energies. On the other hand, the (^{3}He,^{7}Be) reaction seems more likely to proceed via direct α pickup. Détraz[5], et. al. find that at 30 MeV incident ^{3}He energy, the reaction is probably direct. Further work by Détraz[6], et. al. shows that, for the most part, the α particle is transfered in its ground state rather than an isospin 1 excited state.

Target nuclides as heavy as ^{93}Nb[7,8] have been studied at ^{3}He energies as high as 40 MeV. The peak differential cross section is observed to sharply decline from ^{12}C to ^{40}Ca. However the decrease is arrested past calcium. The ^{93}Nb data suggest the cross section may even rise for targets of greater mass. The present work has sought to extend the

previous work to larger masses. A higher beam energy, 70 MeV, is used to assure a direct reaction mechanism, to avoid the Coulomb barrier of heavier nuclides, and to raise the ^{7}Be ejectile energy, thus easing detection difficulties. For application to the (^{3}He,^{7}Be) reaction, a detection system should be able to resolve the peak pairs caused by the particle stable 432 keV first excited state of ^{7}Be. The resolution attainable with semiconductor counter telescopes, used for most previous work, is limited by kinematic broadening. Since the cross sections for (^{3}He,^{7}Be) reactions are very small, less than 1 μb/str for heavy targets, as large an acceptance solid angle as possible is desirable. Therefore, for the present work, an Enge[9] split pole double focusing magnetic spectrograph is used to analyze the reaction products. Its kinematic focusing feature eliminates the kinematic broadening problem, allowing use of a relatively large entrance slit.

In addition to nuclear structure information, the (^{3}He,^{7}Be) reaction presents the opportunity to study nuclides for which little information is available. In particular, the masses and some energy levels of ^{44}Ar, ^{60}Fe, and ^{120}Cd are measured.

II. EXPERIMENT

The experimental arrangement used has four primary constituents: the cyclotron and beam transport system, the spectrometer magnet and camera box, the proportional counter photomultiplier detection system, and the electronic analysis equipment. The Michigan State University sector focused cyclotron is used to accelerate $^{3}He^{++}$ ions to 70 MeV. $^{3}He^{++}$ ions are produced at the center of the cyclotron by a water cooled gas discharge ion source. In order to conserve the expensive isotope, vacuum system exhaust is recovered, circulated through a liquid nitrogen cooled carbon trap, and returned to the ion source. Slits located at the eighteenth and twenty-eighth orbit radii stop errant $^{3}He^{++}$ ions in order to precisely define phase and energy of the beam and to reduce hazardous radiation by stopping the particles while still at a relatively low energy. Beam energy definition of better than 0.1% is routinely achieved. Because of the small differential cross sections of the reactions herein described, an effort was made to maximize the beam current reaching the target. Specifically, the ion source was operated at maximum power level and, after initial adjustment of the cyclotron, the twenty-eighth turn slit was removed. Extraction efficiency remained greater than 90%. Beam current passing through the target typically ranged from 2 to 3 microamperes, except for those target materials intolerant of such high current levels, for which the current was reduced

to a safe value. The beam transport system contains a pair of 45° bending magnets which bend the beam a total of 90° and serve to precisely define the beam energy, which is calculated from a standard calibration[10] using a proton nuclear magnetic resonance measurement of the magnetic field magnitude. As shall be discussed, the major contribution to the experimental resolution of peaks in the measured spectra is due to energy loss in the target; the energy distribution of the cyclotron beam being somewhat better than necessary for the experiments here discussed.

An Enge split pole magnetic spectrograph[9] analyzes the momenta of the reaction products. Two motor driven screws in the camera box allow remote control of the detector position and orientation. For a given beam energy, target, and scattering angle, the detector is placed to minimize the effect on resolution of the energy spread due to acceptance of particles scattered into a range of angles (kinematic broadening). The Enge spectrograph is a double focusing instrument which, together with the kinematic focusing, allows use of a relatively large solid angle, typically 2° x 2° (1.218 millisteradians). Use of an angular interval as large as 2° with a typical counter telescope system would be prohibited by the large values, particularly for light target nuclei, of kinematic broadening for the (^{3}He,^{7}Be) reaction. Although the spectrometer has an entrance aperature of 5.6°, a 2° slit was the largest used. Structure of the angular distributions warrant 2° resolution. Furthermore, time resolution of the

particle identification system is directly proportional to the angular acceptance of the spectrometer. Therefore the slit width was limited to maintain adequate particle identification.

In a typical experiment, the yield for ions such as ^{3}He, α, t, and ^{6}Li is much greater than that for ^{7}Be. Thus the rate at which ^{7}Be ions are detected is a small fraction of the total count rate. Furthermore, the differential energy loss of $^{7}Li^{+++}$ ions crossing the focal plane at a given point is very nearly the same as that for $^{7}Be^{4+}$ ions at the same point. These facts present a severe challenge to the reliability and efficiency of a particle identification system. The basic detector[11] used is a single wire gas filled proportional counter. Thin windows of Havar, Mylar, or Kapton, 1 cm high by 25 cm long on either side of a slotted 1 cm thick aluminum block contain a gas mixture consisting of He 10%, Ne 85%, and CO_2 5%[12]. A nichrome wire 10 or 20 μm in diameter runs the length of the counter and is attached to external connectors at either end. Each end of the counter is fitted with a gas connection to allow a flow of gas through the counter, both to maintain the quality of the gas and to satisfy the requirements of a pressure regulation device.

Charge from an ion passing through the gas is collected at the two terminals; the ratio of the charges collected at the two terminals being inversely proportional to the ratio of the separations of the event from the respective terminals. The outputs of the two terminals are amplified, added,

digitized, and sent to the comptuer. A second input to the computer is the amplified and digitized signal from one end of the counter. The sum signal represents the total energy deposited in the counter by the passing ion; or equivalently, the differential energy loss of the event. The second signal represents the product of the energy loss by the relative position of the event. The computer program TOOTSIE[13] accepts the digitized signals then divides the second input by the first, yielding the position of the event. The results are plotted on an oscilloscope screen. The vertical axis of the display is the energy loss while the horizontal axis is the position of the event. Each event produces a dot at the appropriate point on the screen. The dots distribute themselves in horizontal bands corresponding to the differential energy loss of the different species detected. Lines may be drawn on the screen to specify to the computer regions to be accepted. Unfortunately, while this method of particle identification performs well for some applications, it is inadequate for the (^{3}He,^{7}Be) reaction. The energy resolving power of the proportional counter is inadequate to provide band separation sufficient to assure reliable particle identification. Measurement of the ion time of flight in the spectrograph supplies the additional information needed for a satisfactory solution. As illustrated in Figure 2.1, a plastic scintillator with attached photomultiplier tube (RCA 8575) is placed behind the proportional counter. The amplified signals from the phototube start a time to amplitude converter

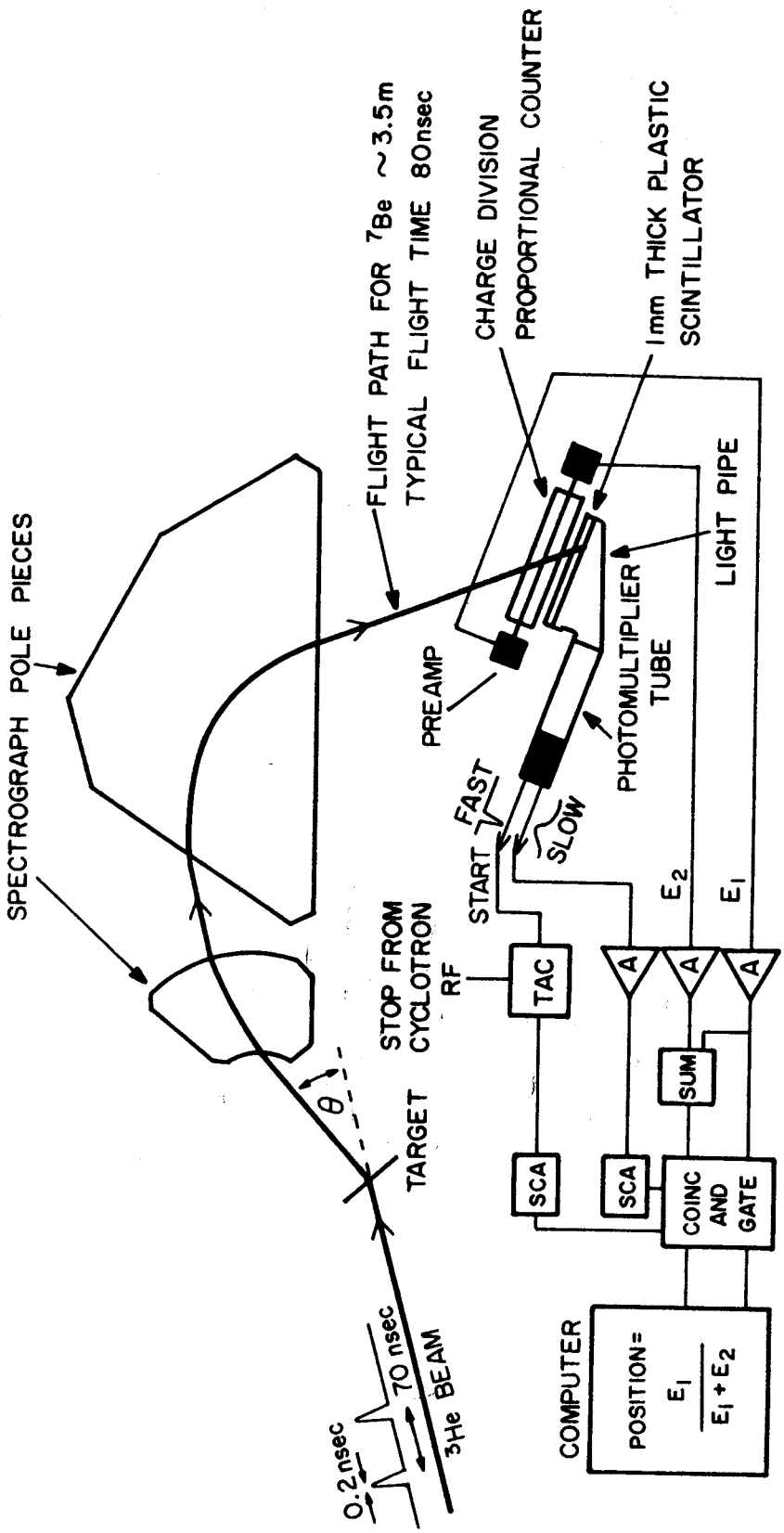

Figure 2.1 TIME OF FLIGHT PARTICLE IDENTIFICATION IN THE SPECTROGRAPH

which is stopped by the cyclotron radio frequency signal. Since the time of flight of a charged particle in a magnetic field is inversely proportional to its charge to mass ratio, the time spectrum so obtained may be used to discriminate ions of different charge to mass ratios. Fortunately no light ion other than $^{7}Be^{4+}$ has a charge to mass ratio of 4/7. Provided the time resolution of the system is adequate, $^{7}Be^{4+}$ ions may be identified uniquely. $^{6}Li^{3+}$, α, and d with a charge to mass ratio of 1/2 and $^{3}He^{++}$ with a ratio of 2/3 are those ions which have flight times closest to $^{7}Be^{4+}$. A typical flight time for a $^{7}Be^{4+}$ ion in the spectrometer is 80 nsec. The corresponding time for an ion of ratio 1/2 is 91 nsec while a $^{3}He^{++}$ ion is in flight for 69 nsec. Figure 2.2 shows a typical time of flight spectrum for a spectrometer entrance slit of $2^{\circ} \times 2^{\circ}$. The time spread of a peak is proportional to the angular acceptance of the spectrometer. For the 2° slit the time resolution is adequate to achieve excellent particle identification. Although an energy signal from the photomultiplier is available, it is ignored because, under the conditions of these experiments, its use does not significantly improve the operation of the system.

Unfortunately, useful spectra are not ensured by good particle identification. Target quality is critical. Because of the relatively large differential energy loss of ^{7}Be ions, the targets must be thin, 200 to 500 $\mu g/cm^2$ depending on atomic number, in order to resolve the double peak for a given level of the residual nuclide. Each level of the

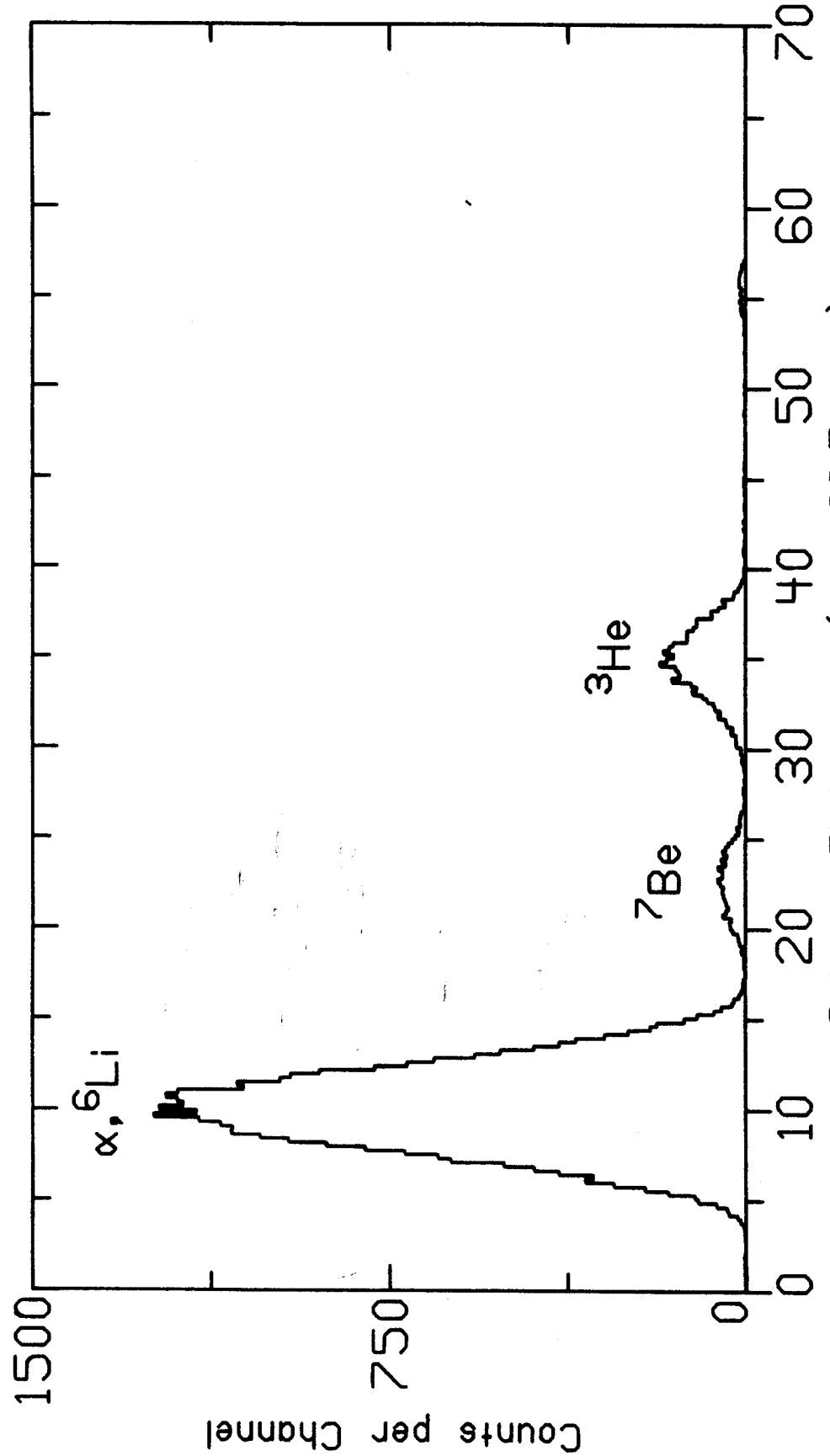

Figure 2.2 Time of flight spectrum for a ^{12}C target.

residual nuclide produces two peaks: the primary peak corresponding to the ground state of ^{7}Be and the secondary peak for the 432 keV first excited state of ^{7}Be. A negligible broadening of the secondary peak is caused by the γ decay of the ^{7}Be 432 keV excited state (Appendix B). Furthermore, the differential cross section for the (^{3}He,^{7}Be) reaction on ^{12}C and ^{16}O is somewhat larger than that for other targets. Consequently contamination of another target material by carbon or oxygen, a condition difficult to avoid, produces in the spectra interfering peaks which often mask the regions of interest. As the target materials used are chemically quite dissimilar, each requires its own special set of precautions. Therefore the preparation and handling of each target shall be discussed individually along with the corresponding reaction.

III. DATA ANALYSIS

Because of the strength of contaminant peaks and the appearance of double peaks for each energy level of the residual nuclide, extraction of accurate information from the spectra is difficult. In order to determine the position and size of each peak, a computer program was used which is able to disentangle overlapping peaks from one another as well as from a smooth background. A spectral intensity function

$$I(x) = \sum_{i=1}^{n} \frac{A_i}{\sqrt{2\pi}\,\sigma_i} \exp -\tfrac{1}{2}\left(\frac{x-\mu_i}{\sigma_i}\right)^2 + \sum_{j=0}^{k} a_j x^j,$$

is constructed by specifing a range of channels in the spectrum to be considered, the number n, of peaks in the interval, the degree k, of the polynomial to represent the smooth background, and approximate values μ_i, σ_i, and A_i for respectively the position, width, and area of each peak. The subroutine CURFIT[14] then calculates increments by which the parameters are to be changed in order to decrease the quantity $\chi^2 = \sum_{j=c_1}^{c_2} \frac{[m_j - \int_j^{j+1} I(x)dx]^2}{m_j}$, where m_j is the number of counts in channel j. The parameters are successively reincremented until χ^2 ceases to decrease appreciably from one iteration to the next. Let

$$I_p(x) = \sum_{i=1}^{n}{}^{(p)} \frac{A_i}{\sqrt{2\pi}\,\sigma_i} \exp -\tfrac{1}{2}\left(\frac{x-\mu_i}{\sigma_i}\right)^2 + \sum_{j=0}^{k} a_j x^j,$$

where $\sum^{(p)}$ indicates deletion from the sum of the p^{th} term. From the data value of channel j is subtracted the quantity $\int_j^{j+1} I_p(x)dx$. The remaining counts are those for peak

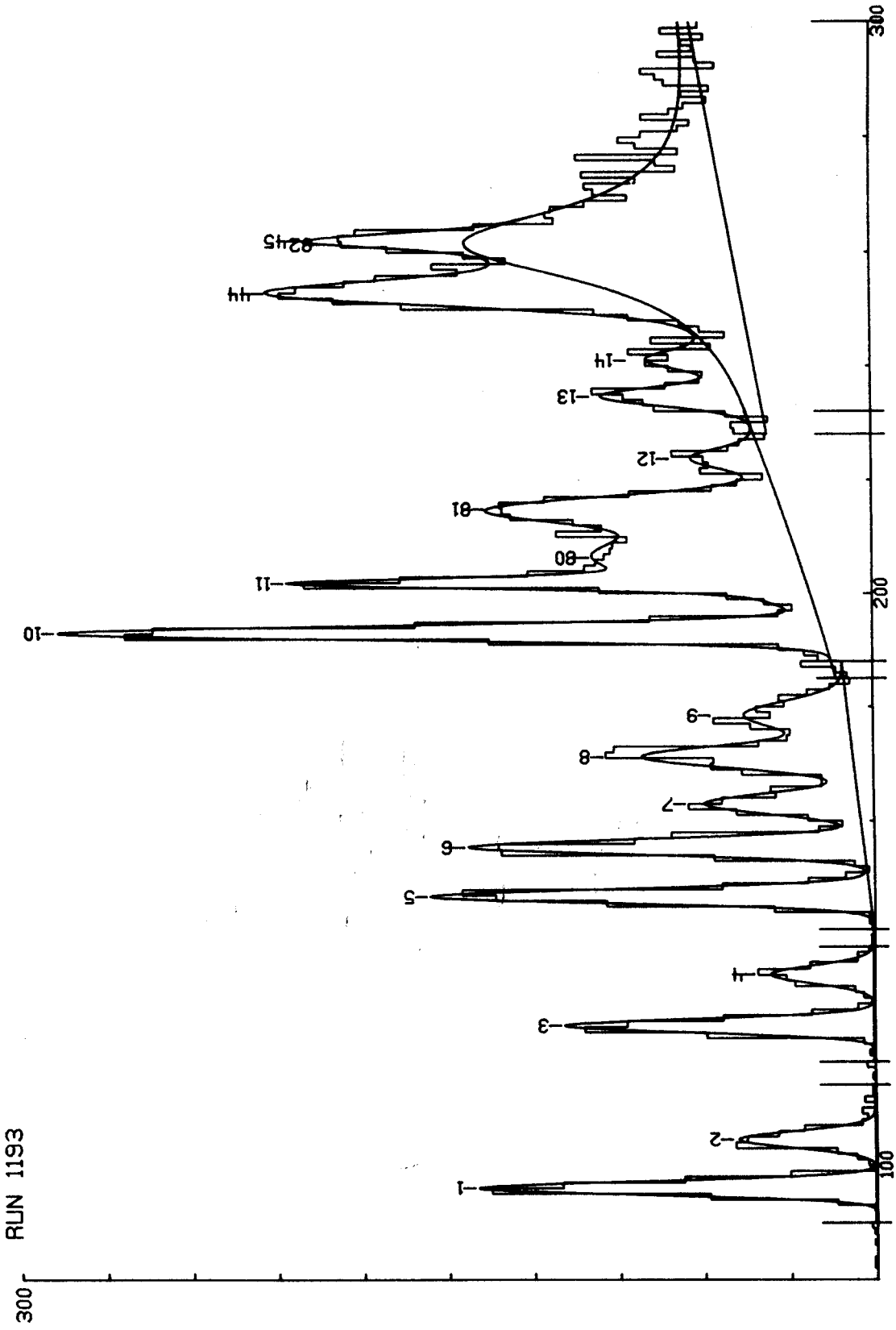

Figure 3.1 Peak analysis for ^{58}Ni spectrum, 10°.

p alone; that is, the smooth background and counts from nearby overlapping peaks have been eliminated. The size of peak p is then calculated by adding the values of each channel of the processed data. The peak position is taken to be the average channel number weighted by the number of counts per channel. In order to identify peaks in a spectrum, the peak location together with the magnet calibration is used to calculate the excitation energy of the level to which it corresponds in the product nuclide. Unfortunately, in contrast to the use of photographic plates, the length along the focal plane corresponding to one channel is not directly measurable. Therefore the use of a proportional counter introduces an additional unknown into the calibration procedure. To determine the calibration, the excitation energy of a known level for which a peak appears in the spectrum is used to compute the ^{7}Be energy, hence momentum, and, via the spectrometer calibration and magnetic field value, the peak position along the focal plane. These data, for several known levels, establish a least squares straight line giving distance along the focal plane in terms of channel number. The excitation energy corresponding to a heretofore unknown peak is computed by using the focal plane position as determined by the peak's channel number and the spectrometer calibration to calculate the effective radius of curvature of the ^{7}Be ions. The magnetic field value from the nuclear magnetic resonance measurement yields the momentum, hence the kinetic energy of the ^{7}Be ion. A correction is made for energy loss

in the target according to the formula of Williamson[15], et. al.; then the excitation energy computed by the formula listed in Appendix A.

Once the peaks have been identified and processed, the area information of the peaks may be used to calculate the differential cross sections for the reactions to the corresponding final states. The differential cross section is computed according to the following formula:

$$\frac{d\sigma}{d\Omega} = \frac{N}{\Delta\Omega} \cdot \frac{\cos\phi}{\rho\Delta x} \cdot \frac{A}{Q}\frac{n}{} \cdot \frac{e}{N_0} .$$

$\Delta\Omega$ is the solid angle subtended by the spectrometer entrance slit.

N is the peak area.

ϕ is the target angle.

$\rho\Delta x$ is the areal density of the target in gm/cm^2.

e is the electron charge, 1.6022×10^{-19} Coulomb.

N_0 is Avogadro's number, 6.0222×10^{23}.

A is the atomic mass of the target.

Q is the charge in Coulombs collected in the course of accumulating

N counts in the peak. And

n is the charge number of the projectile.

If $\Delta\theta$ and $\Delta\phi$ are the angles subtended by the rectangular aperature of the spectrometer entrance slit, the solid angle subtended is $\Delta\Omega = 4 \sin^{-1}\{\sin(\frac{1}{2}\Delta\theta) \sin(\frac{1}{2}\Delta\phi)\}$. The cross sections thus obtained are converted to the center of mass

coordinate system by multiplying by the center of mass to laboratory cross section ratio. The formulae for computation of the cross section ratio and the center of mass scattering angle are listed in Appendix A.

IV. DATA

A. $^{12}C(^{3}He,^{7}Be)^{8}Be$

Energy levels of ^{8}Be are given in Table 4.1. Levels through 17.64 MeV may be observed with this reaction, but the peaks for this level and the ground state may not be simultaneously placed on the counter system because it is not long enough. Therefore measurement of spectra for the ^{12}C target was split into two series of experiments; one each for two ranges of excitation energies in ^{8}Be. A 100 $\mu g/cm^2$ commercially obtained target was used for both sets. Contamination is not a problem for a carbon target, however energy loss of ^{7}Be in carbon is particularly severe because of the target's small atomic mass. Therefore in order to secure adequate resolution, a thin target is necessary, target thickness being the factor limiting resolution. As a check, a 200 $\mu g/cm^2$ target was used and resolution was degraded as expected. Figure 4.1 displays two spectra for the $^{12}C(^{3}He,^{7}Be)^{8}Be$ reaction at two angles. Noting that the separation of the ground state peaks is about 400 keV, the resolution for the forward angle is about 150 keV, whereas the resolution for the 22° spectrum is somewhat poorer because of the decreased ^{7}Be energy. The broad 2^+ and 4^+ states at 2.9 and 11.4 MeV respectively, increase relative to the ground state as the scattering angle increases. Figure 4.2 is a spectrum including the 16.63 - 17.6 MeV excitation energy region of ^{8}Be. Because the 16.63 MeV and

Table 4.1 Energy levels of $^{8}Be^{29}$.

E_x (MeV)	Γ (keV)	J^{π}
0.00	6.8 ev	0^+
2.94	1560	2^+
11.4	7000	4^+
16.627	107	2^+
16.911	77	2^+
17.642	10.7	1^+
18.154	138	1^+
18.91	48	2^-
19.06	270	3^+

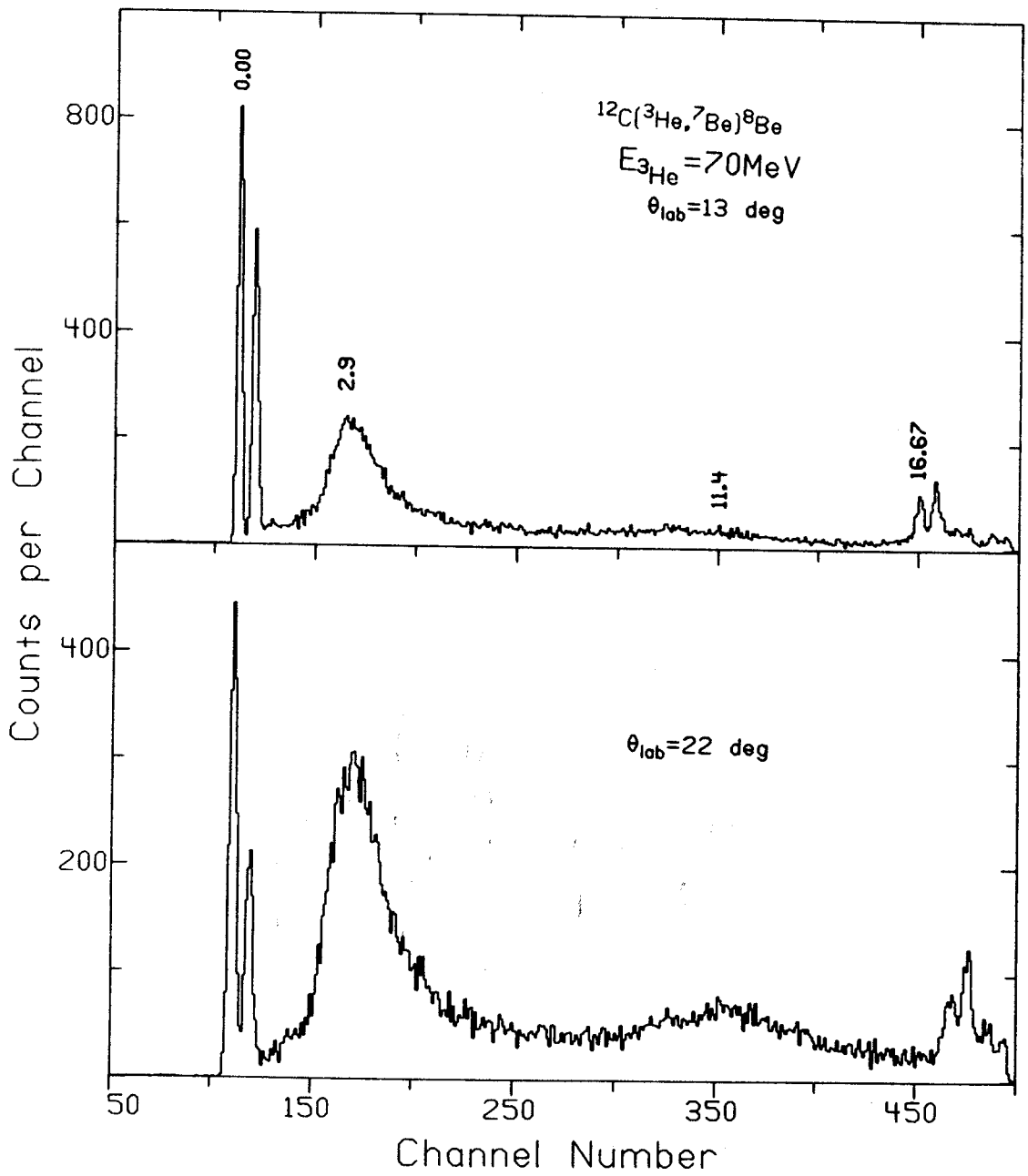

Figure 4.1 Spectra measured with the proportional counter.

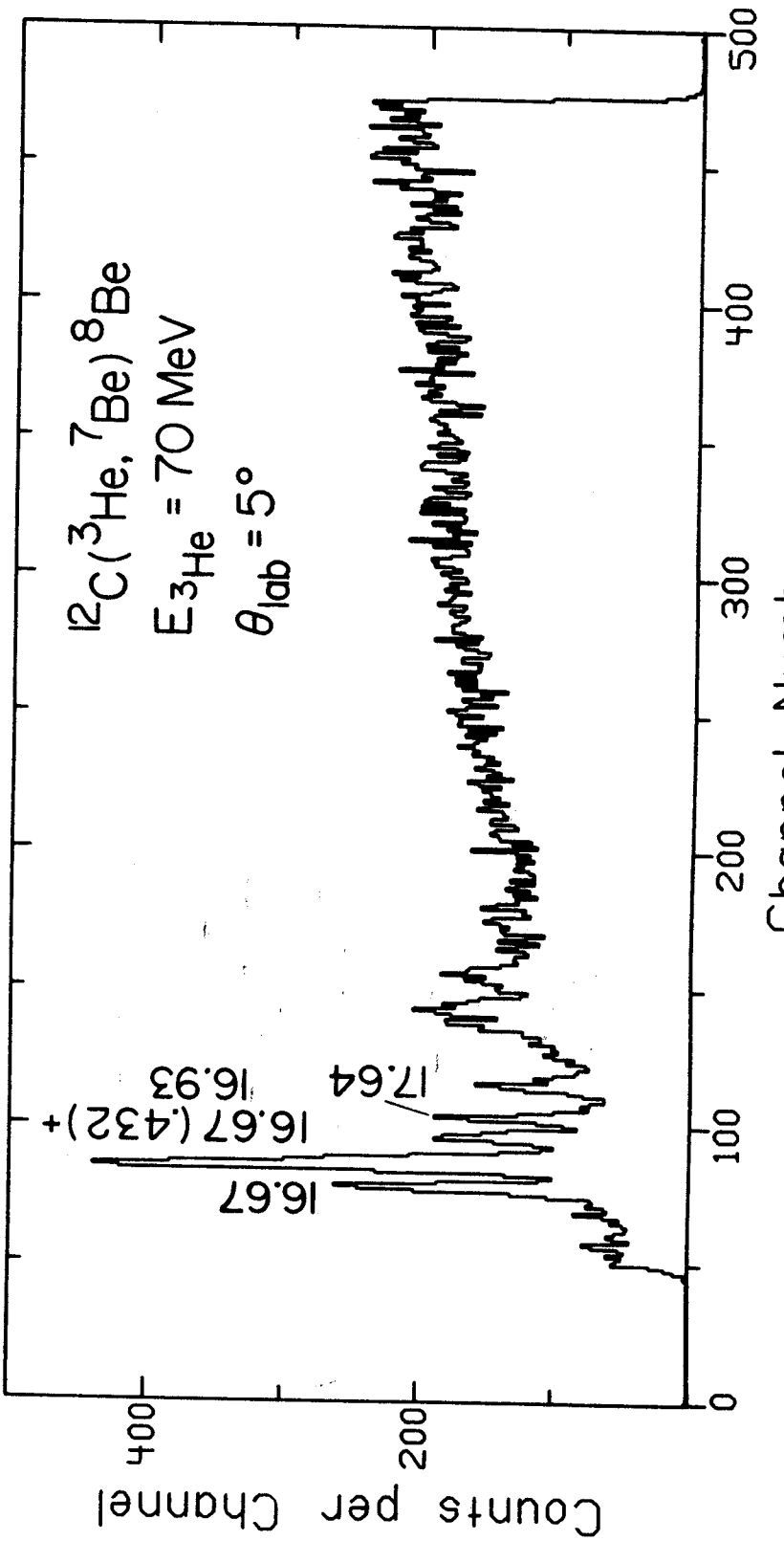

Figure 4.2 As for 4.1.

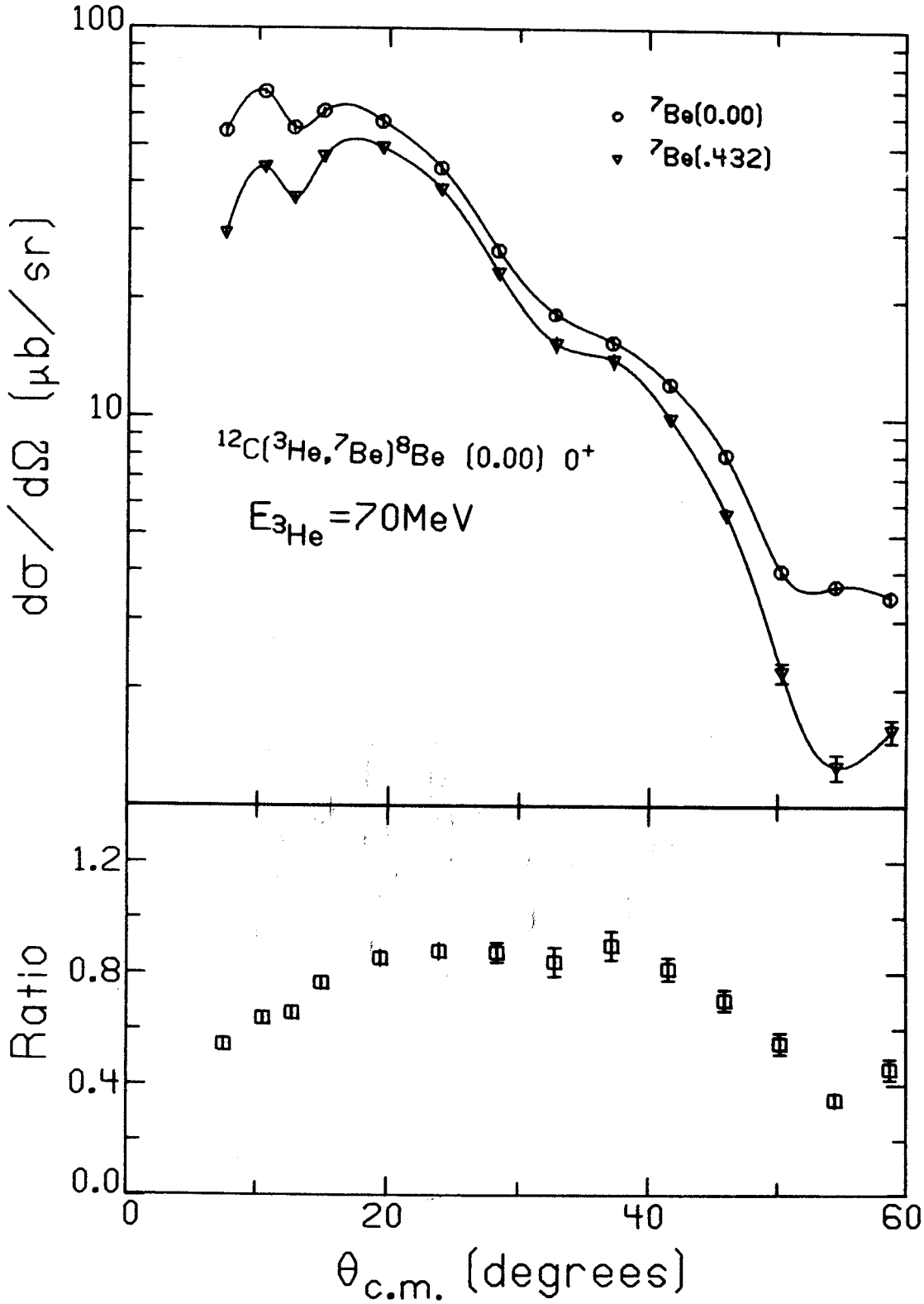

Figure 4.3 Angular distribution together with secondary to primary ratio. The curves are simply for visual convenience.

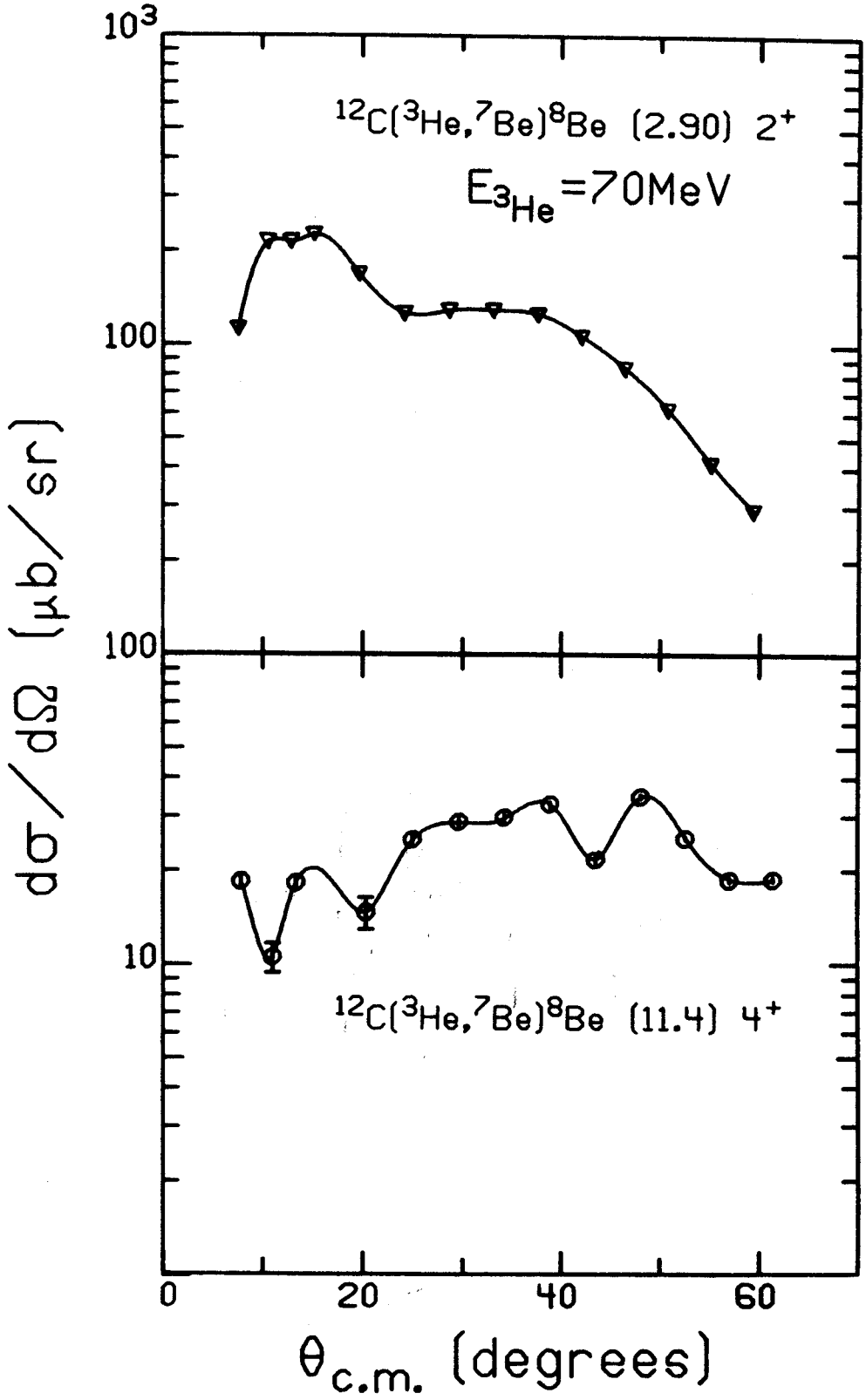

Figure 4.4 Angular distributions.

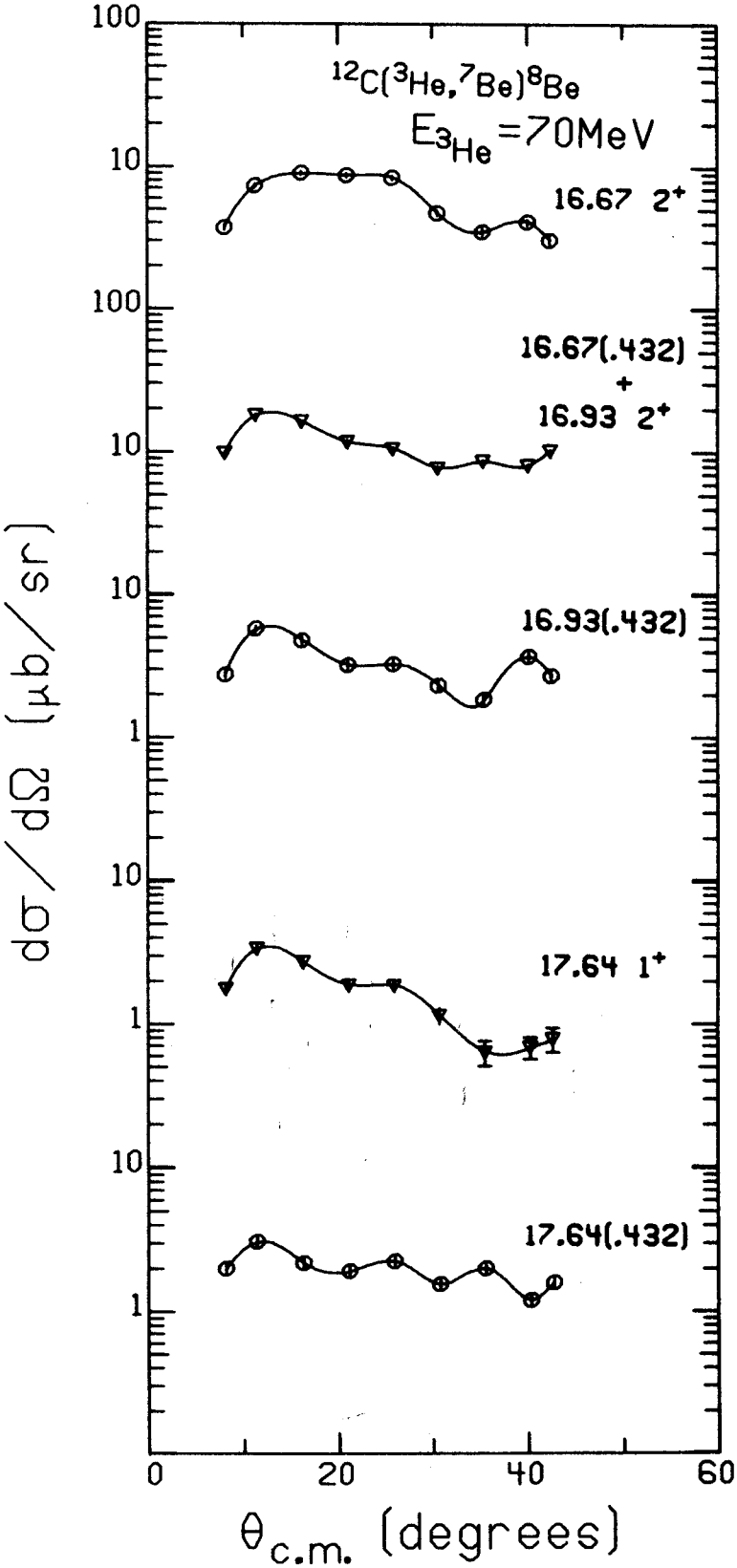

Figure 4.5 As for 4.4.

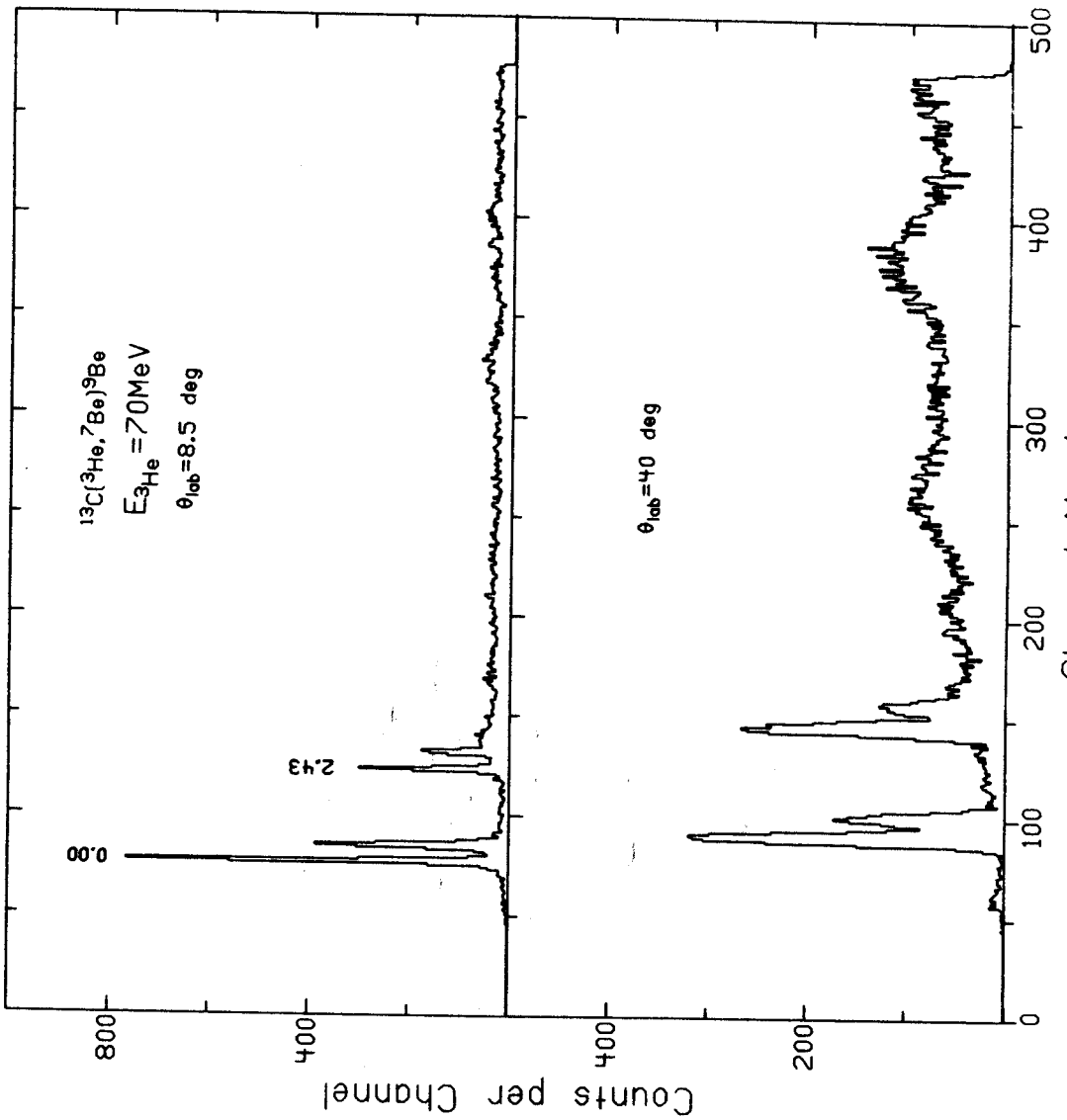

Figure 4.6 As for 4.1.

16.91 MeV states are separated by about the same amount as the ground state and first excited state of ^{7}Be, the primary 16.91 peak and the secondary 16.63 peak cannot be resolved. Therefore the angular distribution in Figure 4.5 is the sum of the 16.91 primary and the 16.63 secondary distributions. The distributions in Figure 4.4 for the 2.9 and 11.4 MeV levels are, of course, sums of the respective primary and secondary distributions as the levels are much too broad to resolve their primary and secondary constituents. The ground state angular distribution is shown in Figure 4.3; both primary and secondary distributions together with the ratio of the secondary to primary cross sections. Note that this ratio distinctly deviates from the expected constant value ½.

B. $^{13}C(^{3}He,^{7}Be)^{9}Be$

Two sharp levels in ^{9}Be are observed with this reaction and, as may be seen from Figure 4.6, several broad levels appear at backward angles. A 200 $\mu g/cm^2$ enriched ^{13}C target was used so the resolution is not as good as for the ^{12}C experiment but nevertheless is adequate to resolve primary and secondary peaks of the sharp states. The broad 2.78 MeV level under the pair of sharp peaks representing the 2.429 MeV level may be seen in addition to the ground state peaks. No evidence at any angle is discernable for the 210 keV wide 1.68 MeV level. The primary and secondary angular distributions together with the secondary to primary cross section

ratios are plotted in Figures 4.7 and 4.8 for the ^{9}Be ground state and 2.429 state. The angular distributions are smooth with very little structure and the ratios are more nearly constant than those for ^{8}Be.

C. $^{16}O(^{3}He,^{7}Be)^{12}C$

The oxygen target was fabricated by evaporating tungsten oxide (WO_3) onto a 250 $\mu g/cm^2$ gold foil. Tungsten and gold were chosen since their ^{7}Be yield from the (^{3}He,^{7}Be) reaction is probably negligible compared to that from ^{16}O. The amount of oxygen on the target was determined by comparing with the ^{7}Be yield from a ¼ mil Mylar target at 17.5°. The oxygen areal density was measured to be 11 $\mu g/cm^2$ or 53 $\mu g/cm^2$ WO_3. Despite the attempt to make a clean target, the presence of a significant amount of ^{12}C is apparent in Figure 4.9 which is a spectrum measured at 20°. The ^{12}C ground state and 4.439 2^+ first excited state are strongly excited. The 7.653 0^+ and 9.64 3^-, on the other hand, are very weak, appearing only at some angles. Higher levels are absent except for a group of weak unresolved levels around 13.35 MeV excitation energy. Angular distributions and ratios are plotted for the 0^+ ground state and the 2^+ 4.439 level in Figures 4.10 and 4.11.

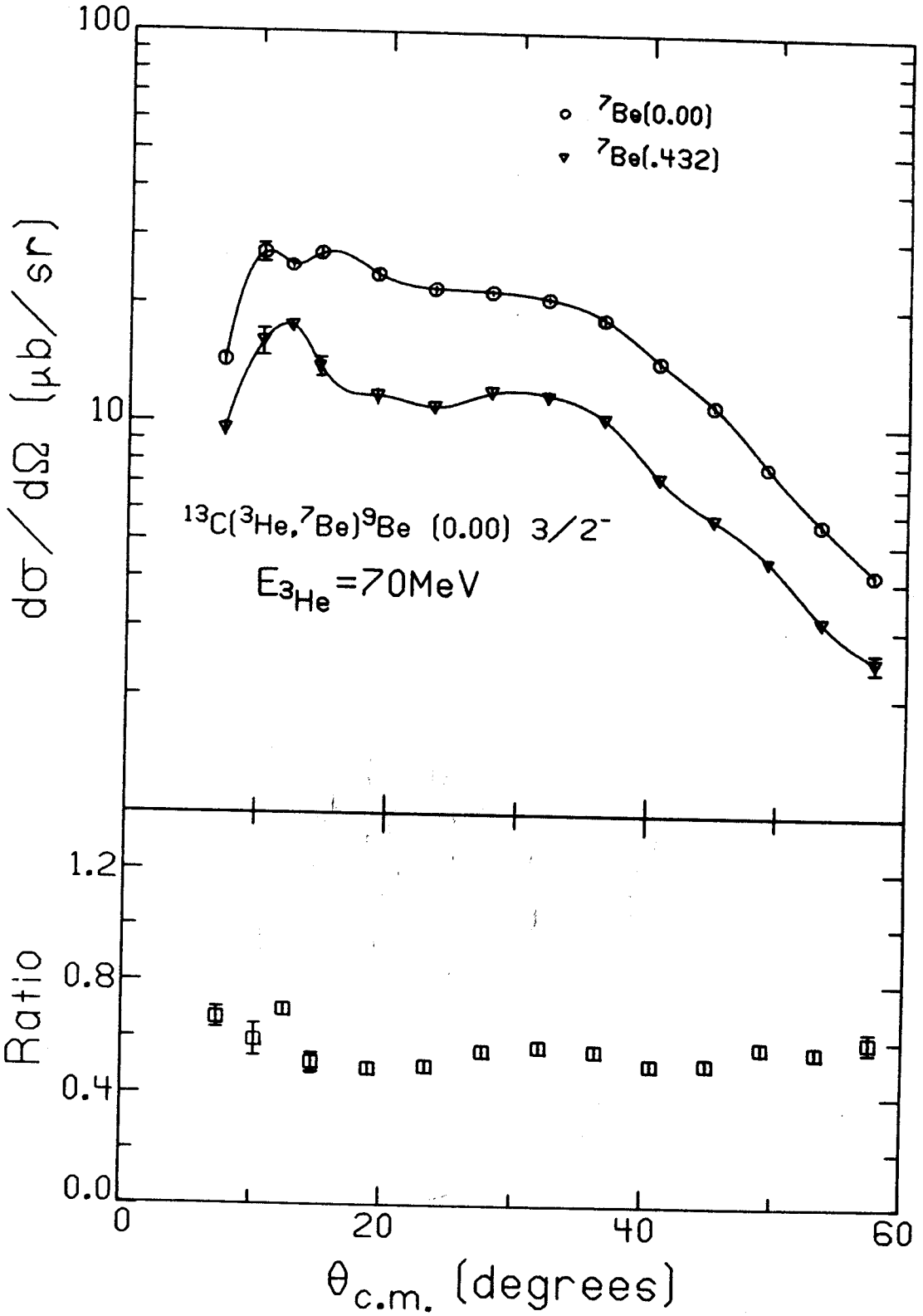

Figure 4.7 As for 4.3.

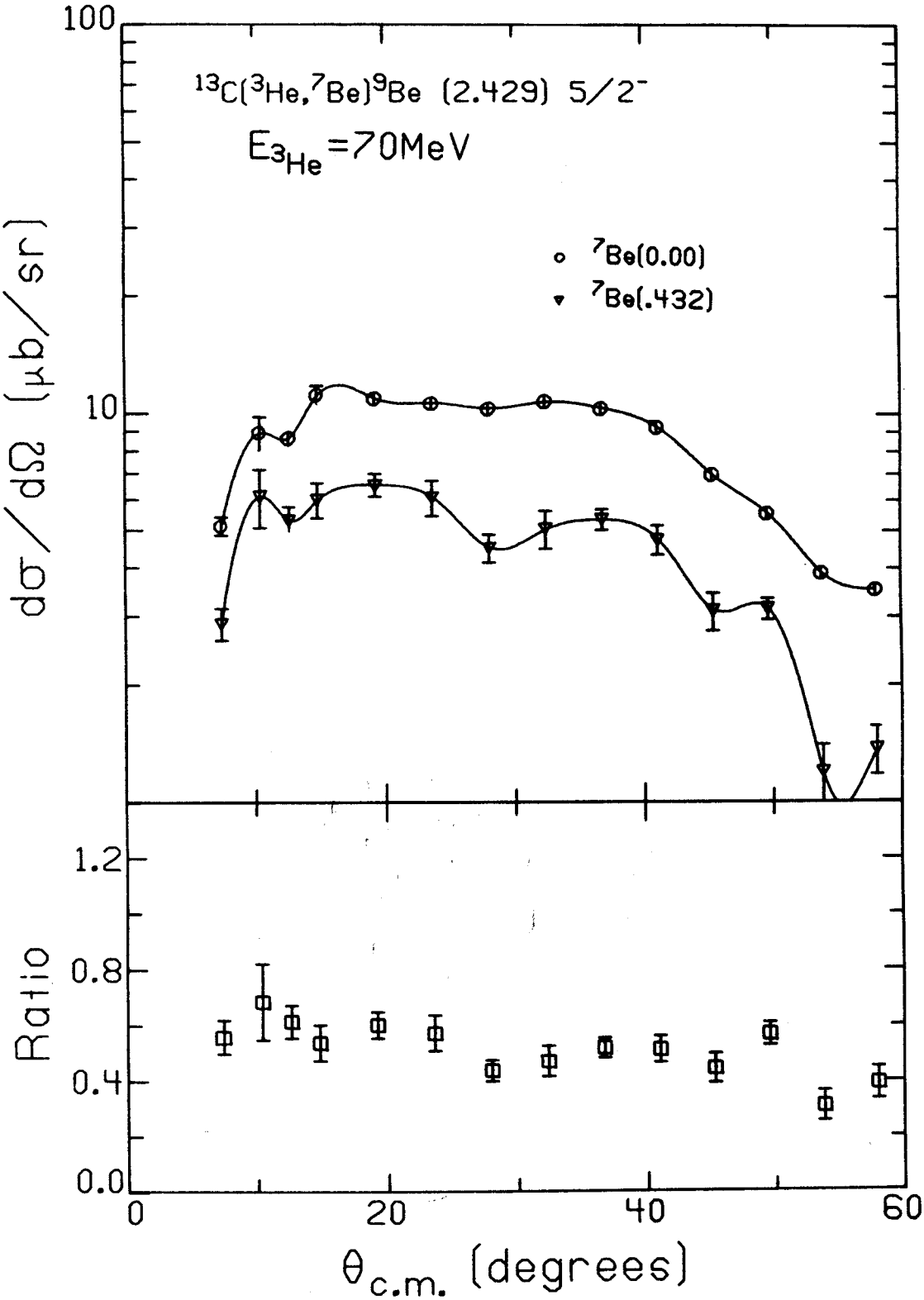

Figure 4.8 As for 4.3.

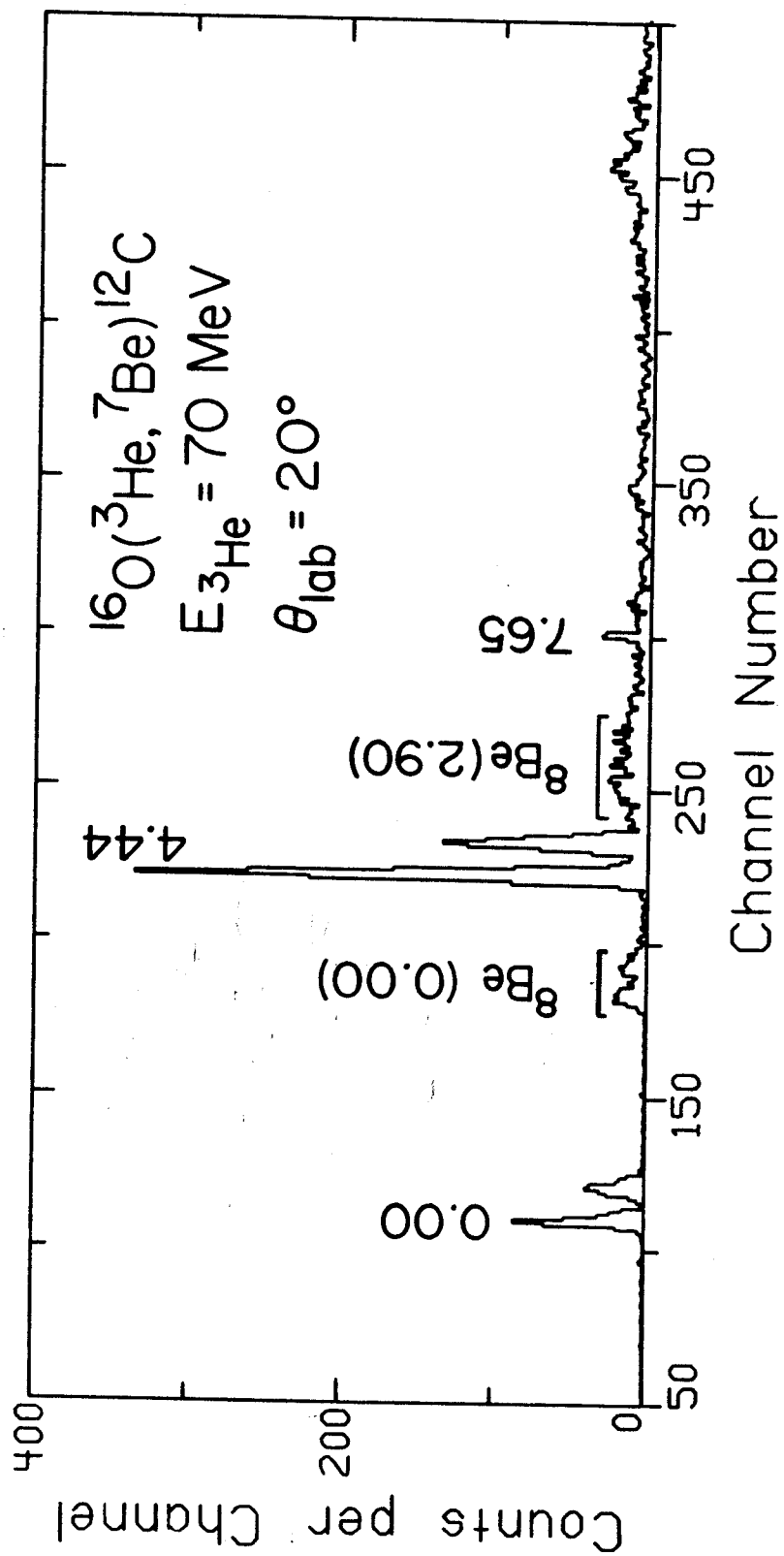

Figure 4.9 As for 4.1.

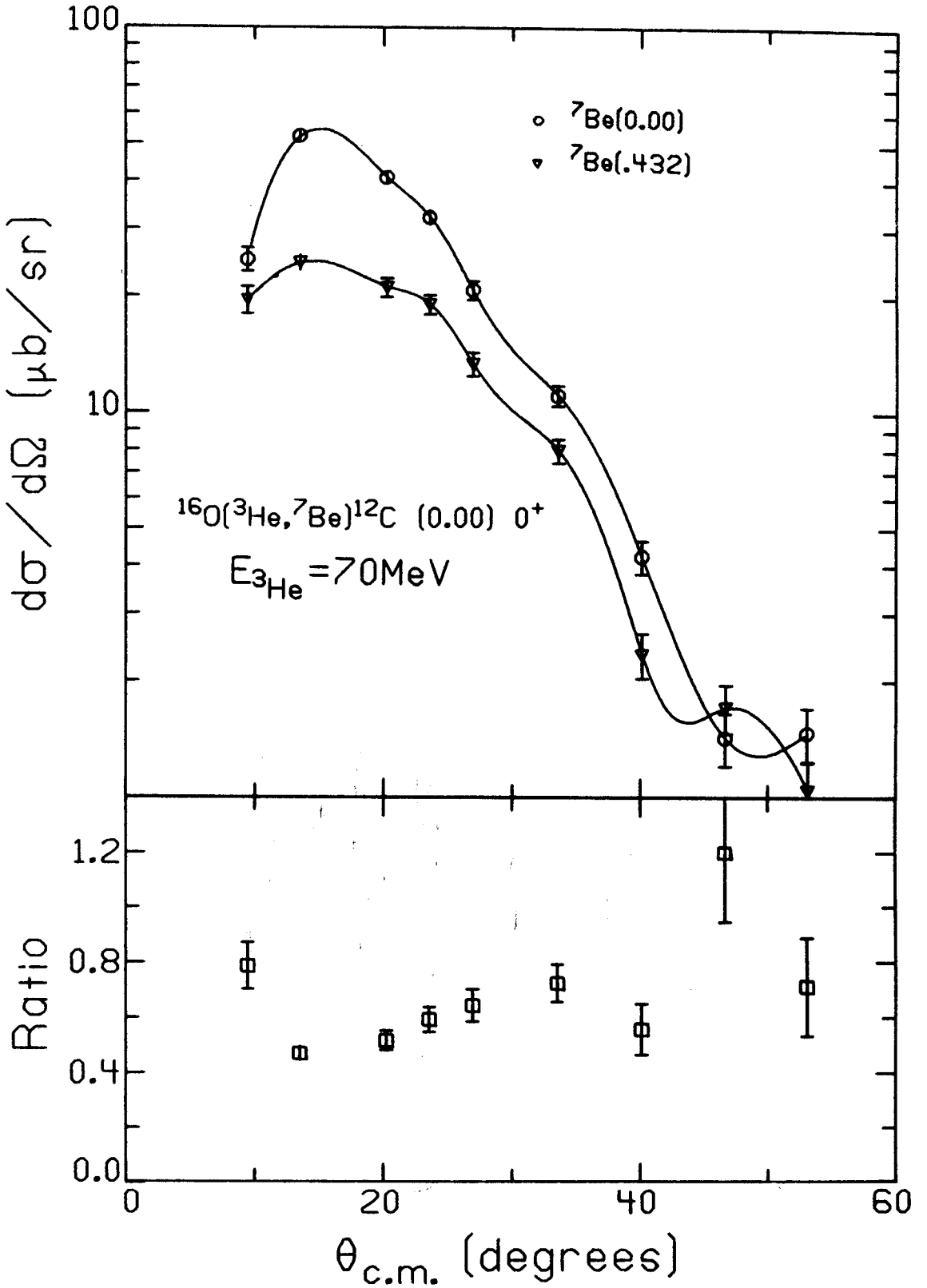

Figure 4.10 As for 4.3.

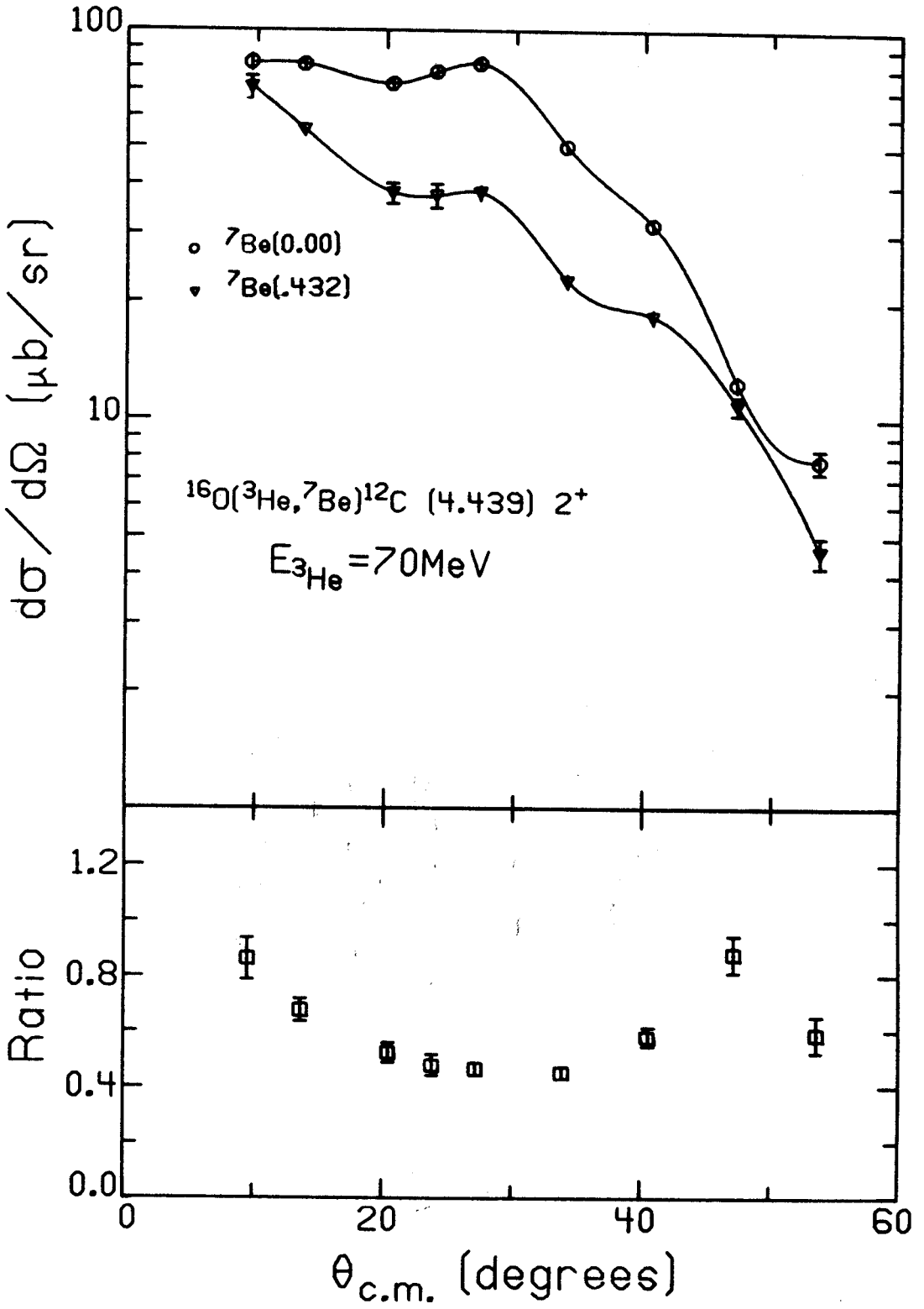

Figure 4.11 As for 4.3.

D. $^{24}Mg(^{3}He,^{7}Be)^{20}Ne$

The target used for this experiment is a 300 $\mu g/cm^2$ self supporting enriched ^{24}Mg foil. The thickness of the target was determined by passing α particles from the decay of ^{241}Am through the target and noting the energy loss. The areal density of ^{24}Mg causing the observed energy loss was computed with the aid of the energy loss formula of Williamson[15], et. al. Not having been prepared especially for this work, the target had been used previously and stored in the atmosphere. Consequently, carbon and oxygen contamination is particularly severe. The 27.5° spectrum plotted in Figure 4.12 is relatively contaminant free as the cross section for carbon and oxygen decrease more rapidly with increasing angle than the cross section for magnesium. The four most strongly excited ^{20}Ne levels all appear unobscured in this spectrum; the 0^+ ground state, 1.63 2^+, 4.25 4^+, and 5.62 3^-. A pure α transfer reaction will not excite unnatural parity states. Nonetheless, the 4.97 2^- is present. Although weakly excited, it appears at enough angles to measure the angular distribution plotted in Figure 4.17. States of higher excitation energy appear but are not resolved.

Because of a sharp dip noticed in the ground state's secondary to primary cross section ratio at 10°, particular attention was given to the ground state at forward angles. Several spectra were obtained at angles around 10° in 1° steps, using a 1° wide by 2° tall spectrograph entrance slit rather than the usual 2° x 2° slit to improve angular

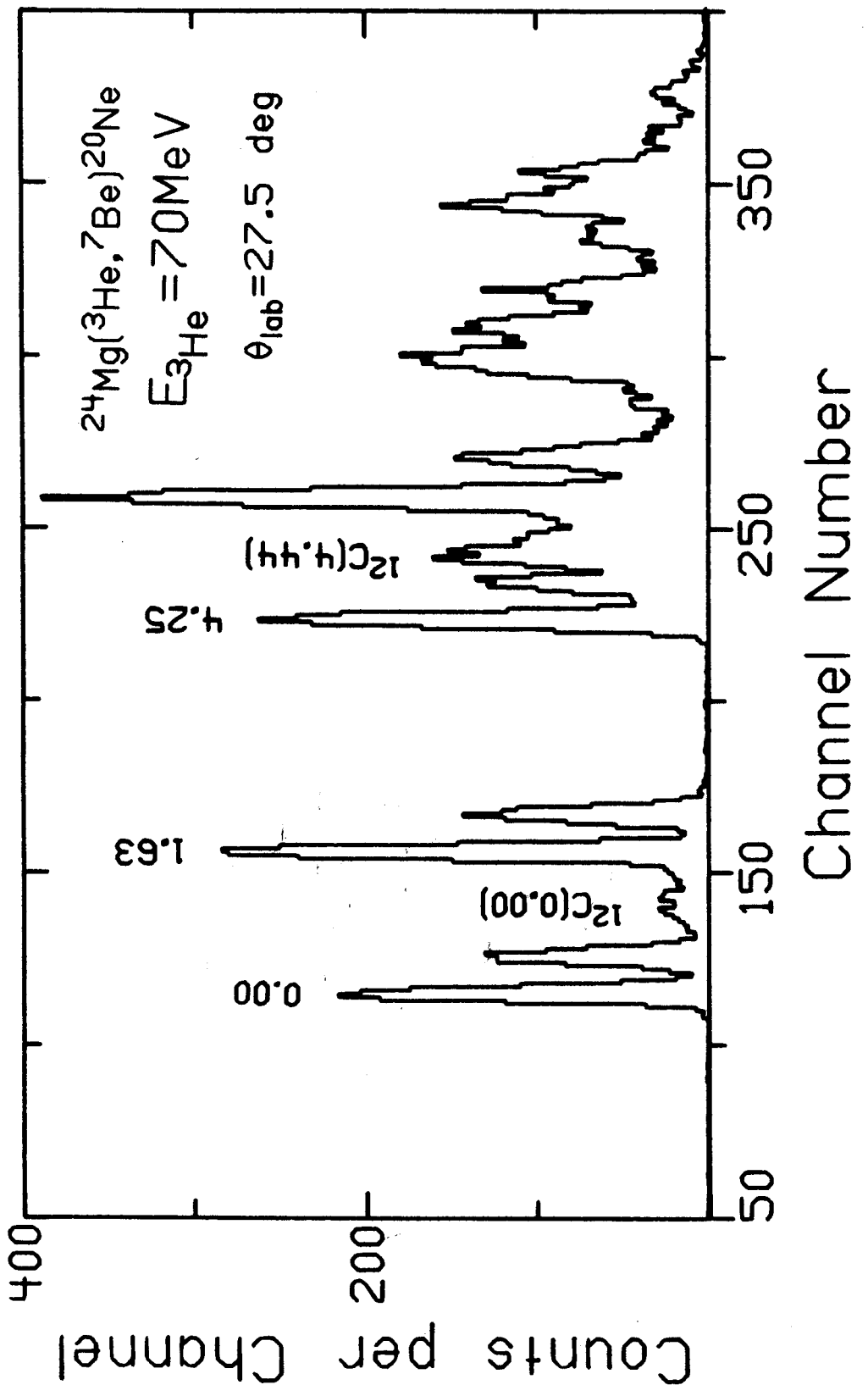

Figure 4.12 As for 4.1.

resolution. The result, plotted in Figure 4.13, is a deep minimum in the ratio at 13° center of mass angle. Angular distributions and ratios for the other three strong states are plotted in Figures 4.14, 4.15, and 4.16.

E. $^{26}Mg(^{3}He,^{7}Be)^{22}Ne$

A self supporting 250 $\mu g/cm^2$ enriched ^{26}Mg target was used for this reaction. This target, as the ^{24}Mg target, was previously used; however, it had been stored in a vacuum chamber ($\sim 10^{-3}$ torr). Nevertheless, contamination is a serious problem, causing gaps in angular distributions of some states. Numerous states in ^{22}Ne are excited by this reaction, particularly in the range 5 - 9 MeV excitation energy. The observed levels in ^{22}Ne are listed in Table 4.2 together with $^{22}Ne(\alpha,\alpha')$ spectral measurements of Ollerhead[30], et. al. The 45° spectrum of Figure 4.18 includes all states observed. At this large scattering angle, the contaminant peaks pose no problem, having significantly decreased in magnitude relative to the ^{22}Ne peaks. The largest peak in the spectrum, at 7.53 MeV, is the strongest peak at most angles. Angular distributions for the ^{22}Ne states are presented in Figures 4.19 to 4.25.

F. $^{48}Ca(^{3}He,^{7}Be)^{44}Ar$

This experiment was undertaken primarily to measure the mass of the nuclide ^{44}Ar. Additionally, excitation energies of some low lying levels were determined. The ^{48}Ca target

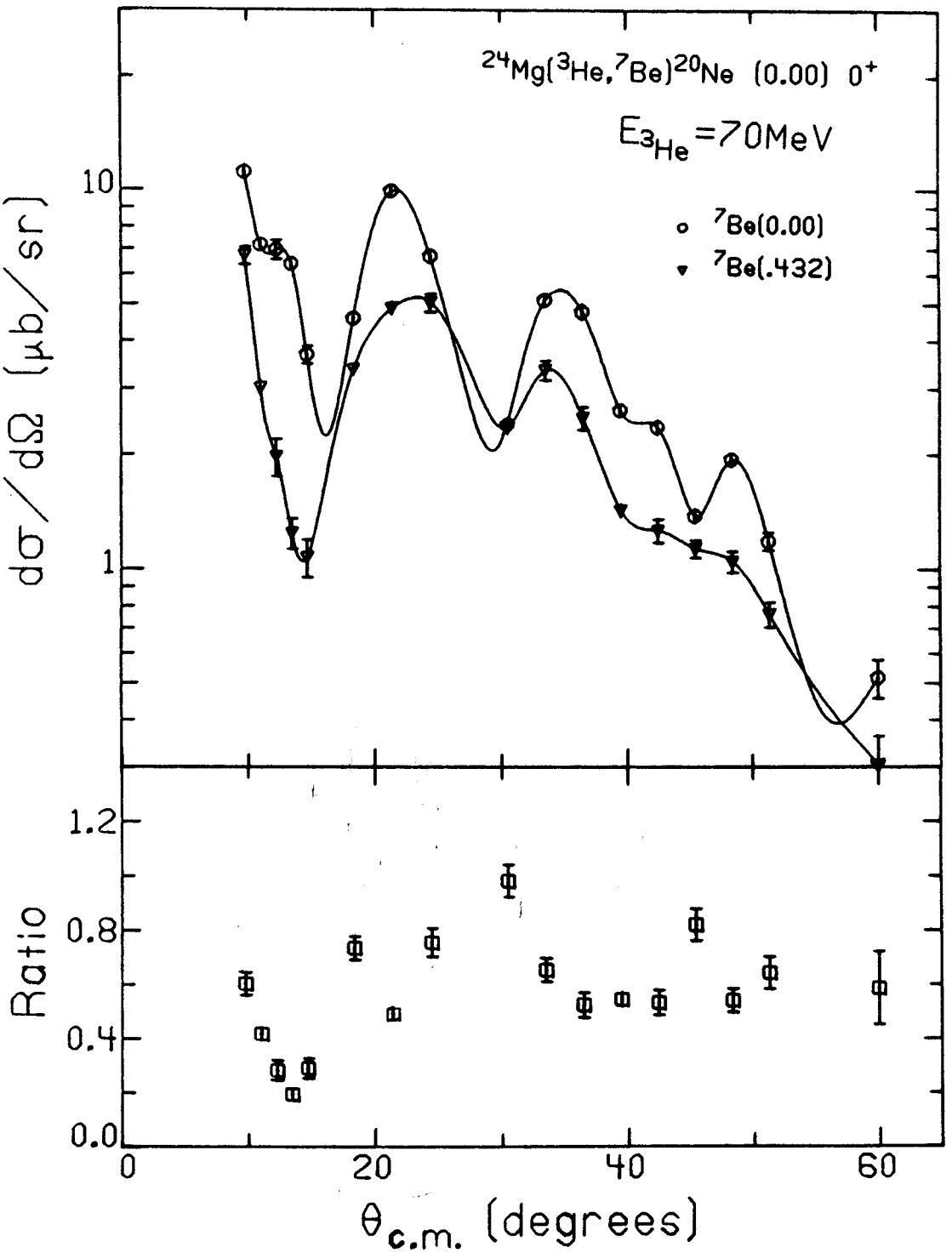

Figure 4.13 As for 4.3.

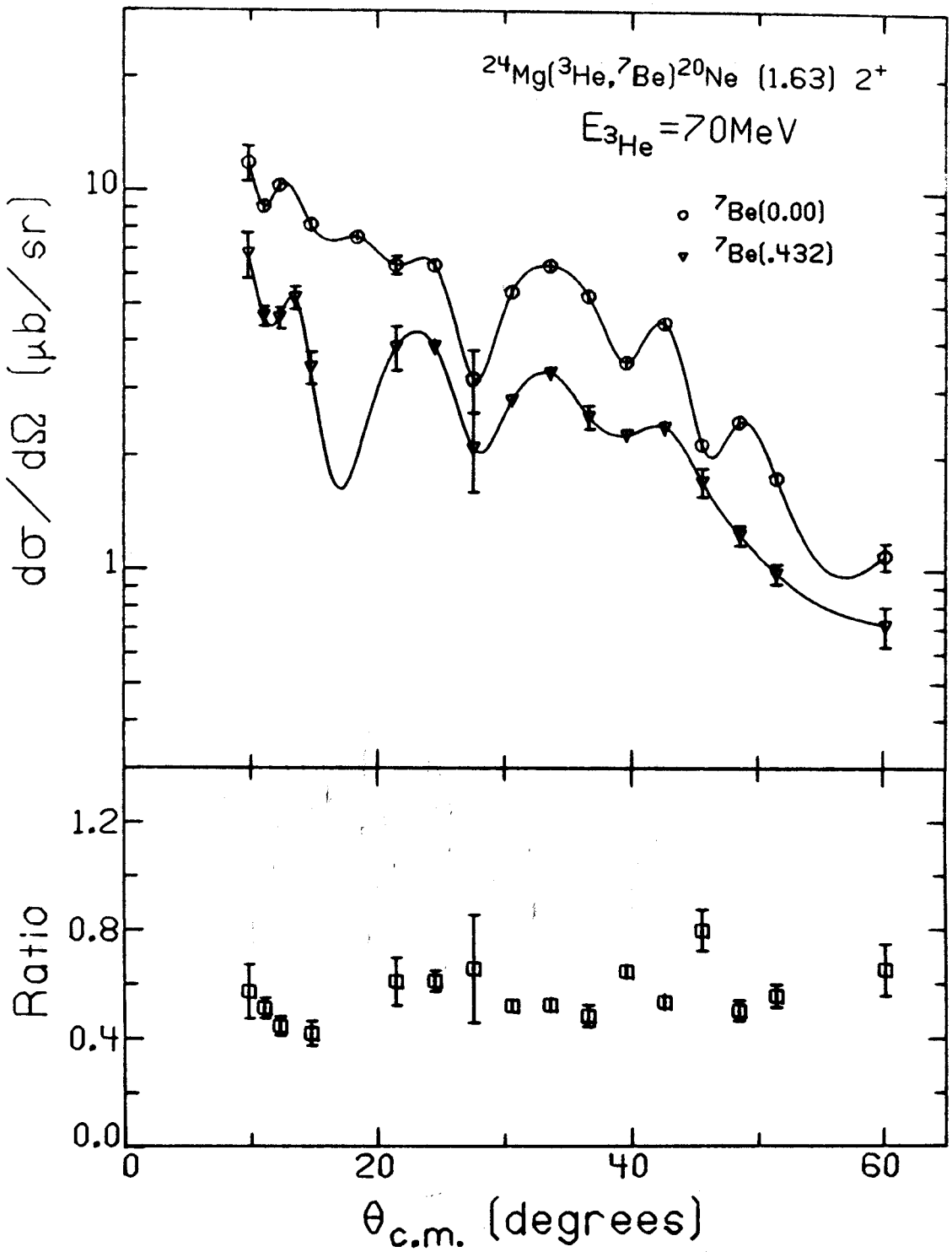

Figure 4.14 As for 4.3.

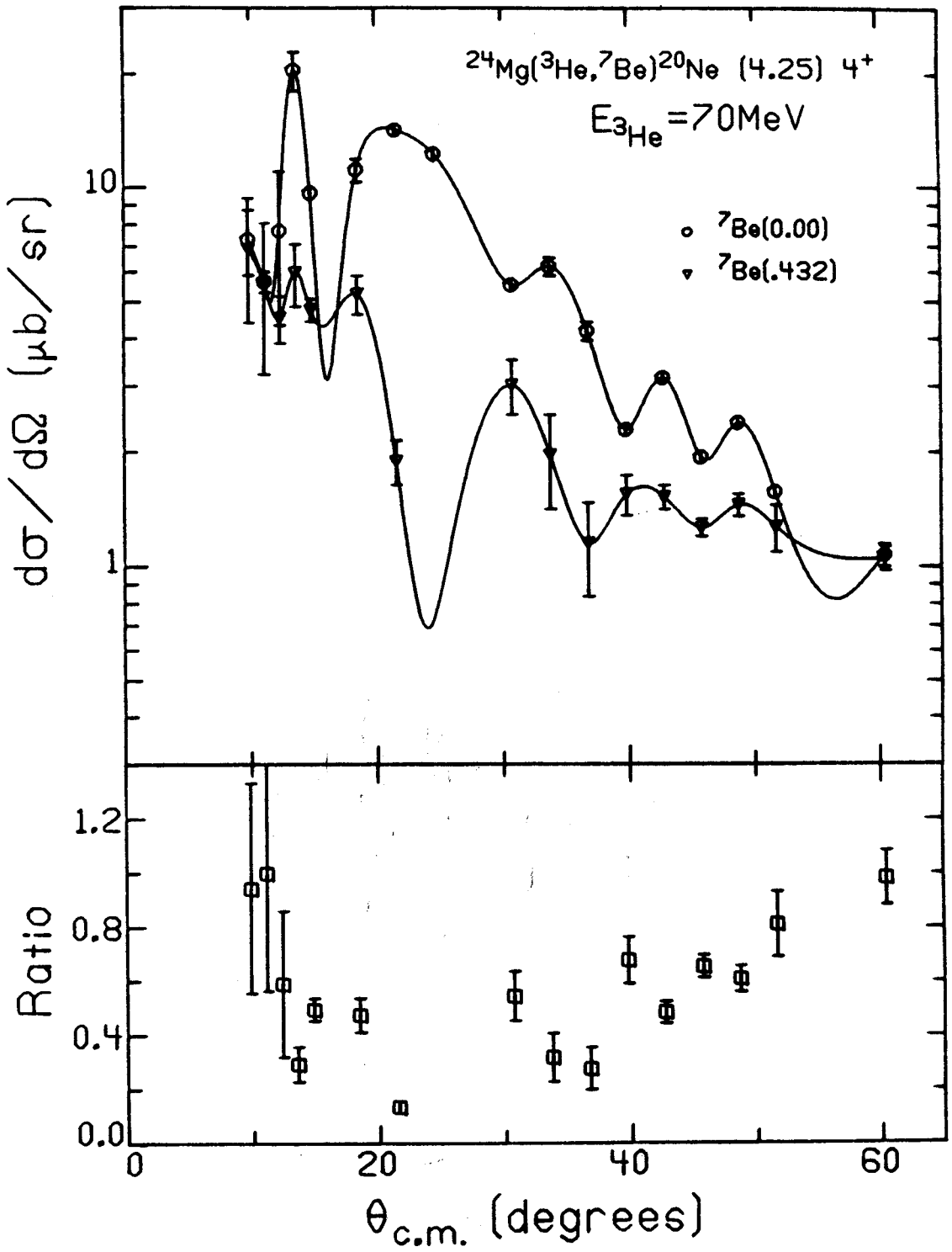

Figure 4.15 As for 4.3.

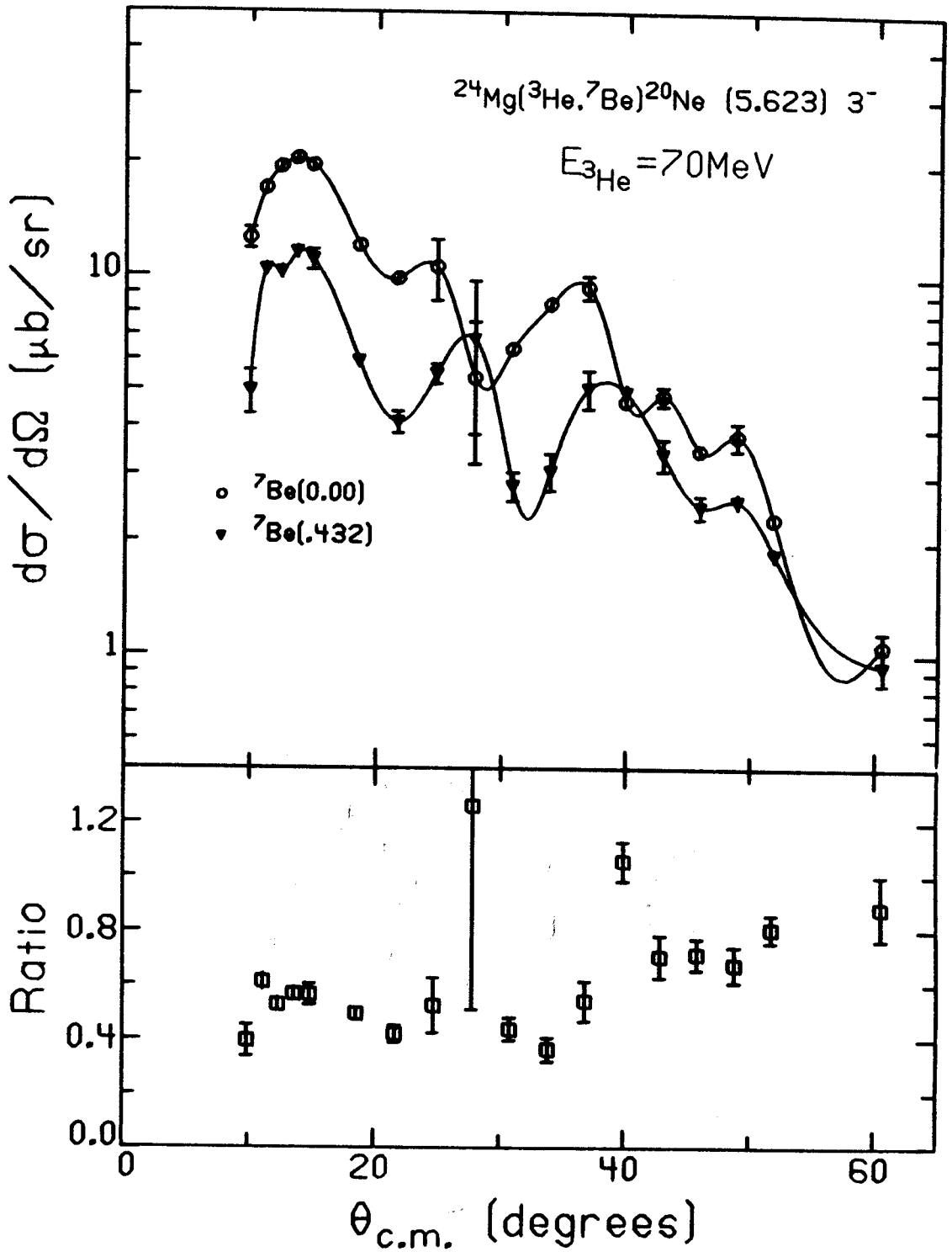

Figure 4.16 As for 4.3.

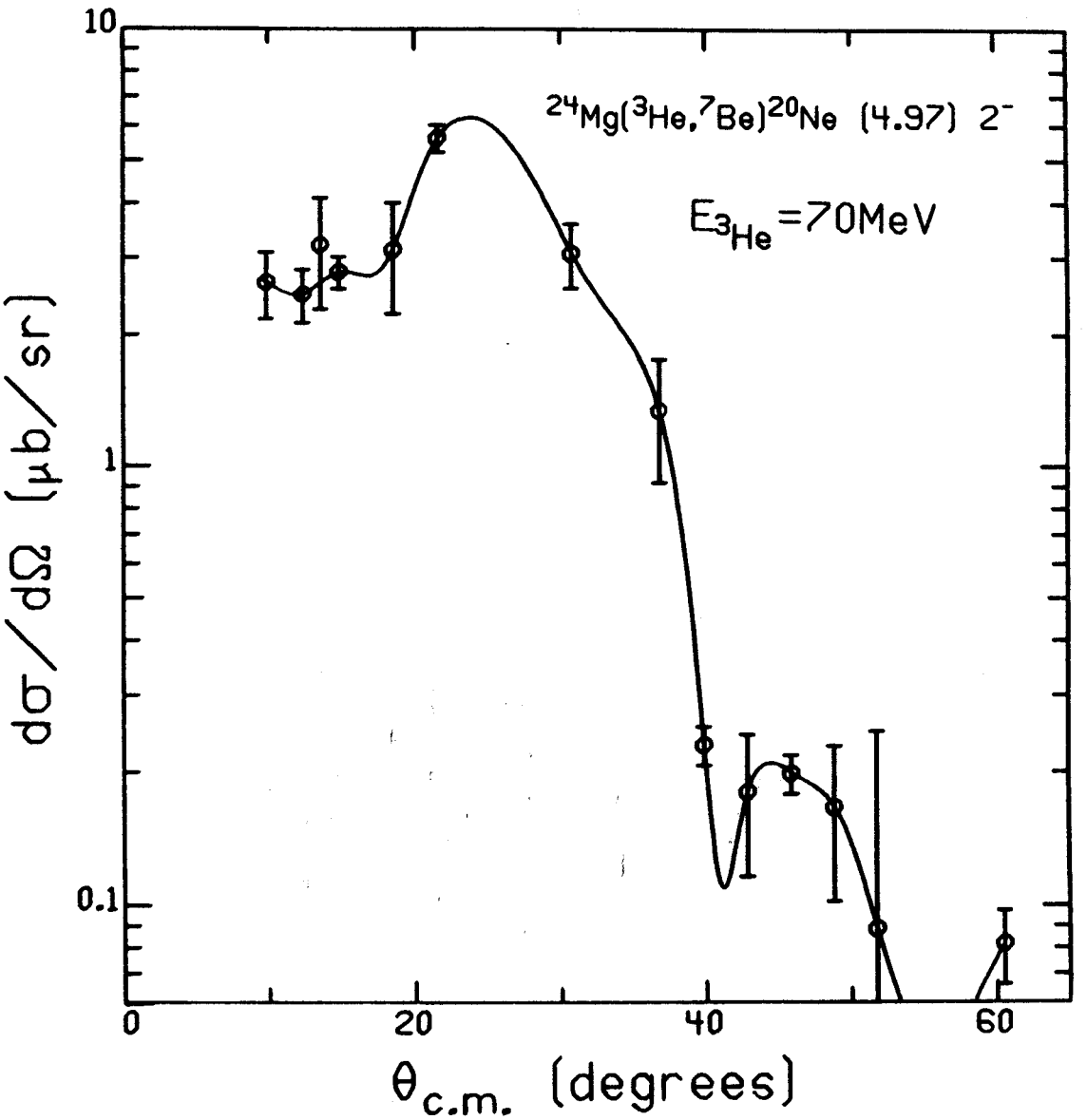

Figure 4.17 Angular distribution.

Table 4.2 Energy levels of ^{22}Ne.

Present Work	Previous Work		
E_x (MeV)	E_x (MeV)	J^π	ref.
0.00	0.00	0^+	30,34,35
1.265 ± .03	1.28	2^+	30,34,35
3.350 ± .04	3.36	4^+	30,34,35
4.470 ± .05	4.46	2^+	30,34,35
	5.14	2^-	30,34,35
	5.33	$(1)^+$	30,34
	5.36	$(2)^+$	30,34,35
5.57 ± .16	5.52	4^+	30,34,35
	5.64	3^+	30,34,35
6.00 ± .17	5.93	2^+	30,35
	6.12	(3^-)	30,34,35
	6.24	0^+	30,35
6.42 ± .17	6.35	6^+	30,34,35
	6.64	+	30,34
	6.70		30,35
	6.82	2^+	30,34,35
	6.86	$(1)^+$	30,34
	6.90	0^+	35
	7.05*	1^-	30,34,35
	7.34*	0^+	34,35
	7.41	-	34,35
7.52 ± .20	7.49*	1^-	34,35
	7.64*	2^+	34,35
	7.66*	-	34
	7.73*	3^-	34,35
	7.93	+	34,35
	8.08	+	34,35
	8.14*	2^+	34,35
8.30 ± .27	8.38		34,35
	8.50	+	34,35
	8.55	+	34
	8.59	2^+	34,35
8.75 ± .35	8.74	-	34
	8.86	+	34
	8.90	-	34
	9.04		34
9.15 ± .40	9.10	-	34
9.82 ± .75			

* The states most strongly excited by (^{7}Li,t).

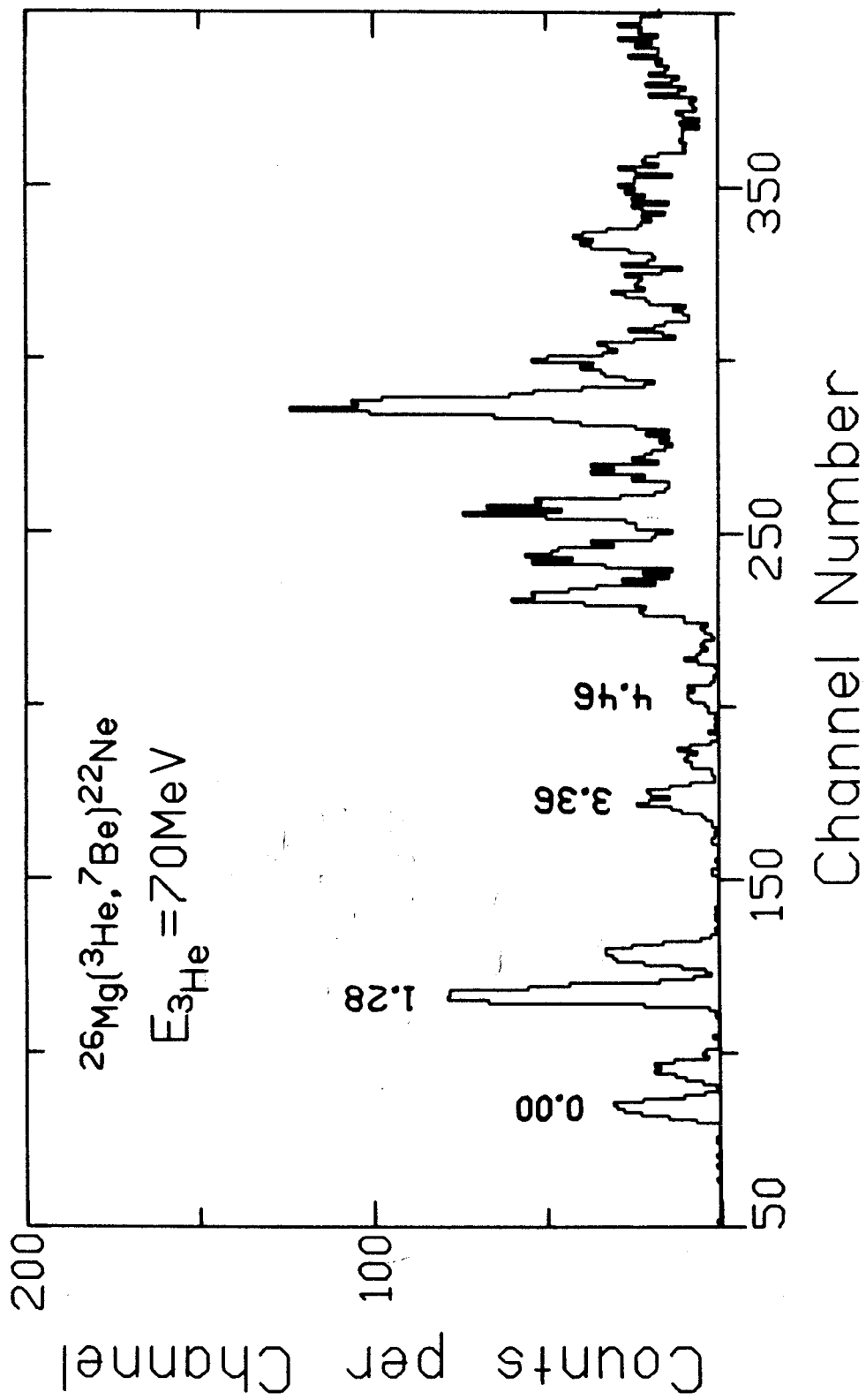

Figure 4.18 As for 4.1.

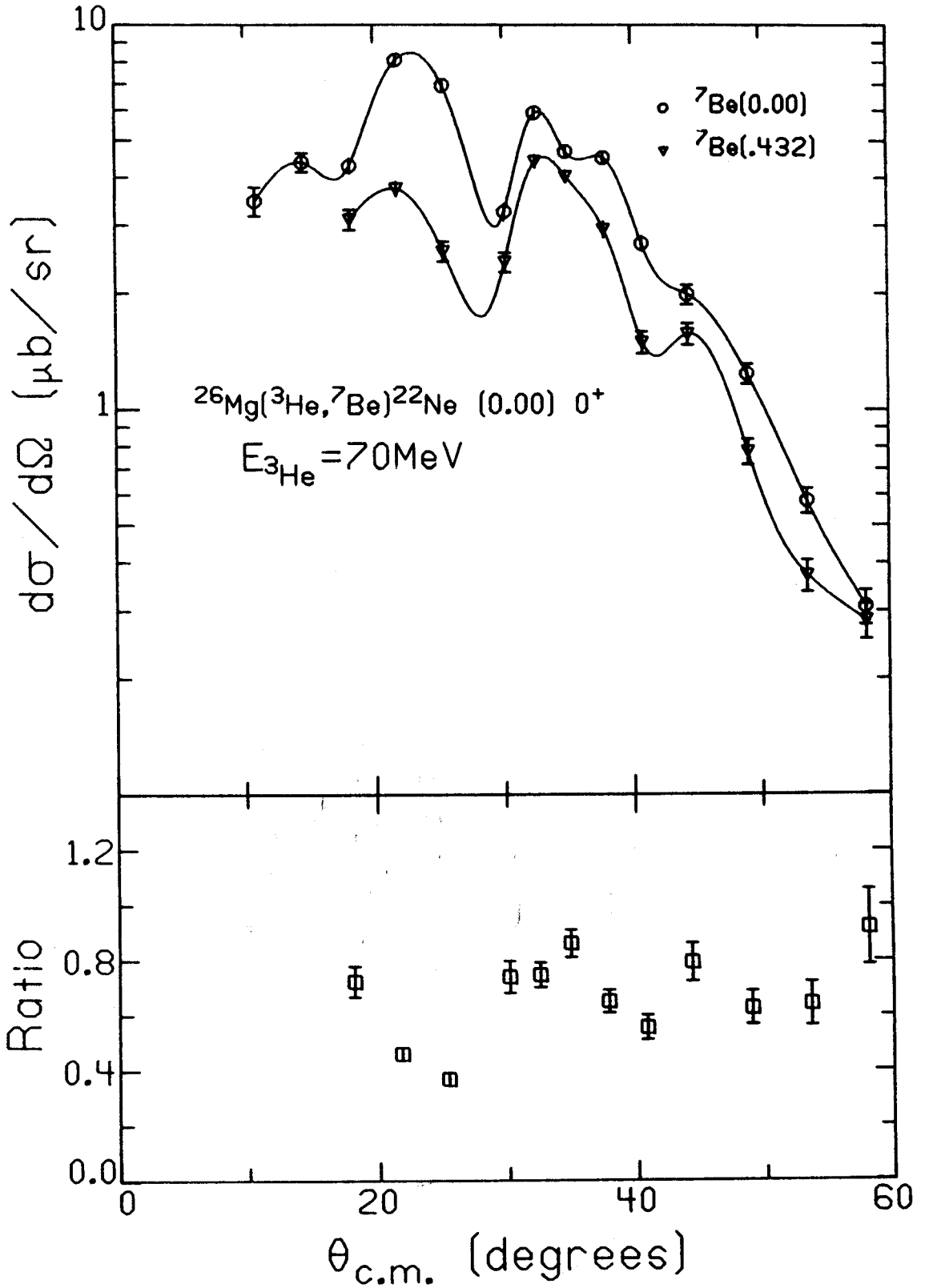

Figure 4.19 As for 4.3.

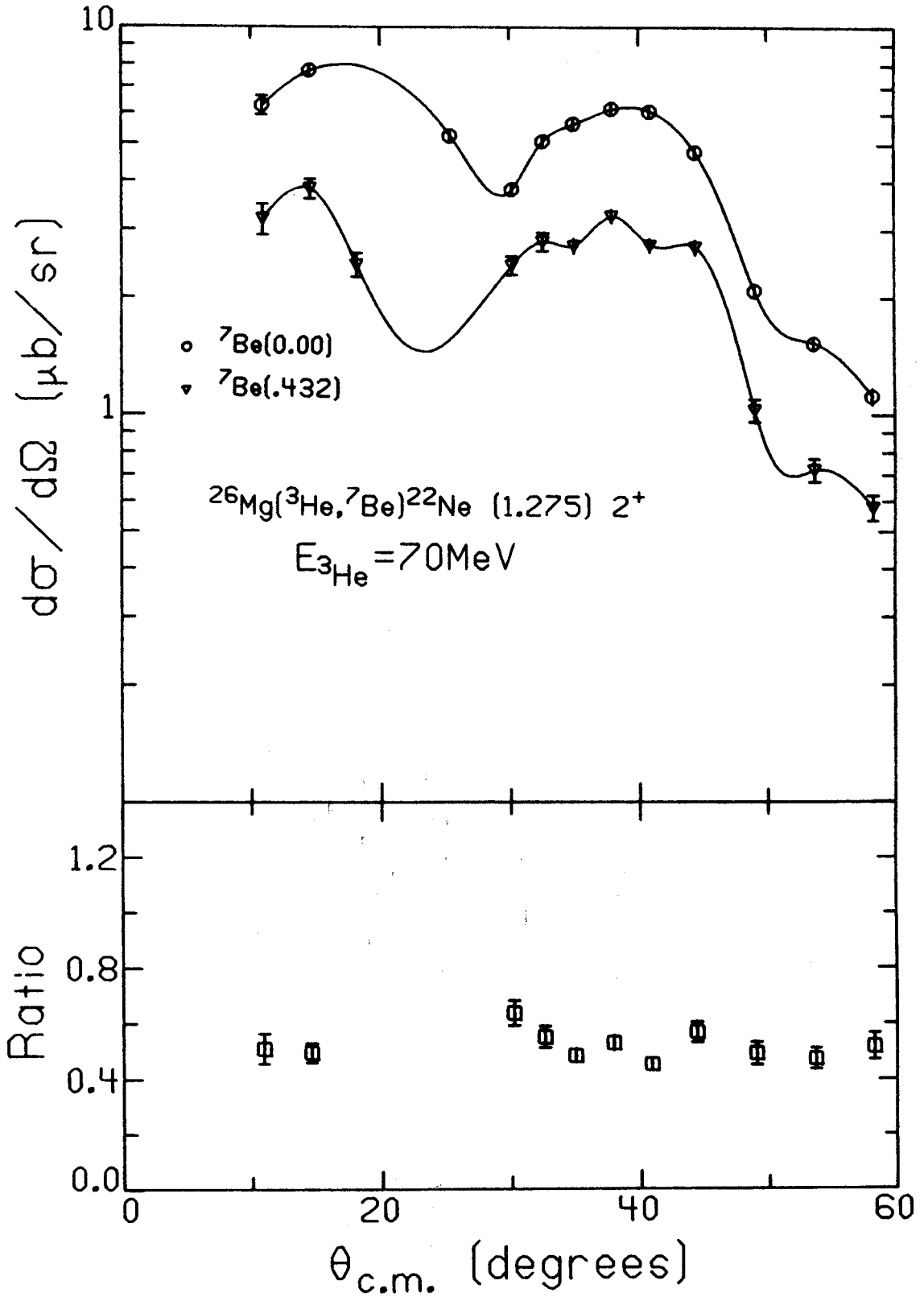

Figure 4.20 As for 4.3.

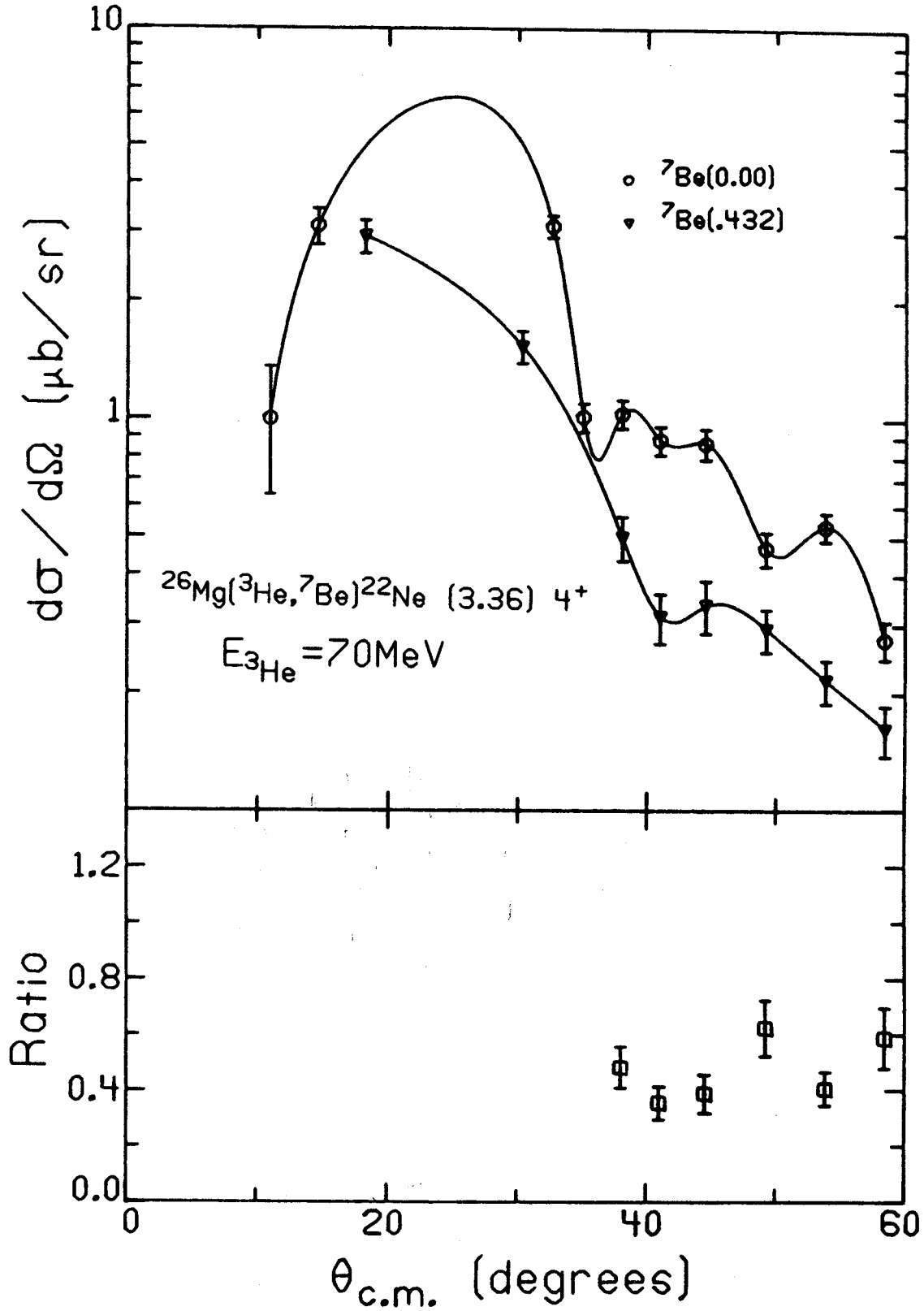

Figure 4.21 As for 4.3.

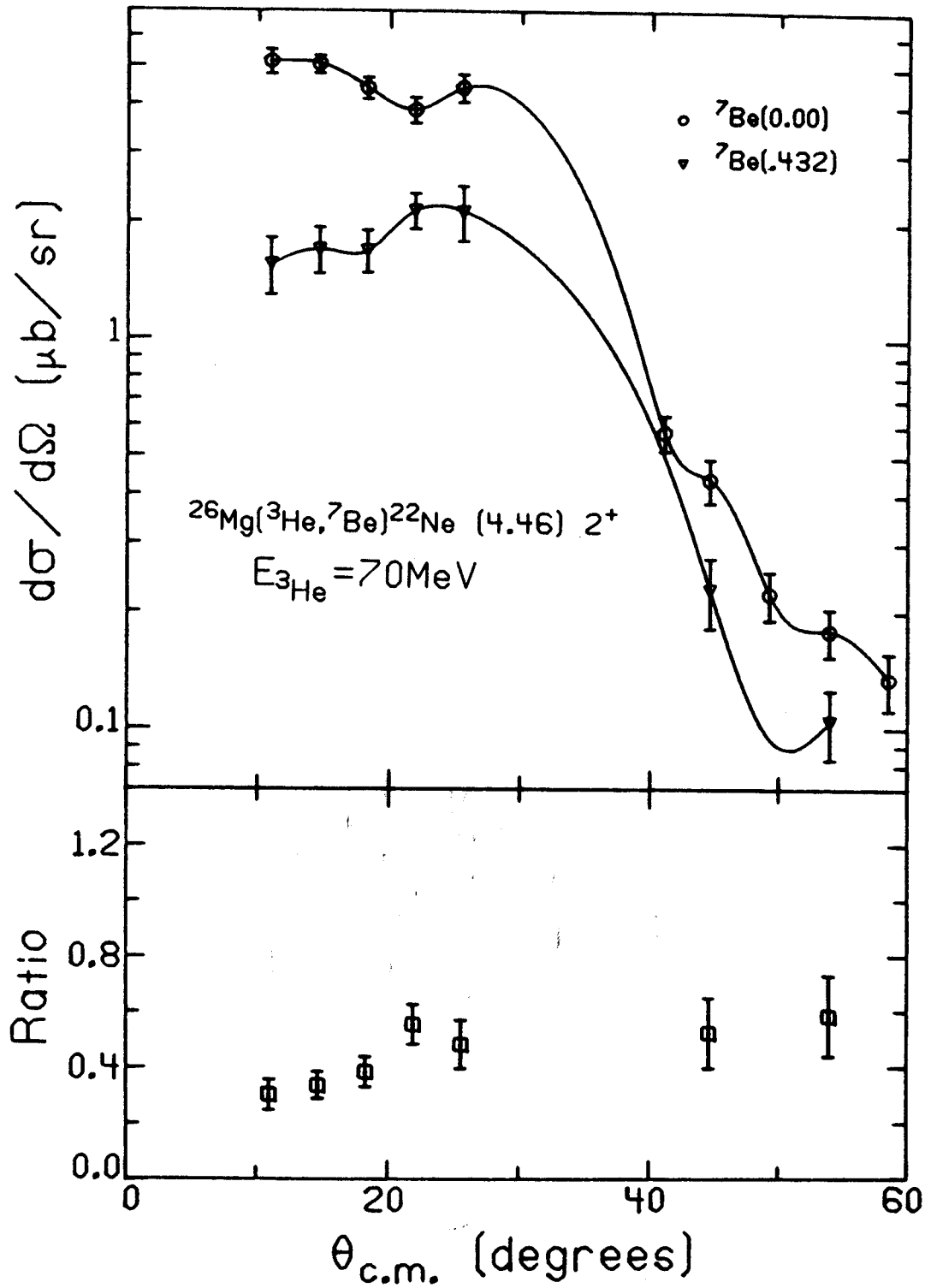

Figure 4.22 As for 4.3.

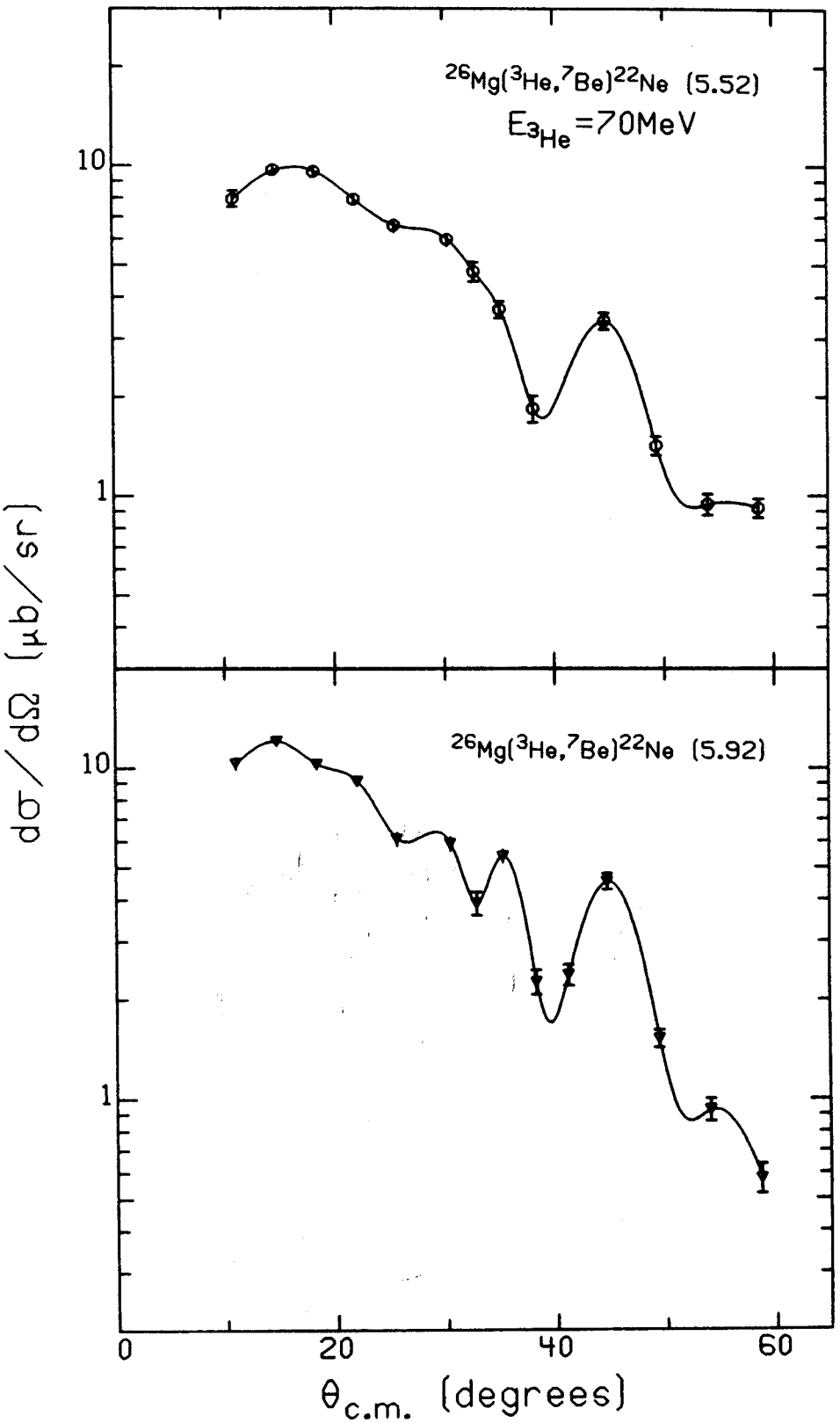

Figure 4.23 As for 4.4.

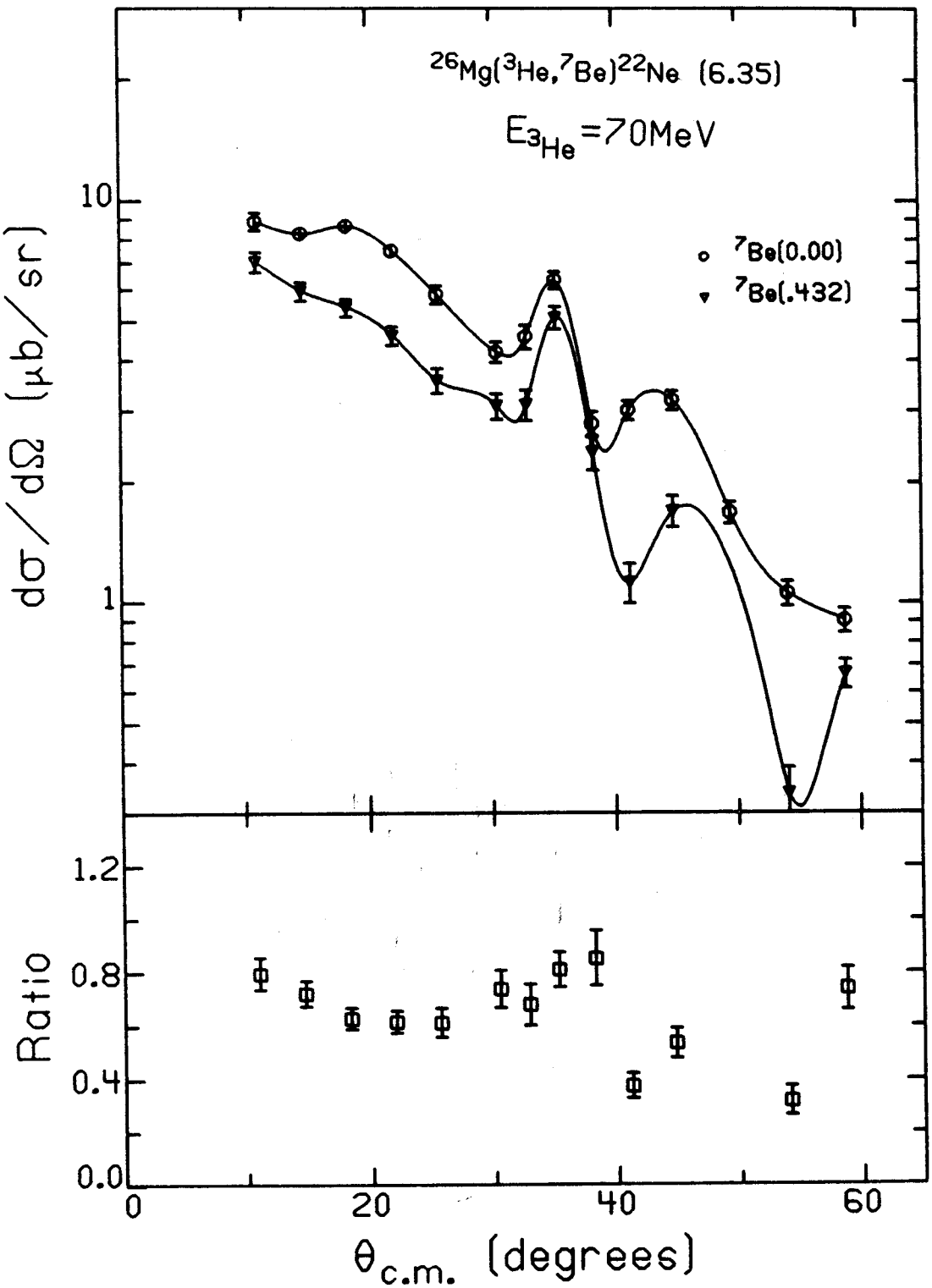

Figure 4.24 As for 4.3.

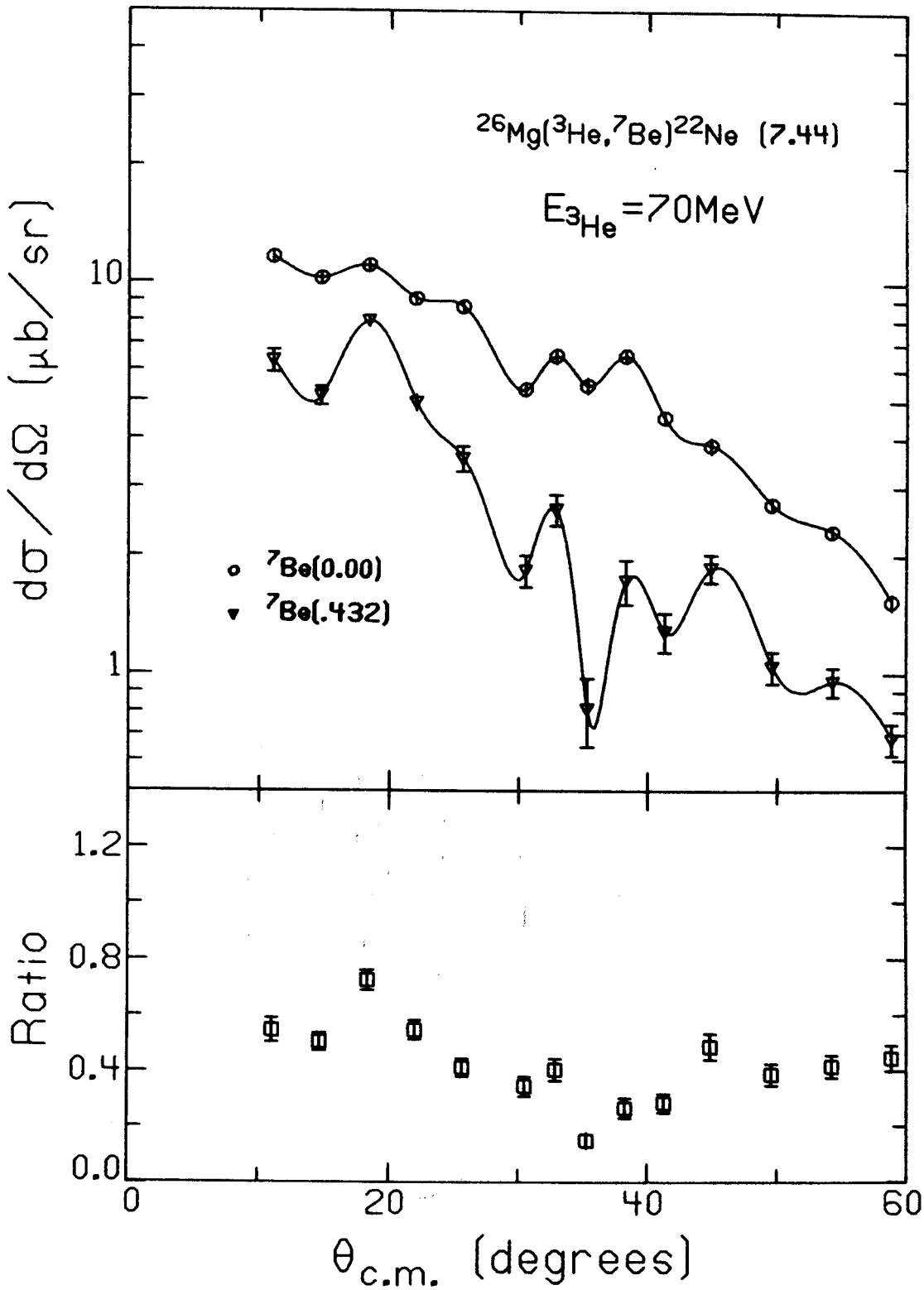

Figure 4.25 As for 4.3.

was prepared by reducing with zirconium powder 97.16% isotopicly enriched $^{48}CaCO_3$, condensing the liberated calcium metal on a 500 $\mu g/cm^2$ gold foil. Preparation, storage, and transfer of the target were carried out in high vacuum apparatus, the pressure never exceeding 10^{-4}torr, except perhaps momentarily during transfer. The thickness of the target was indirectly estimated to be 200 $\mu g/cm^2$ by measuring the yield from the $^{40}Ca(^3He,^7Be)^{36}Ar(1.977)$ reaction using a commercial ^{48}Ca target of known thickness and isotopic composition, and comparing with the yield from the target in question. Eight spectra were measured at angles ranging from 5° to 10°. A 7° spectrum is plotted in Figure 4.26. Small angles were chosen to maximize the separation from contaminant peaks of the peaks corresponding to ^{44}Ar. At angles large enough to shift the contaminants from the critical region of the focal plane, the differential cross section for the reaction becomes so small as to preclude a practical experiment. Even at 5°, the peaks corresponding to the lowest observed level of ^{44}Ar are very close to the peaks representing the 4.44 MeV level in ^{12}C. This pair, together with the background produced by the broad 2.9 MeV level of ^8Be, could obscure peaks from potential lower levels of ^{44}Ar. In order to check this possibility, the reaction was carried out at a lower energy, 37.5 MeV. The experiment becomes more difficult at the lower energy because the ^7Be ions lose a large amount of energy in the target, thus degrading resolution. Furthermore, since the ^7Be ions have insufficient

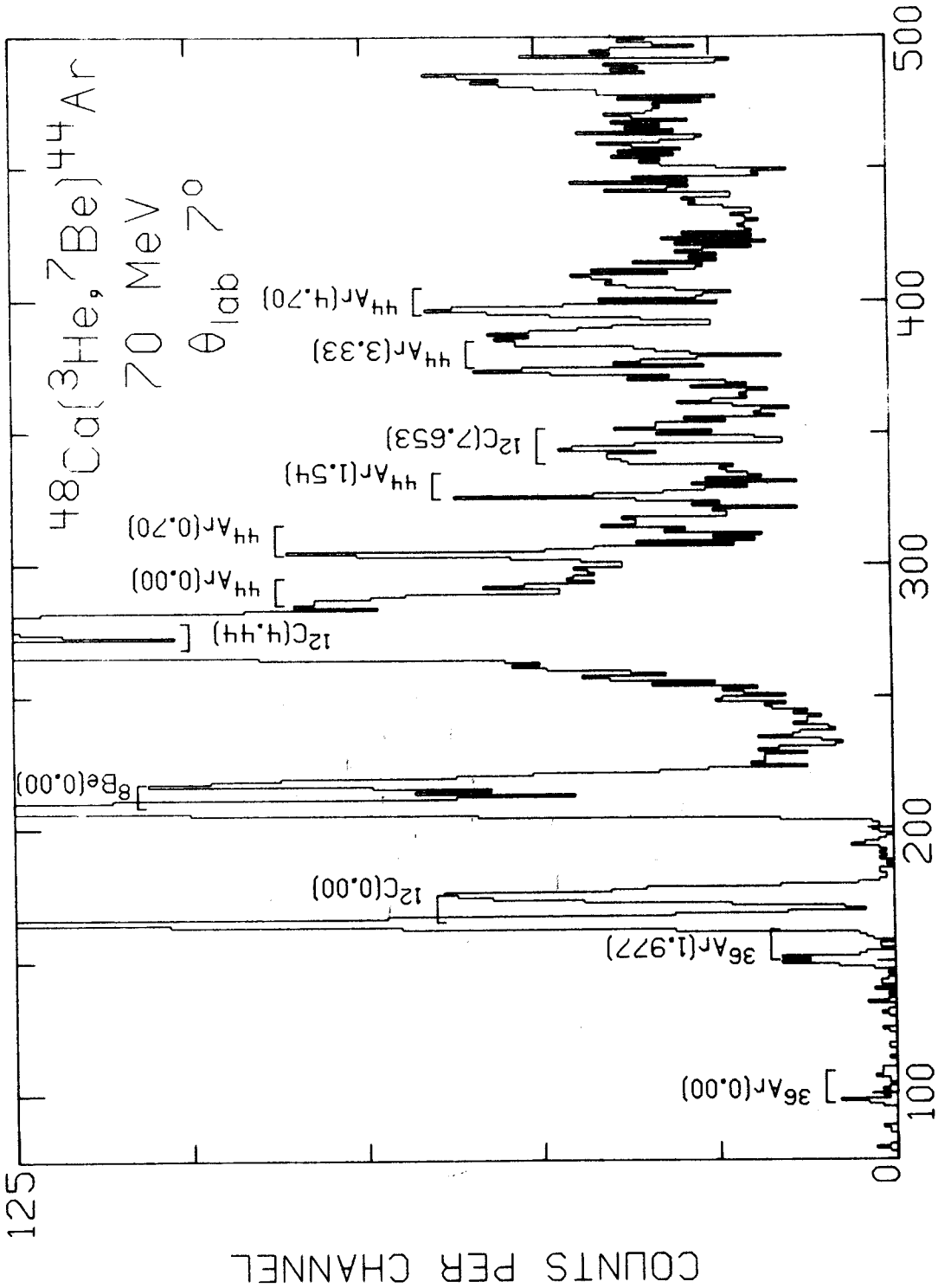

Figure 4.26 As for 4.1.

energy to pass through the proportional counter and produce a significant pulse in the scintillator, time of flight information is lost. As a result, particle identification is incomplete and other ions, particularly $^{7}Li^{3+}$, are introduced into the ^{7}Be spectrum. Nevertheless, a pair of peaks is observed at a position consistent with that expected of the presumed ^{44}Ar ground state deduced from the 70 MeV data. As a result of reducing the incident ^{3}He energy from 70 to 37.5 MeV, the kinematical shift clears of contaminants a 1.5 MeV region of excitation in ^{44}Ar below the alleged ground state peaks. Were the true ground state peaks still lower, the ^{44}Ar mass would disagree with the Garvey-Kelson[17] prediction by more than 1 MeV. Since no peaks appear in this contaminant free area, the lowest observed level of ^{44}Ar must be the ground state.

Table 4.3 summarizes the mass excess and excitation energies of levels identified as belonging to ^{44}Ar. Both the primary and secondary peaks corresponding to a given level have been used in calculation of its entry. The errors are derived from the spread of the values of the eight measurements. While levels above 4 MeV are observed, contaminant peaks make the assignment of excitation energies very difficult. The ground state mass excess differs from the Garvey-Kelson[17] prediction by about 500 keV, which is about 10 times the average deviation found in their table. A new calculation by Borysowicz[18], also listed in Table 4.3, which uses more recent masses and which includes a weighting for the

Table 4.3 Measured energy levels of ^{44}Ar.

Level	Mass Excess (MeV)	E_x (MeV)
1	-32.27 ± .04[†]	0.00
2	-31.55 ± .04	0.70
3	-30.71 ± .09	1.55
4	-28.91 ± .18	3.34
5*	-27.56 ± .16	4.69

[†] Garvey-Kelson prediction for ground state mass excess: -32.76 MeV. Borysowicz prediction for ground state mass excess: -32.60 MeV.

* The fifth level is included only tentatively.

actual errors in the 1972 mass table[19], is closer to the measured value for ^{44}Ar but still differs by about 350 keV.

Because of the ^{40}Ca impurity in the target, a comparison of the ^{40}Ca(^{3}He,^{7}Be)^{36}Ar and ^{48}Ca(^{3}He,^{7}Be)^{44}Ar reactions is possible. Unfortunately the ^{36}Ar ground state transition occurs in only a few spectra so the cross section ratio of ^{36}Ar(0.00)/^{44}Ar(0.00) of approximately 10 is not well determined. The first excited state of ^{44}Ar has an unusually low excitation energy of 700 keV; lower than the first excited state of lighter even even nuclides.

G. ^{58}Ni(^{3}He,^{7}Be)^{54}Fe

A commercial 275 μg/cm^2 99.89% enriched ^{58}Ni target made by rolling thin a pellet of isotopic material, was used. Contamination by carbon and oxygen does not interfere with the low excitation energy levels of the iron isotopes because the Q-values for ^{58,60,62,64}Ni(^{3}He,^{7}Be)^{54,56,58,60}Fe are all somewhat greater than the Q-values for the corresponding reactions on ^{12}C and ^{16}O. Therefore it is ironic that the nickel targets were the cleanest of all targets used in this series of experiments. Table 4.4 is a list of the observed ^{54}Fe levels. Figures 4.27 and 4.28 show spectra from the four nickel isotopes, all taken at 13°. All four reactions are similar; the 0^+ ground state and 2^+ first excited level are excited, as well as a few states in the more densely populated region above 4 MeV. In particular, levels at 4.8 and 5.9 MeV are relatively strongly excited. The 4.8 MeV level could

Table 4.4 Energy levels of ^{54}Fe.

Present Work	$^{54}Fe(p,p'\gamma)^{31}$	
E_x (MeV)	E_x (MeV)	J^π
0.000	0.000	0^+
1.409 ± .006	1.409	2^+
2.530	2.540	4^+
	2.654	0^+
	2.948	6^+
2.956 ± .019	2.959	2^+
	3.164	2^+
	3.296	4^+
	3.345	3^+
	3.838	4^+
	4.029	
	4.048	(4^+)
	4.074	3^+
	4.265	(4^+)
	4.287	(0^+)
	4.579	2^+
	4.656	3,4
	4.700	
4.799 ± .038	4.781	3^-
	4.949	4^+
5.716 ± .249	. . . many higher levels . . .	

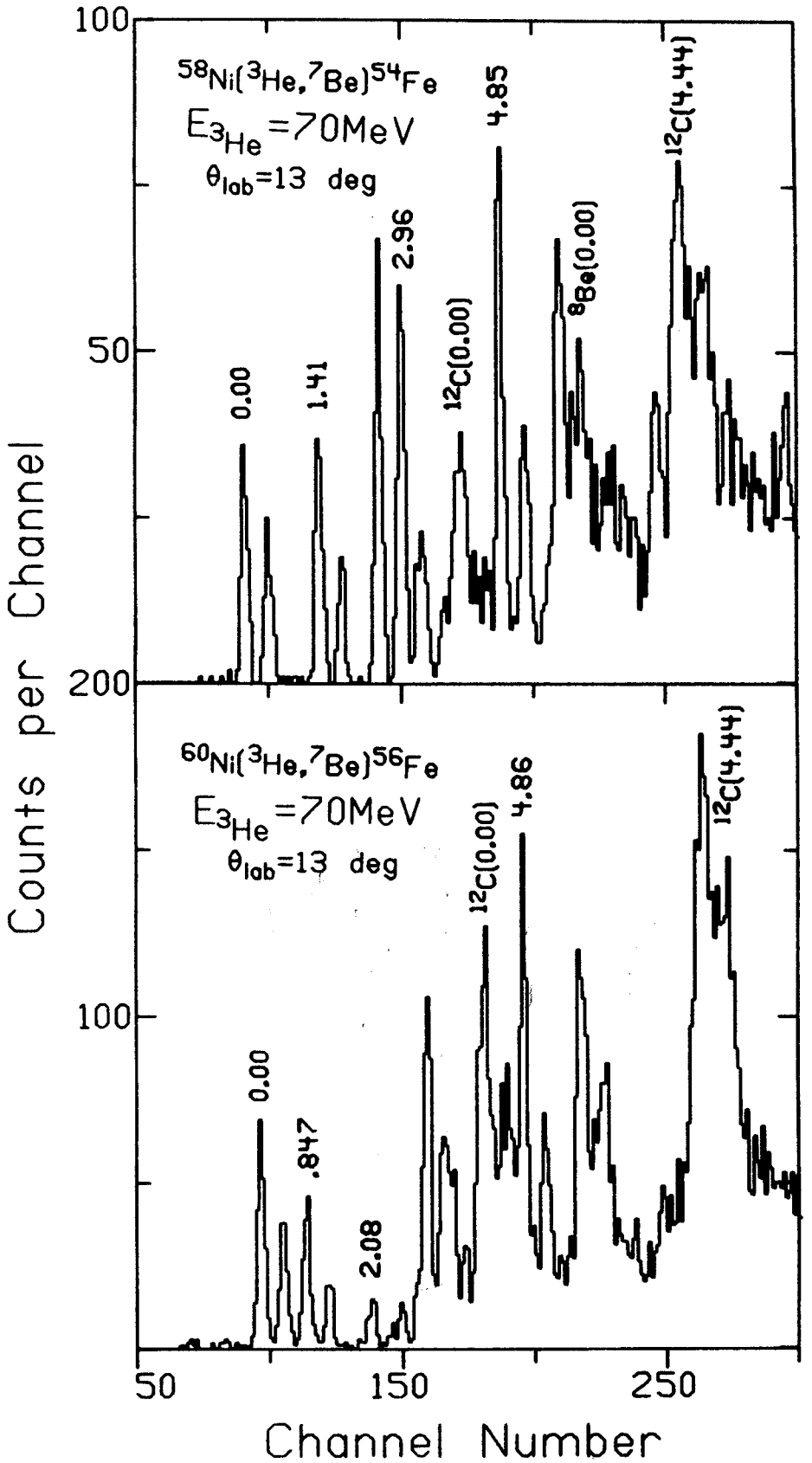

Figure 4.27 As for 4.1.

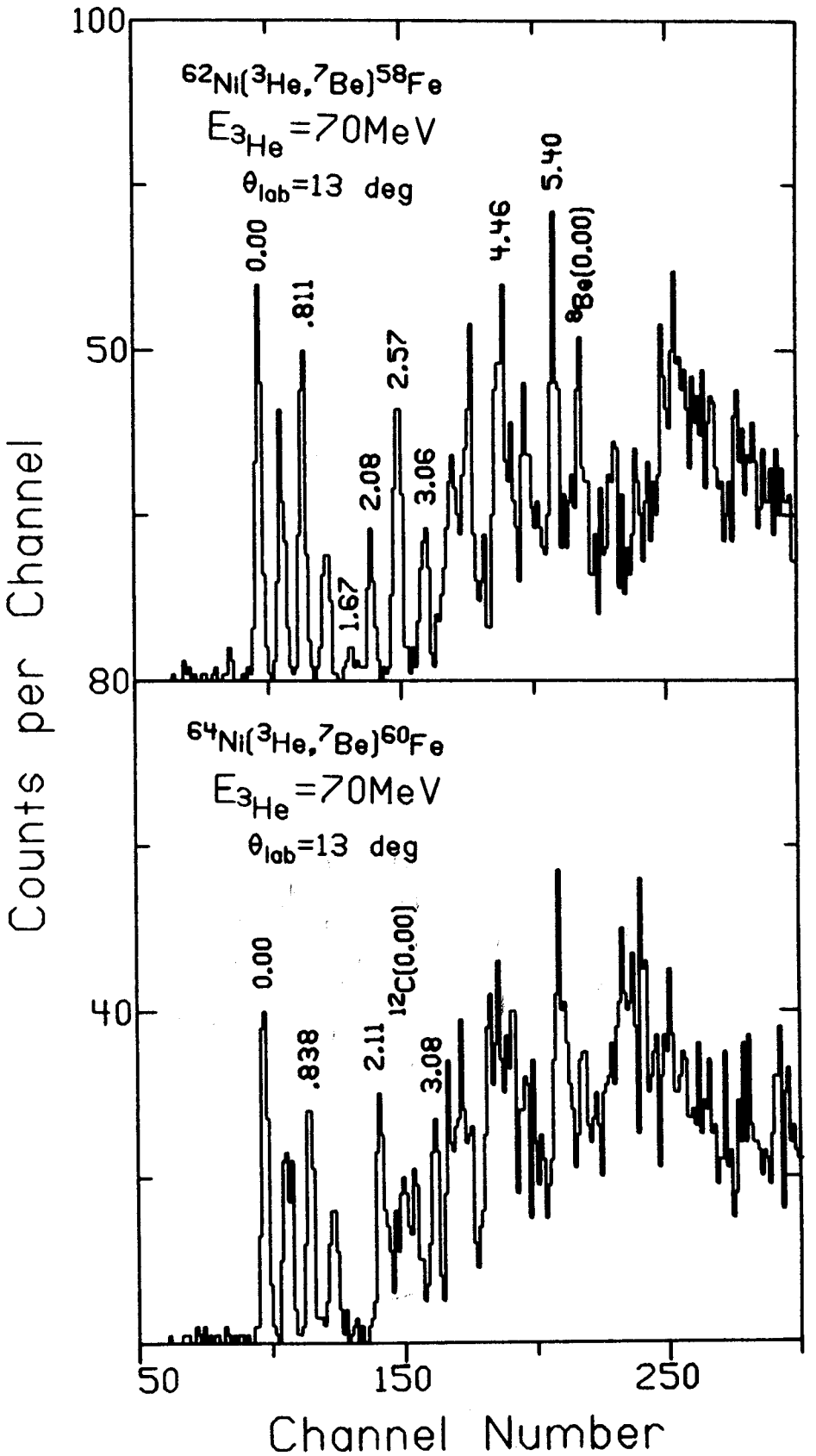

Figure 4.28 As for 4.1.

well be the 3^- established more accurately by other experiments[31] to have an excitation energy of 4.781 MeV. Angular distributions for these and other levels are plotted in Figures 4.29 through 4.33. Secondary to primary ratios for the iron isotopes seem to have more nearly constant values with angle than the ratios for reactions on lighter nuclei. The differential cross sections for reactions to the various levels of ^{54}Fe are small; 2 to 4 μb/str at forward angles, falling rapidly with angle to less than 0.2 μb/str at 30° center of mass angle. Most distributions show a forward peak at 8° to 10°; the cross section declining at smaller angles and sharply decreasing with increasing angle. Moderate diffraction structure is evident.

H. ^{60}Ni(^{3}He,^{7}Be)^{56}Fe

The 218 μg/cm^2 commercially obtained ^{60}Ni target was rolled from 99.79% enriched ^{60}Ni. The 13° ^{56}Fe spectrum in Figure 4.27 shows the 847 keV 2^+, 2.085 4^+, and 2.685 2^+ levels to be excited as well as the 0^+ ground state. Additionally, two higher lying states at 4.86 and 5.90 MeV are relatively strongly excited. They are possibly 4^+ states observed by Mani[32] with inelastic proton scattering. Table 4.5 lists the measured levels. Like those of ^{58}Ni, the angular distributions for the ^{60}Ni reaction, shown in Figures 4.34 to 4.38, indicate small differential cross sections, however the magnitude does not decrease as rapidly with increasing angle.

Table 4.5 Energy levels of ^{56}Fe.

Present Work	Previous Work		
E_x (MeV)	E_x (MeV)	J^π	ref.
0.000	0.000	0^+	32,37
0.848 ± .012	0.847	2^+	32,37
2.057 ± .019	2.085	4^+	32,37
2.628 ± .049	2.658	2^+	32,37
	2.940	0^+	37
	2.960	2^+	37
3.074 ± .032	3.120		37
	3.123		37
	3.159	4^+	32
	3.370	2^+	37
	3.383		37
	3.411	$(6^+),2^+$	32
	3.445	(3,4)	37
	3.450		37
3.592 ± .061	3.598	0^+	37
	3.604	2^+	37
	3.635	2^+	32
	3.748		37
	3.826		37
	3.850	2^+	32
	3.857	$(3,4)^+$	37
	4.049	$(3,4)^+$	37
	4.100	$(3,4)^+$	37
	4.120	4^+	32,37
	4.298	$(3,4)^+$	37
	4.30	0^+	37
	4.389		37
	4.395	(4^+)	32,37
	4.453	4^-	32,37
	4.505	3^+	32,37
	4.660*	4^+	32
4.846 ± .047	4.860	4^+	32
	5.106	5^-	32
	5.195	(4^+)	32
	5.266	4^+	32
	5.535	2^+	32
	5.763	(5^+)	32
5.873 ± .064	5.880	4^+	32
	6.067	4^+	32
	6.273	4^+	32

* Many levels above 4.66 MeV are refered to in ref. 37. Only those in ref. 32 are listed.

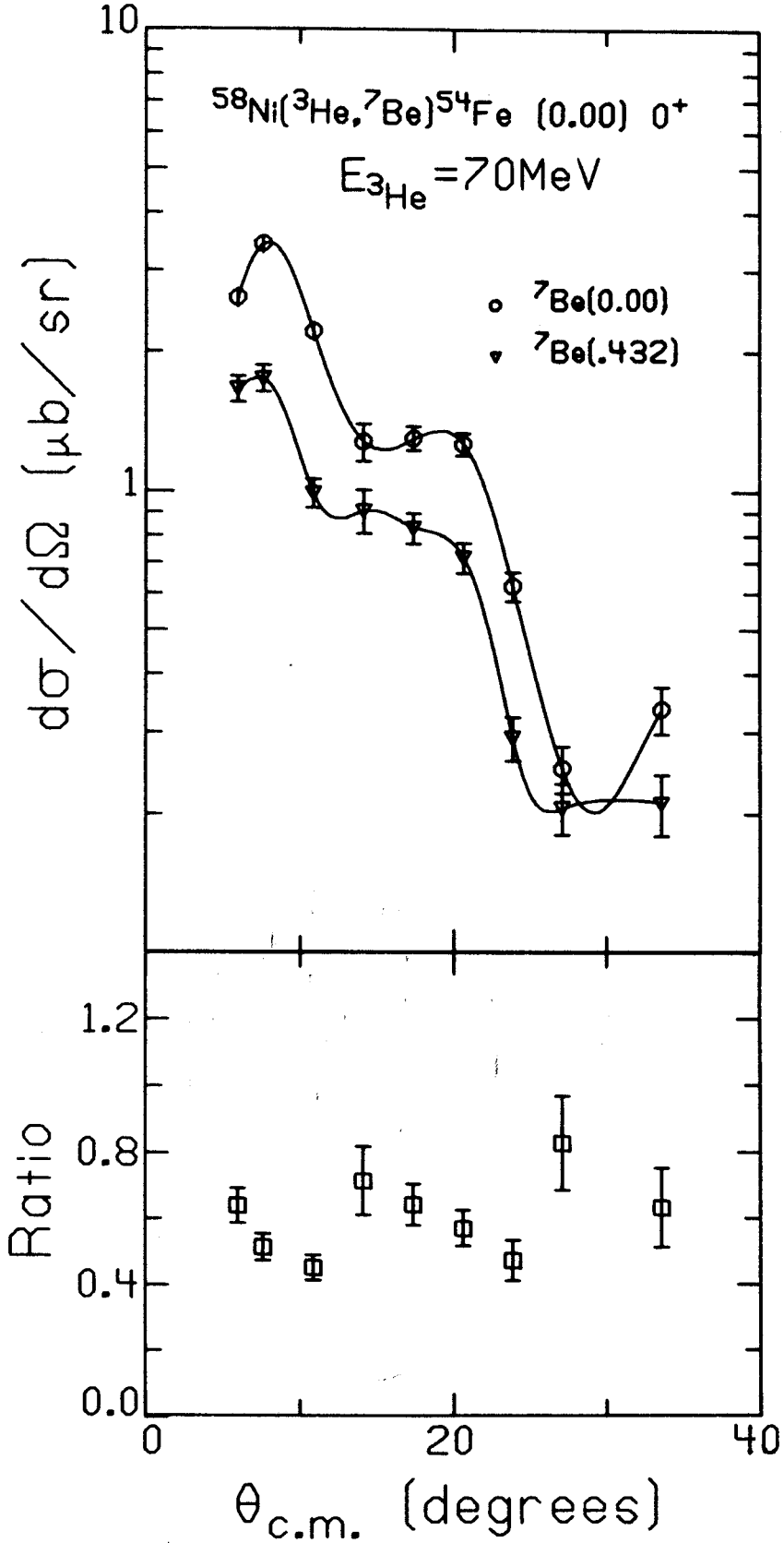

Figure 4.29 As for 4.3.

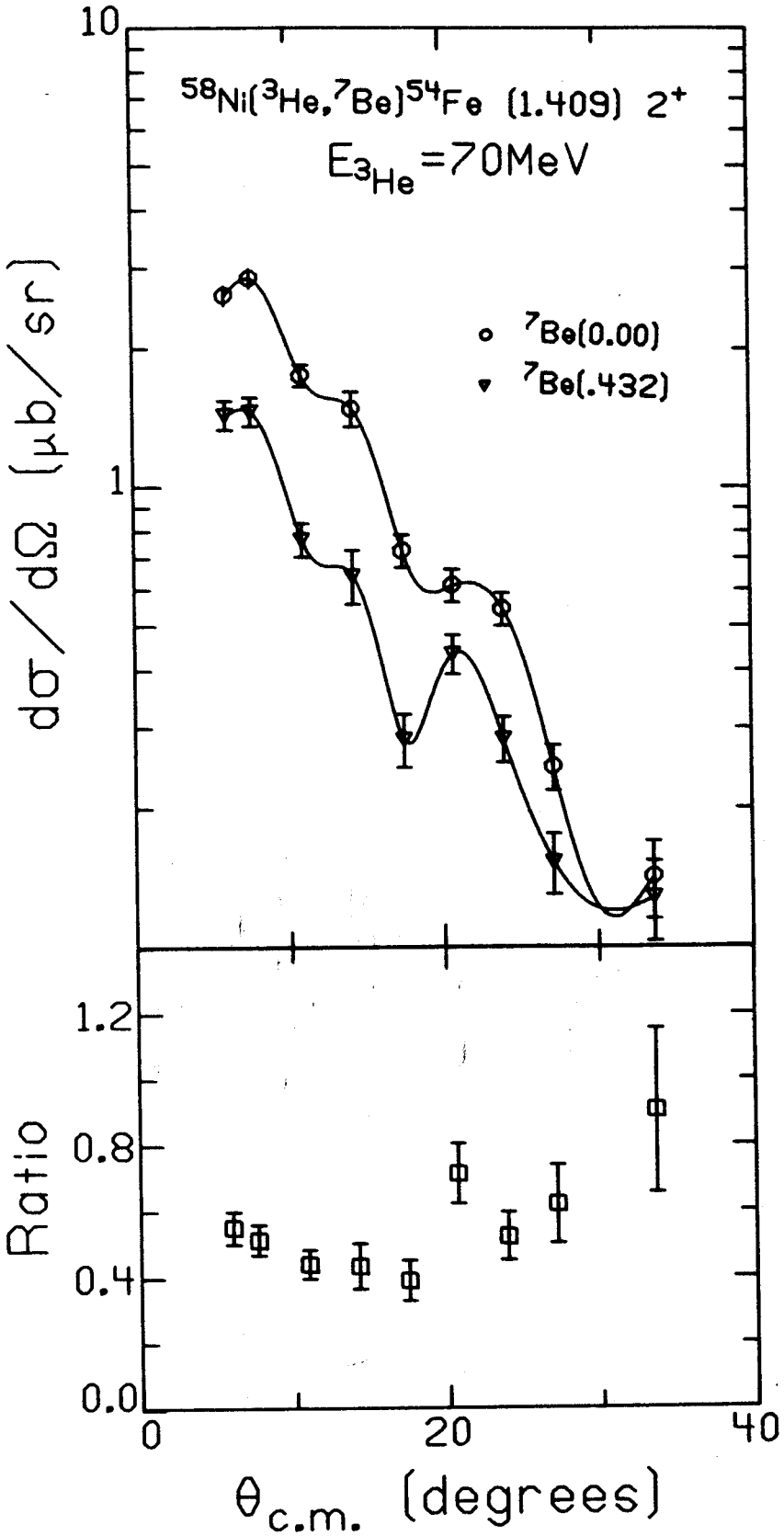

Figure 4.30 As for 4.3.

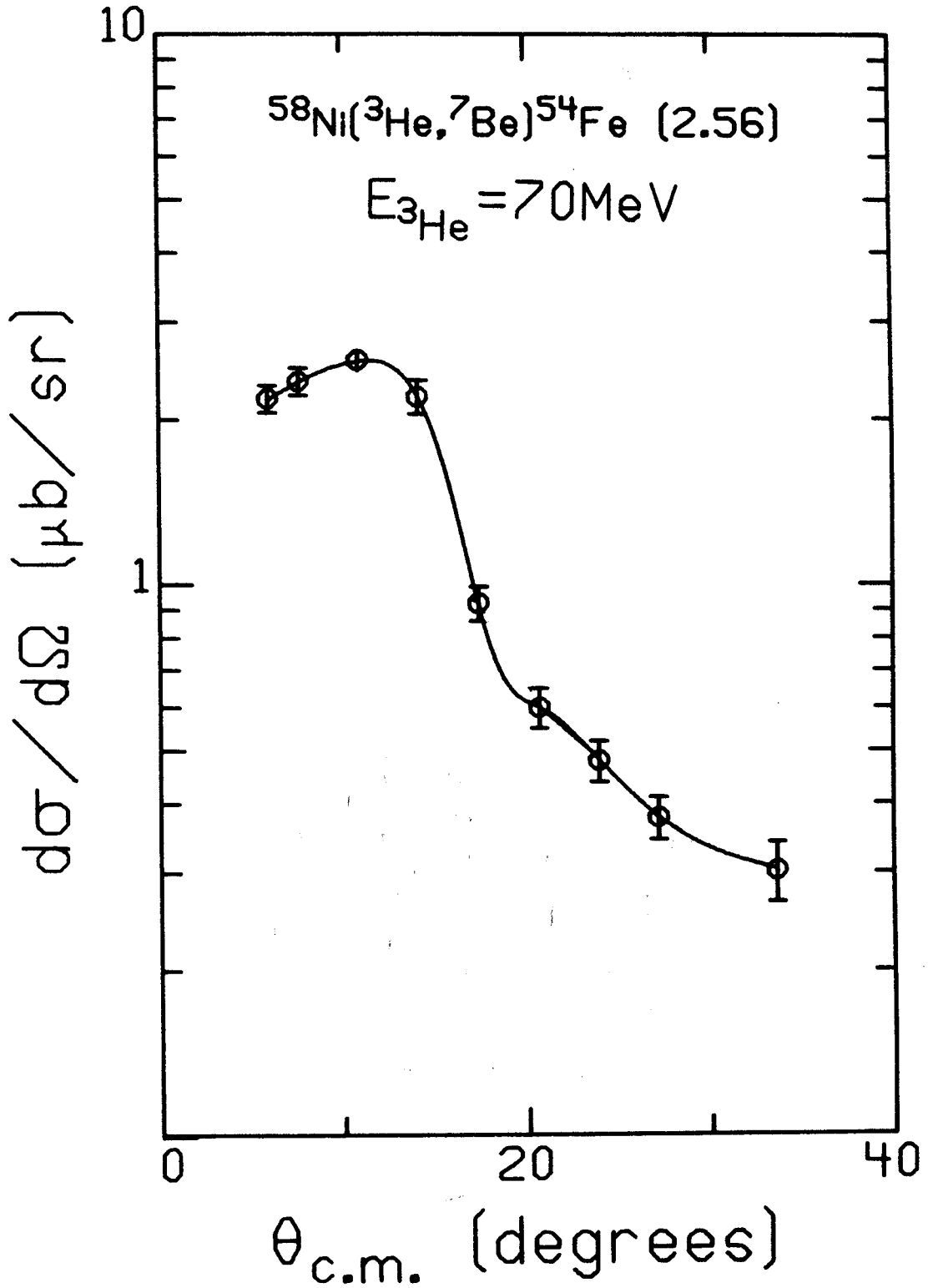

Figure 4.31 As for 4.17.

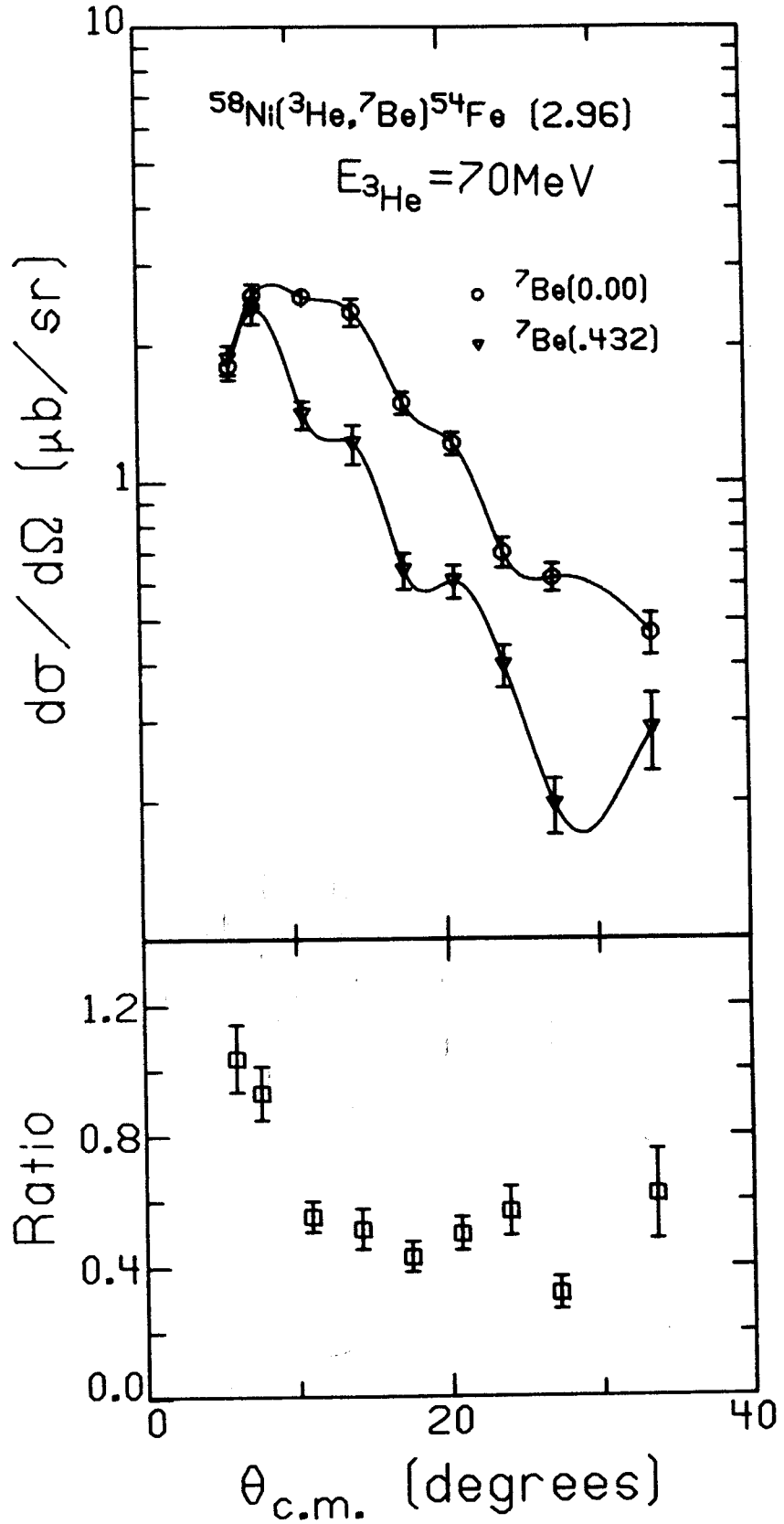

Figure 4.32 As for 4.3.

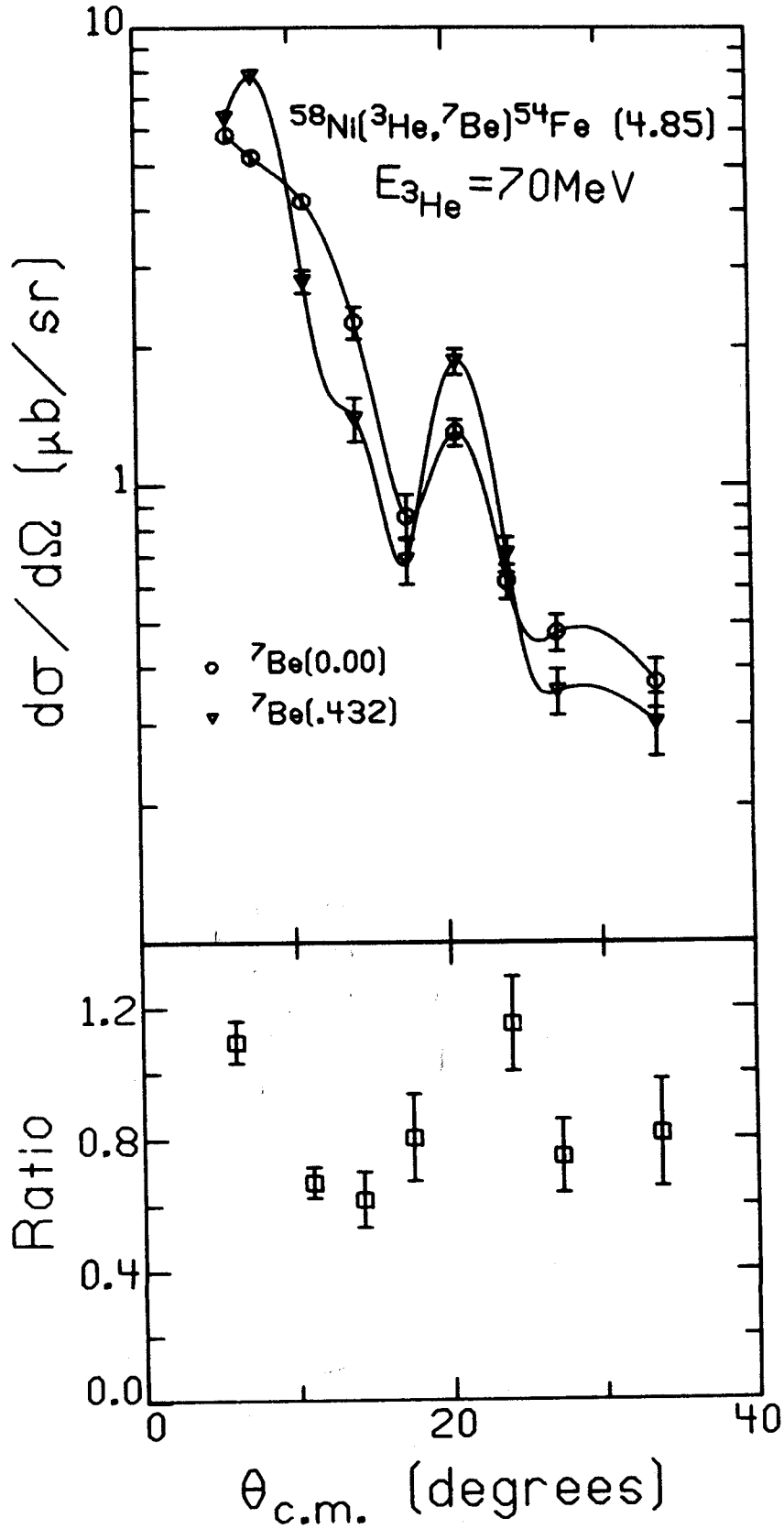

Figure 4.33 As for 4.3.

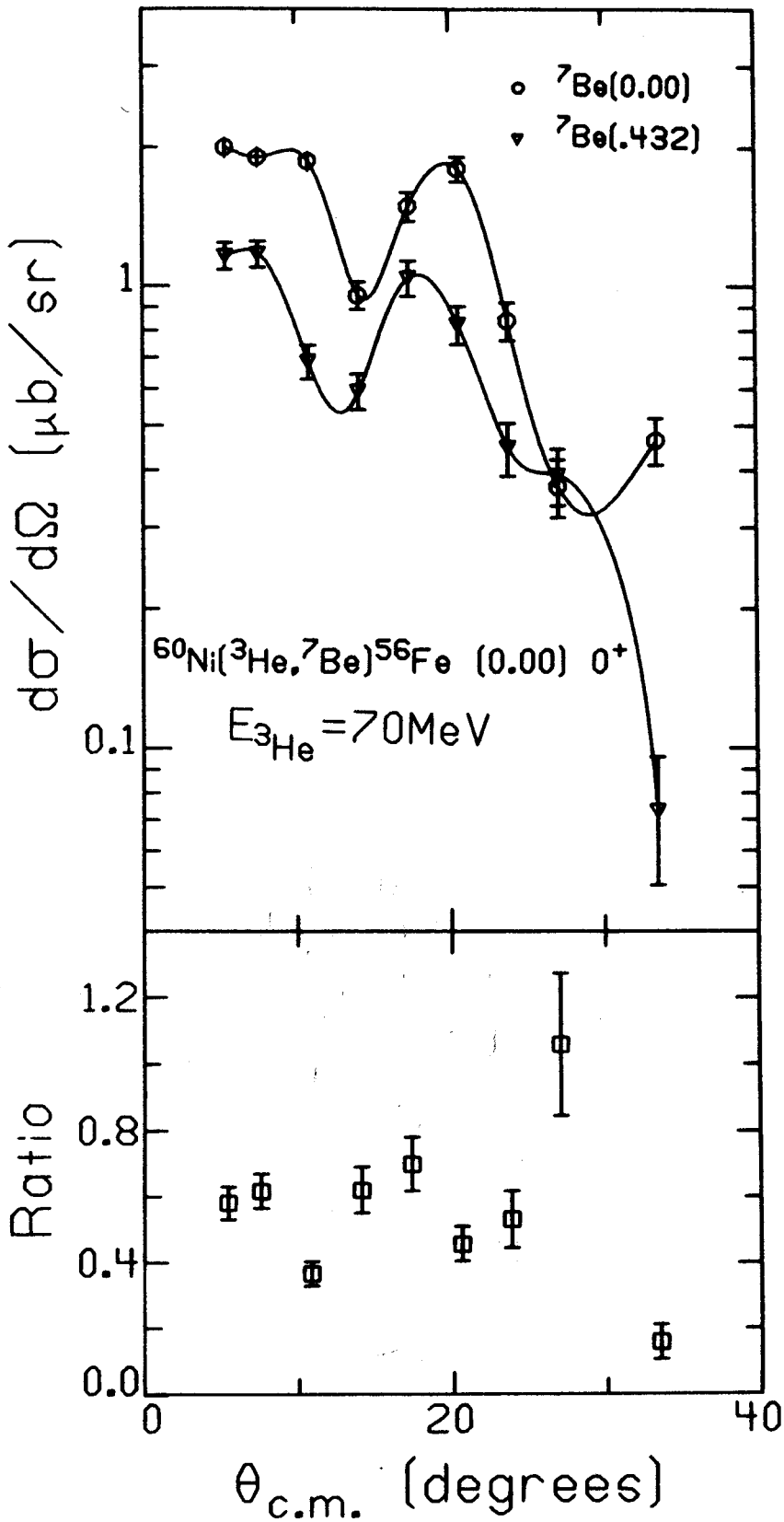

Figure 4.34 As for 4.3.

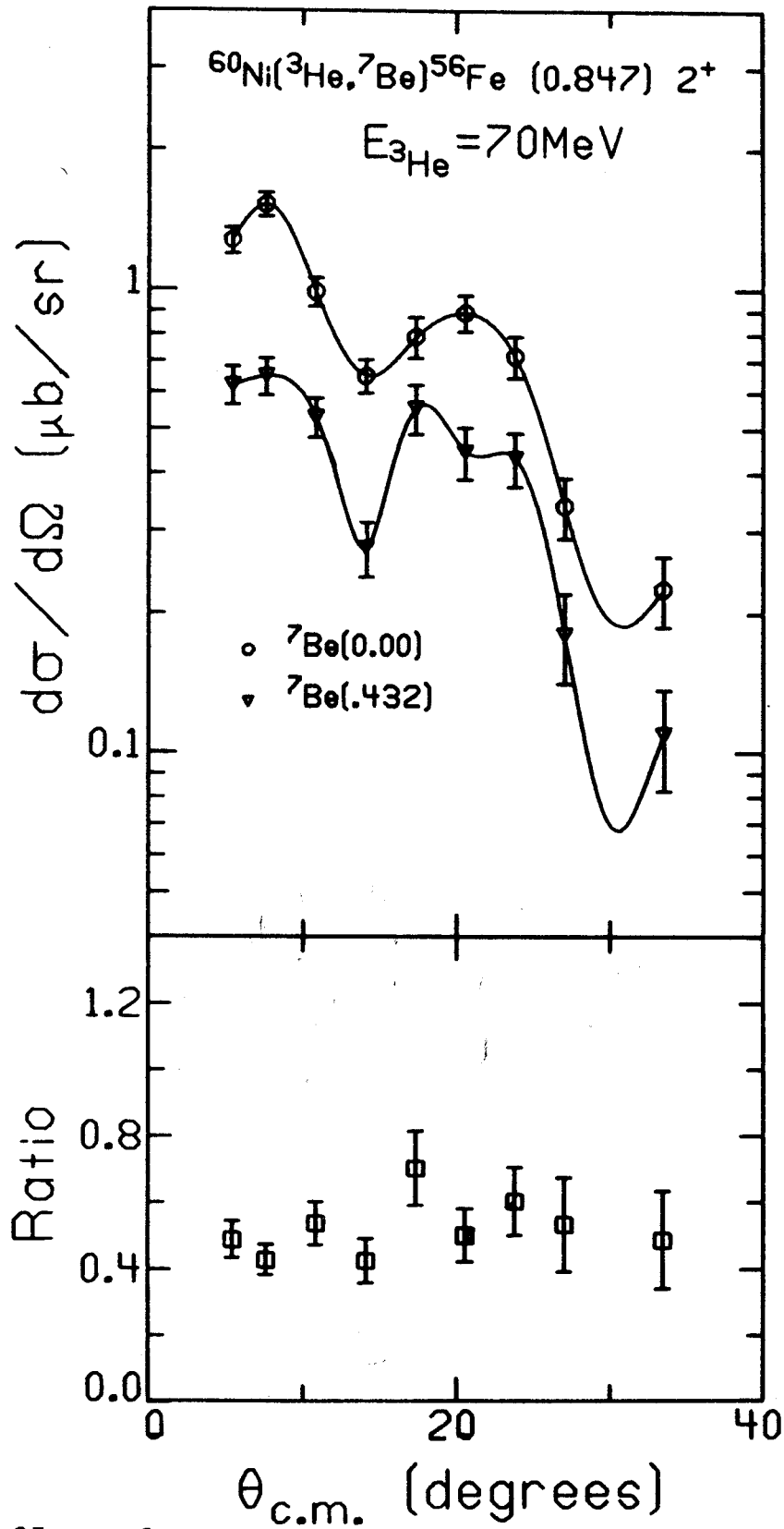

Figure 4.35 As for 4.3.

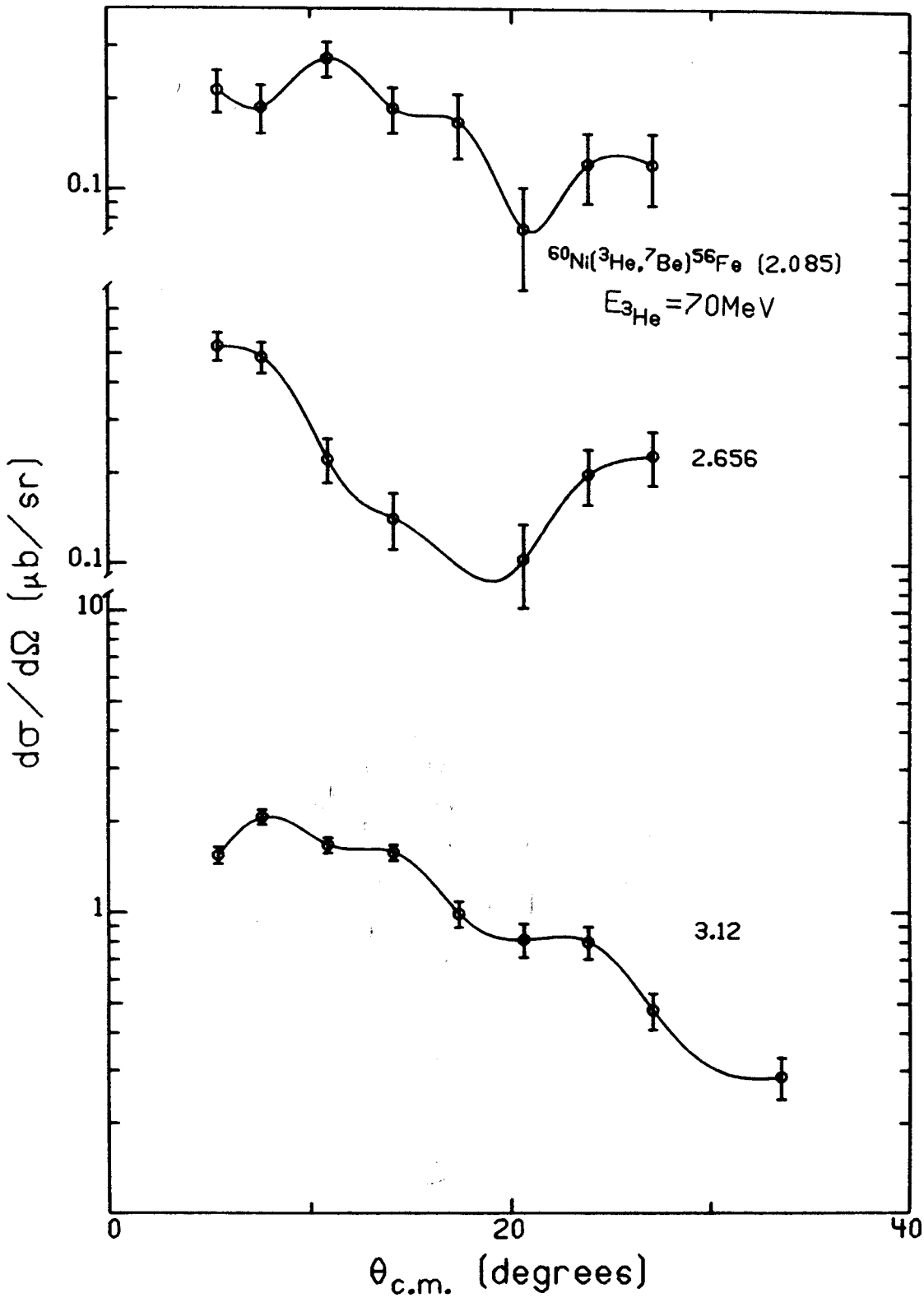

Figure 4.36 As for 4.4.

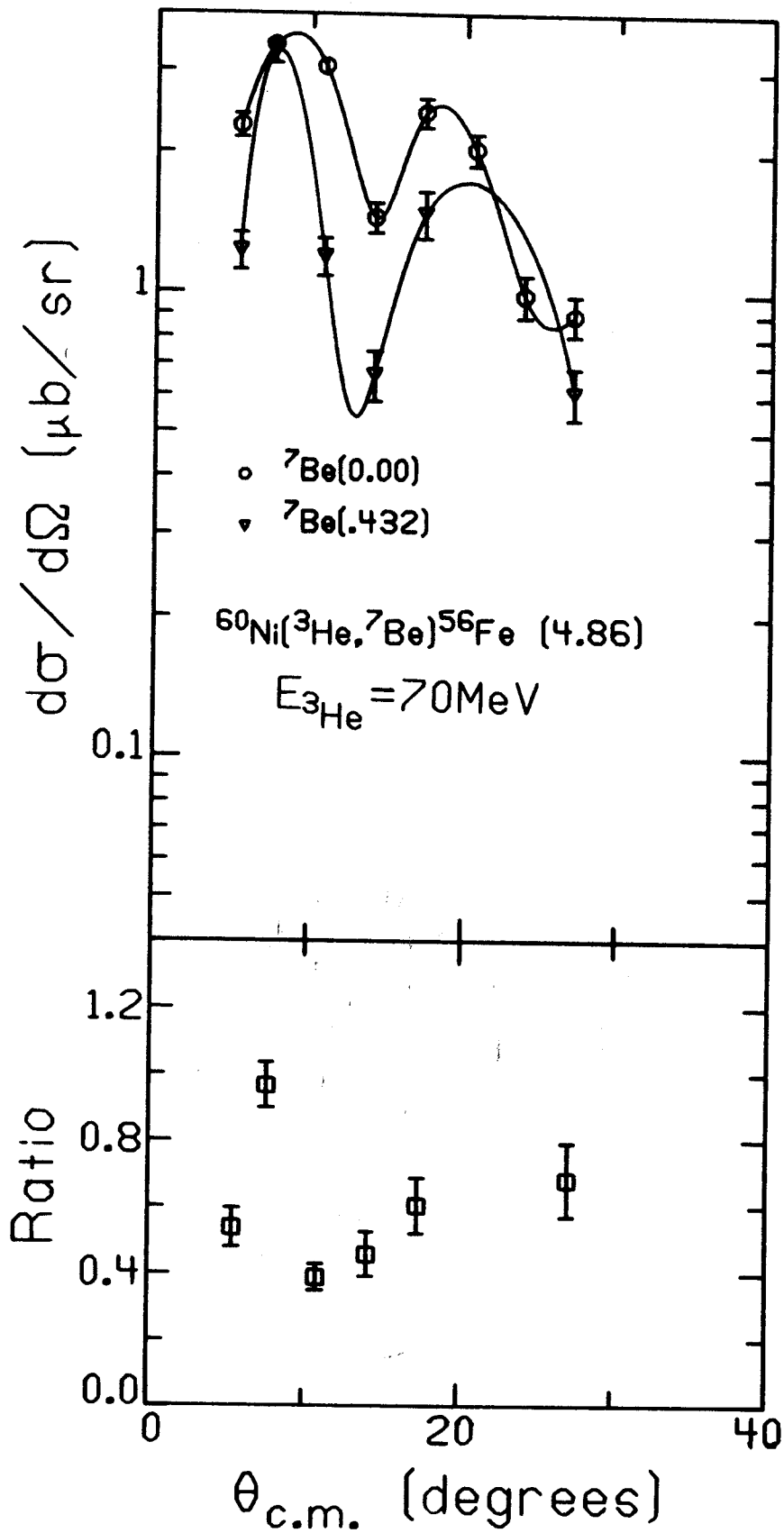

Figure 4.37 As for 4.3.

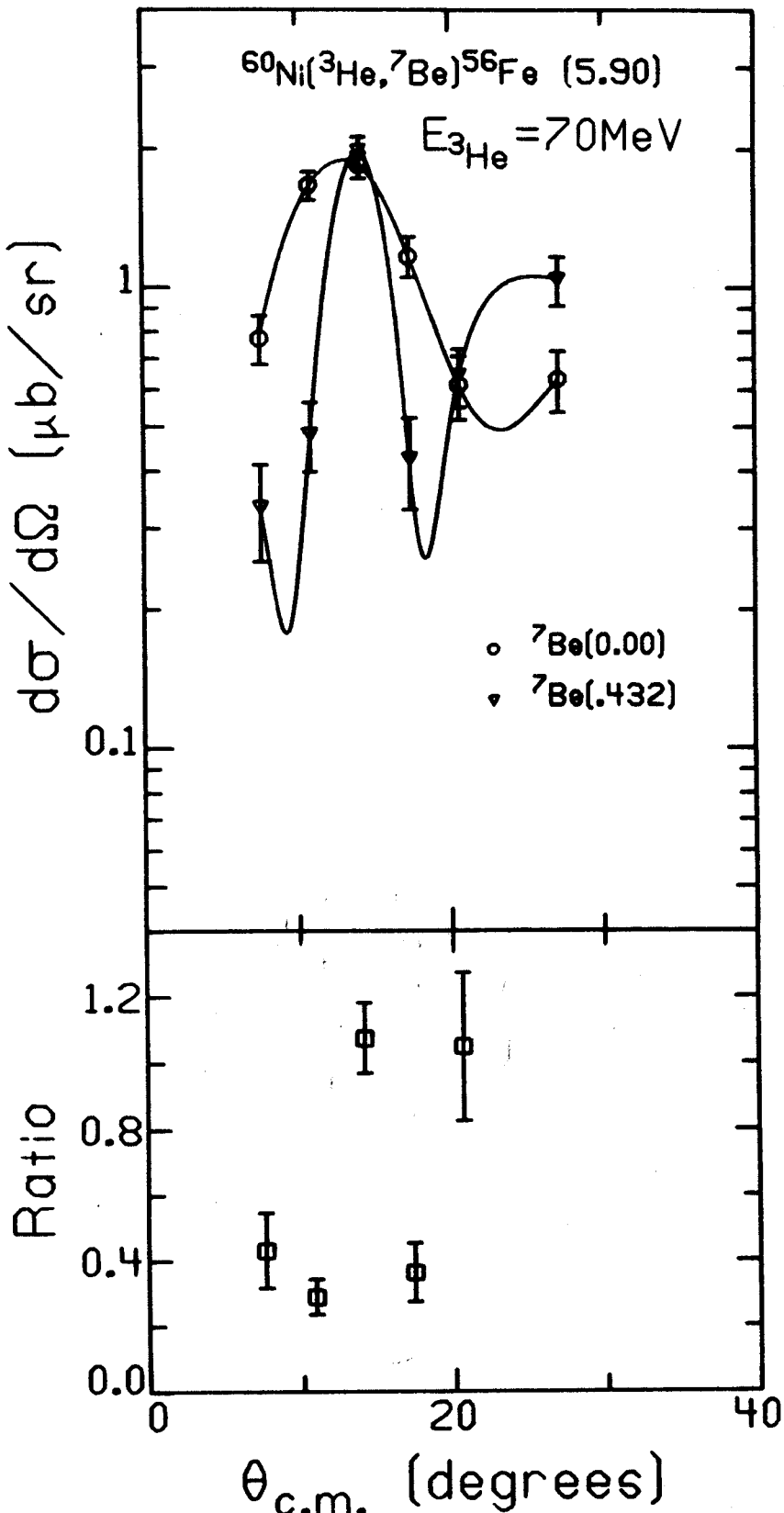

Figure 4.38 As for 4.3.

I. $^{62,64}Ni(^{3}He,^{7}Be)^{58,60}Fe$

The self supporting 260 μg/cm 98.83% enriched ^{62}Ni target, as with the other nickel targets, was prepared commercially by a rolling procedure. This reaction, as well as the ^{64}Ni reaction, was executed primarily to obtain a qualitative comparison of the differential cross section with that of ^{58}Ni and ^{60}Ni. Therefore spectra for only three angles for each were measured. Tables 4.6 and 4.7 list the excitation energies of the levels observed in ^{58}Fe and ^{60}Fe respectively. Little information on the levels of ^{60}Fe is available since the nucleus cannot be produced from a stable target with most standard particle transfer reactions. The differential cross sections for the observed levels are compiled in Tables 4.8 and 4.9.

J. $^{90}Zr(^{3}He,^{7}Be)^{86}Sr$

A self supporting 500 μg/cm^2 enriched ^{90}Zr target was used for this reaction. Even though the target is somewhat thicker than the targets used for the lighter nuclei, resolution does not suffer appreciably because ^{7}Be energy loss is sufficiently less for the larger atomic mass. Figure 4.39 is a spectrum of ^{86}Sr at 21°. The contaminant peaks dominate simply because the differential cross section for the ^{90}Zr reaction is so small, for most levels and angles less than 700 nb/str. Fortunately the Q-value for the ^{90}Zr reaction is sufficiently great so that the contaminants do not interfere with the low lying levels of ^{86}Sr. Table 4.10 lists the ^{86}Sr

Table 4.6 Energy levels of ^{58}Fe.

Present Work	Previous Work		
E_x (MeV)	E_x (MeV)	J^π	ref.
0.000	0.000	0^+	33,38,39
0.812 ± .003	0.811	2^+	33,38,39
1.659 ± .011	1.676	2^+	33,38,39
2.081 ± .012	2.085	4^+	33
	2.132	$(3)^+$	38,39
	2.254	0^+	38,39
2.573 ± .012	2.597	4^+	33,38,39
	2.776	1^+	38,39
	2.874	2^+	38,39
	2.970	5^-	33
3.030 ± .038	3.080	2^+	38,39
	3.133		38
	3.151	4^+	33
	3.230		38,39
	3.244		38
	3.389	2^+	33
	3.451		38,39
	3.522	2^+	33
3.566 ± .022	3.533	1^+	38,39
	3.629	2^+	33,38,39
	3.749		38,39
	3.785		38,39
	3.854	3^-	33,38,39
	3.875	1	38,39
3.883 ± .020	3.894	$(2,3)^+$	38,39
	4.013	2^+	38,39
	4.079	4^+	33
	4.131	$(0,1,2)^+$	38,39
	4.158	0^+	38,39
	4.212	$(2^+,3^+,4^+)$	38,39
	4.230	4^+	33
	4.237	(2^+)	38,39
	4.288	2^+	33,38,39
	4.314	2^+	38,39
	4.348	2^+	38,39
	4.398		38,39
	4.438	2^+	39
	4.441	3^-	33
	4.468	3^-	38,39
	5.315*		39
	5.370		38,39
5.393 ± .025	5.370		38,39
	5.406		38,39
	5.462		38,39
	5.506		38,39

* Some levels not near those excited by (^{3}He,^{7}Be) are excluded.

Table 4.7 Measured energy levels of ^{60}Fe.

Excitation energy (MeV)
0.000
0.835 ± .010
2.109 ± .020
3.077 ± .014

Table 4.8 ^{62}Ni(^{3}He,^{7}Be)^{58}Fe dσ/dΩ(μb/str).

	center of mass scattering angle		
E_x (MeV)	5.4°	9.2°	14.0°
0.000	2.24	2.59	0.86
0.000†	1.21	1.04	0.59
0.812	1.59	1.69	0.74
0.812†	0.90	0.94	0.38
1.659	0.41	0.34	--
2.081	0.43	0.69	0.32
2.573	0.69	1.07	0.79
3.03	0.56	1.03	0.45
3.56	--	1.32	1.04
3.88	--	1.25	0.70
5.39	--	0.58	0.89

† ^{7}Be first excited state peak.

Table 4.9 ^{64}Ni(^{3}He,^{7}Be)^{60}Fe dσ/dΩ(μb/str).

	center of mass scattering angle		
E_x (MeV)	10.8°	14.0°	17.3°
0.00	1.06	0.74	1.21
0.00†	0.37	0.56	0.66
0.84	0.97	0.55	0.62
0.84†	0.58	0.41	0.38
2.11	0.64	0.63	0.34
3.08	0.56	0.44	0.44

† ^{7}Be first excited state peak.

Table 4.10 Energy levels of ^{86}Sr.

Present Work	$^{86}Y(\beta^+)^{34}$*	
E_x (MeV)	E_x (MeV)	J^π
0.000	0.000	0^+
1.085 ± .018	1.077	2^+
1.841 ± .020	1.854	2^+
2.227 ± .052	2.230	4^+
	2.482	3^-
	2.642	(2^+)
2.705 ± .069	2.673	5^-
	2.788	-
	2.878	$3^+,4^+$
	2.997	3^-
3.031 ± .072	3.056	$(4,5)^-$
	3.185	$(3)^-$
3.440 ± .082	3.362	$(3^+,4^+)$
	3.500	$3^-,4^-,5^-$
	3.926	$3^+,4^+,5^+$
	3.942	$3^\pm,4^+$
3.958 ± .068	3.968	$3^\pm,4^\pm,5^\pm$
	4.146	$3^\pm,4^+$

* Some levels not near those excited by (^3He,^7Be) have been excluded. Information similar to that in the quoted reference is contained in the Nuclear Data Sheets[40].

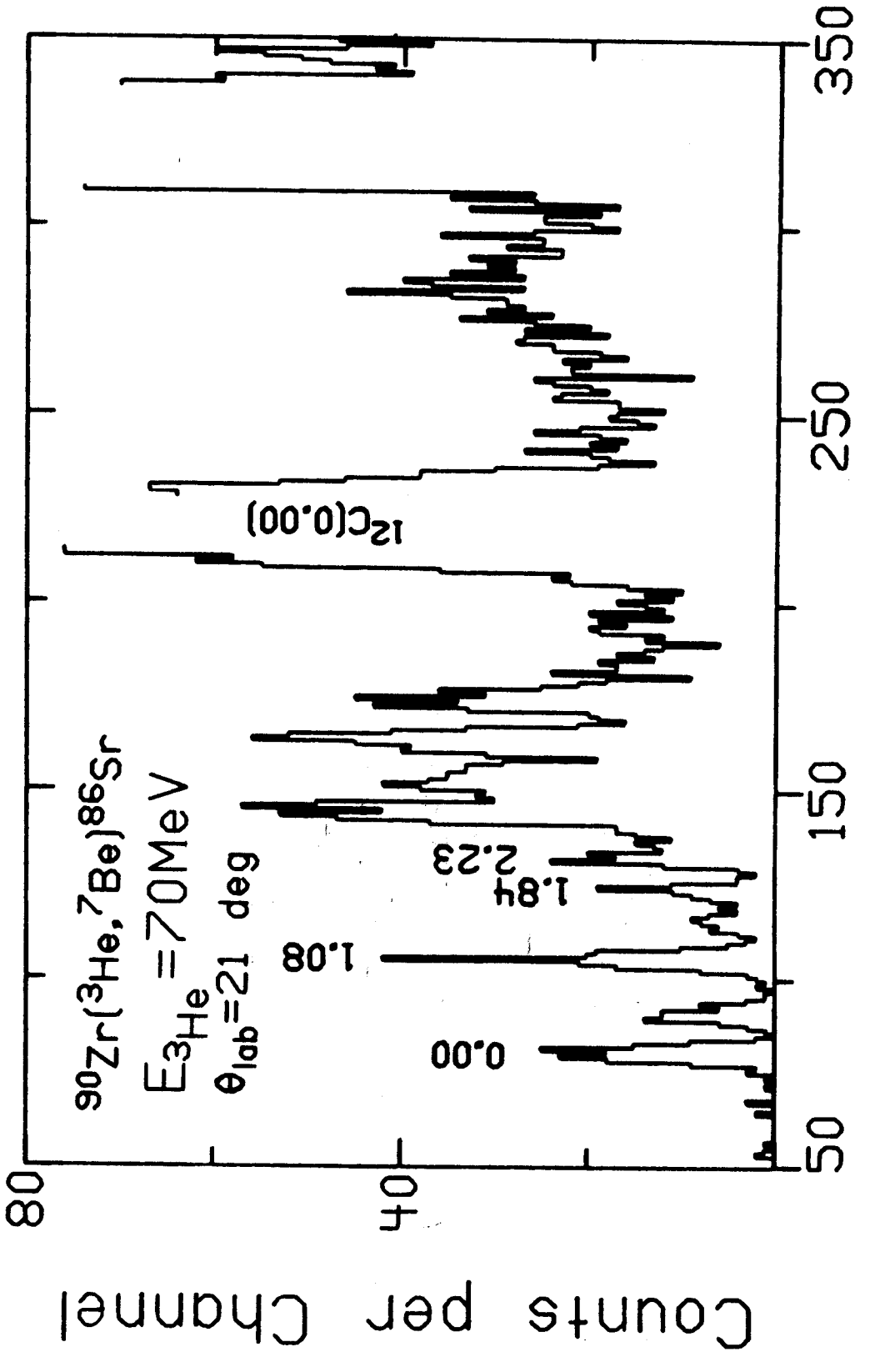

Figure 4.39 As for 4.1.

levels observed, and the angular distributions for these levels are plotted in Figures 4.40 to 4.42.

K. $^{120,124}Sn(^{3}He,^{7}Be)^{116,120}Cd$

$^{120,124}SnO_2$ were reduced in vacuum by passing an electric current through a tantalum tube containing the oxide. The metallic tin evaporated onto a glass substrate coated with a thin film of CsI. The resulting layers of tin were floated off the substrate onto a water surface and picked up onto an aluminum target frame. The results were respectively a 525 $\mu g/cm^2$ and a 290 $\mu g/cm^2$ self supporting tin target. The tin oxide from which the targets were made was isotopicly enriched as follows: 98.39% ^{120}Sn and 96.0% ^{124}Sn respectively for the two oxide samples. The thicknesses were deduced by comparing ^{3}He elastic scattering data at forward angles with the corresponding calculations performed by the optical model program GIBELUMP[16]. The $^{124}Sn(^{3}He,^{7}Be)^{120}Cd$ reaction was done to determine the mass of the heretofore unknown nuclide ^{120}Cd. The ^{120}Sn reaction served to check the accuracy of the energy calibration. Measurements were made at three angles. Although the differential cross sections for both reactions are less than 900 nb/str, distinct ground state peaks are observed for both ^{116}Cd and ^{120}Cd (Figure 4.43). The mass values presented in Table 4.11 are averages of the results for the three measurements, the spread of which determines the listed uncertainties. In addition to new mass information, the reactions provide information useful for

determining the qualitative variation of peak differential cross section with atomic mass. The differential cross sections measured for the ^{116}Cd and ^{120}Cd ground state transitions are compiled in Table 4.12.

Table 4.11 Mass and energy levels of ^{120}Cd.

Level	Mass Excess (MeV)	E_x (MeV)
1	-83.98 ± .03	0.00
2	-83.48 ± .05	0.50
3	-82.68 ± .04	1.30

Garvey-Kelson ground state mass excess: -83.92 MeV.

Table 4.12 ^{120,124}Sn(^{3}He,^{7}Be)^{116,120}Cd $d\sigma/d\Omega$(nb/str).

	center of mass scattering angle			
	7.3°	10.4°	13.5°	16.6°
^{116}Cd (g.s.)	530	850	420	64
^{116}Cd (g.s.)†	560	530	570	64
^{120}Cd (g.s.)	510	630	365	145
^{120}Cd (g.s.)†	425	550	410	85

† ^{7}Be 432 keV first excited state peak.

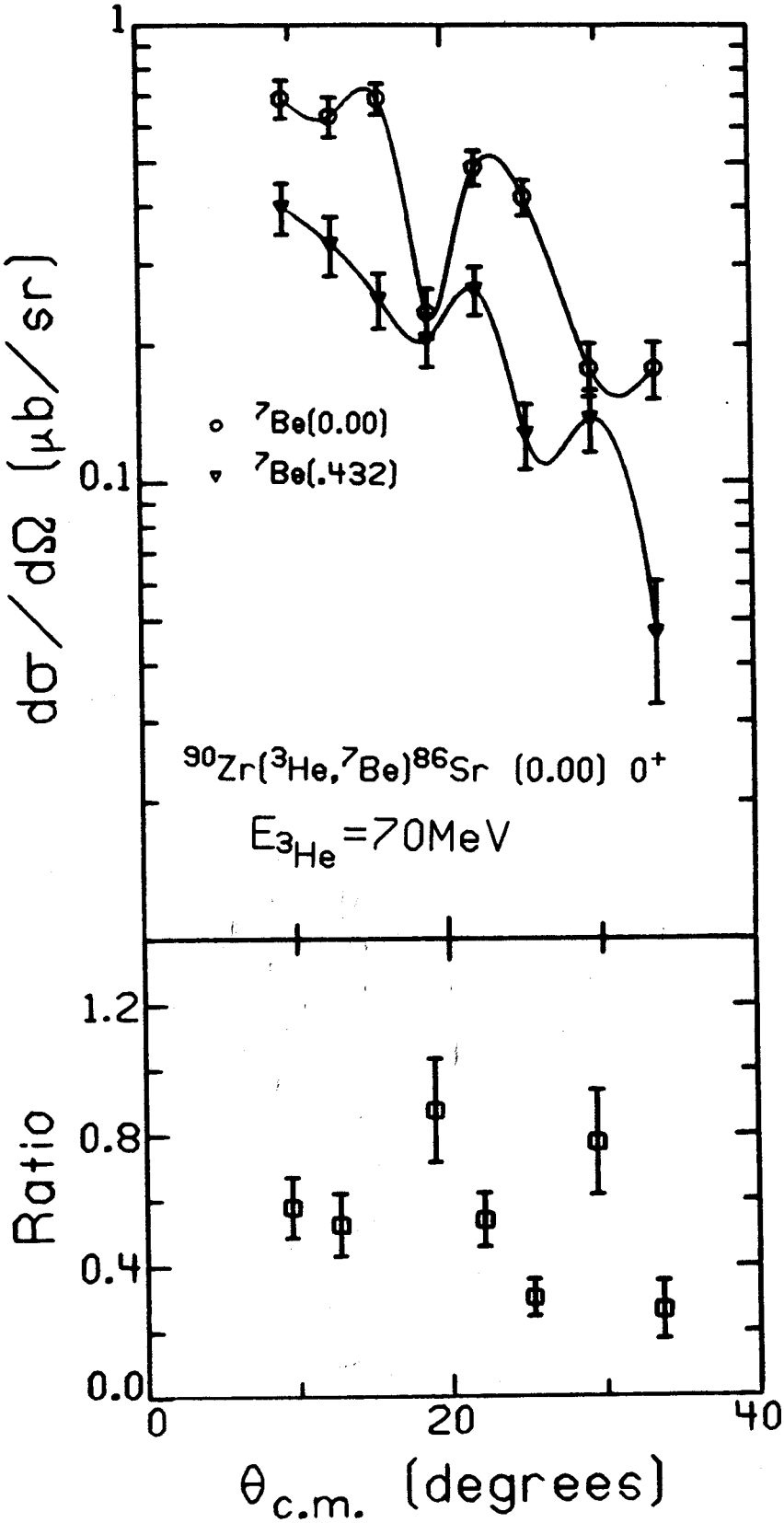

Figure 4.40 As for 4.3.

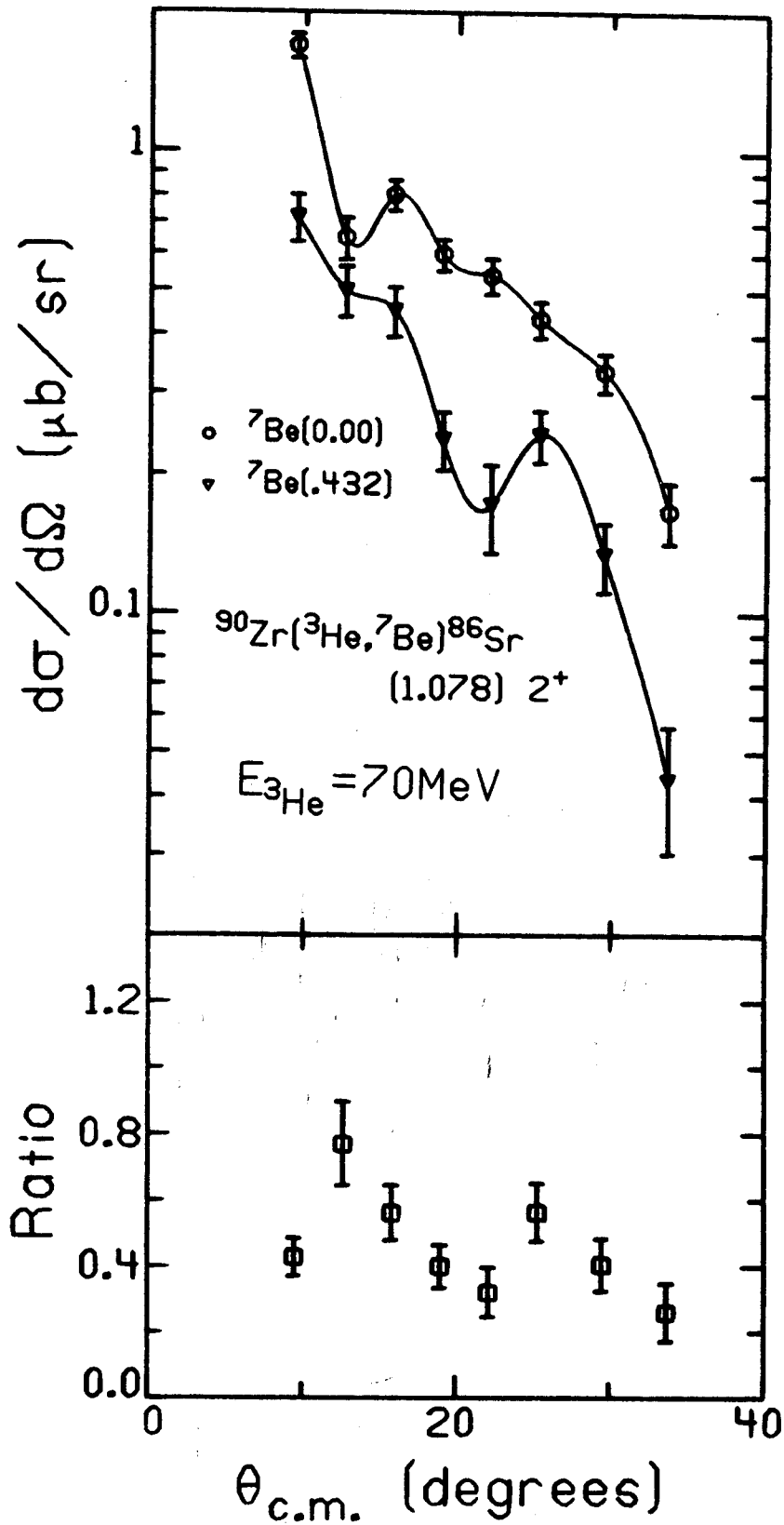

Figure 4.41 As for 4.3.

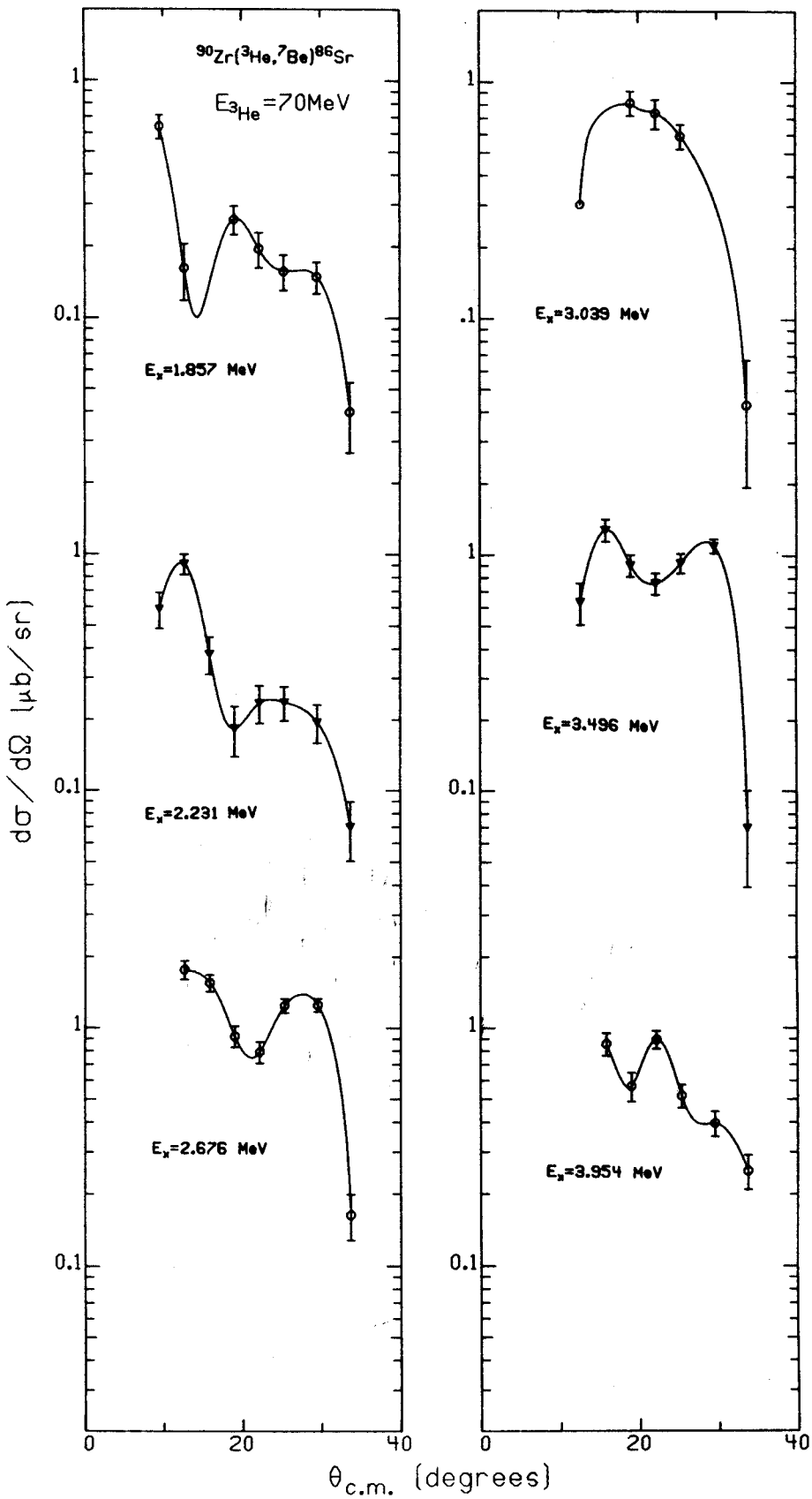

Figure 4.42 As for 4.4.

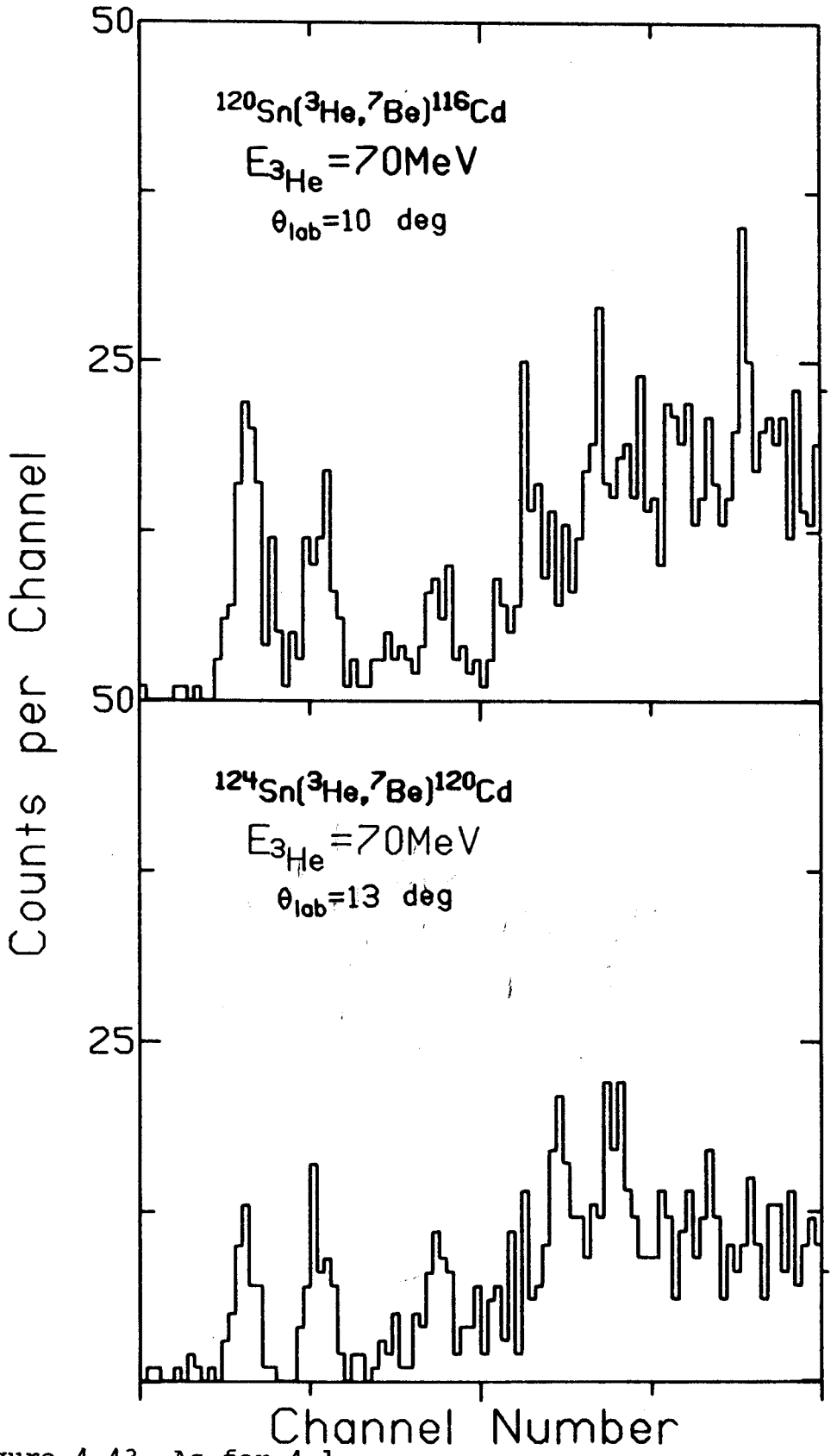

Figure 4.43 As for 4.1.

V. DWBA CALCULATIONS

If the (^{3}He, ^{7}Be) reaction is assumed to pick up an α particle from the surface of the target nucleus, the α spectroscopic factor, $S_\alpha = d\sigma/d\Omega(\text{measured})/d\sigma/d\Omega(\text{reaction theory})$, provides an indication of the extent to which surface α clusters occur. In order to compute the differential cross section, it is necessary to assume that a monolithic α particle is transfered from the nuclear surface to the ^{3}He projectile, thus forming the ^{7}Be ejectile. Most DWBA computer programs employ the zero range approximation which, in this case, assumes the ^{3}He and α particles to interact only when occupying the same point in space. If the ^{7}Be nucleus is viewed as a two particle system, an α particle bound to a ^{3}He nucleus, the α particle has one unit of angular momentum relative to the ^{3}He. Since for such a p state the α - ^{3}He separation is never zero, the zero range approximation is inappropriate. Programs exist which use a finite range approximation, however the program LOLA[20] makes no simplification beyond the usual distorted wave Born approximation. Therefore the program LOLA has been applied to the problem of computing a single particle transfer reaction differential cross section, the transfered particle being an α particle.

In order to use any DWBA program, it is necessary to supply optical model parameters for both the entrance and exit channels. Optical model parameters for elastic scattering of ^{3}He from the various target nuclides are available,

however only for energies somewhat lower than the 70 MeV bombarding energy of the present work. In most cases the parameters used are taken from Doering[21] who used a folding model. Since ^{7}Be has a half life of only 53 days, ^{7}Be beams are unavailable. Therefore ^{7}Be elastic scattering data, from which optical model parameters are deduced, do not exist. In the absence of ^{7}Be parameters, ^{7}Li optical parameters are used instead. Although the ^{7}Li complex optical potential should probably be increased when applied to ^{7}Be to allow for the greater absorption of the more weakly bound ^{7}Be, no adjustment is made. Any such change would be negligible compared to the inherent uncertainty in the parameters. For many cases, several sets of parameters have been tried. The parameters used for the final calculations, along with their sources, are listed in Table 5.1.

The program LOLA computes, for a given transition and orbital angular momentum transfer ℓ, a corresponding differential cross section, $\sigma_{\ell}(\theta)$. The final reaction differential cross section is given by the formula:

$$\frac{d\sigma}{d\Omega}(\theta) = \frac{2s_a+1}{2s_b+1} S_1 S_2 \sum_{\ell} (2\ell+1)\ W^2(\ell_1 j_1 \ell_2 j_2; s_x \ell)\ \sigma_{\ell}(\theta),$$

where $s_x = 0 =$ α spin,

$s_a = 3/2 =$ ^{7}Be spin,

$s_b = 1/2 =$ ^{3}He spin,

$\ell_1 = 1 =$ orbital angular momentum internal to ^{7}Be,

$\ell_2 =$ orbital angular momentum of α in target nuclide,

$j_1 = \ell_1 + s_x = \ell_1$, and

Table 5.1 Optical model parameters.

Reaction	Energy	used for	V(MeV)	r_r(fm)	a_r(fm)	W_v(MeV)	r_i(fm)	a_i(fm)	ref.
$^{3}He \rightarrow {}^{12}C$	70 MeV	$^{12}C, ^{16}O$	120.0	1.16	.933	10.6	1.28	.819	21
$^{7}Li \rightarrow {}^{24}Mg$	34	^{12}C	54.1	1.78	.580	10.95	2.15	1.01	23
$^{3}He \rightarrow {}^{27}Al$	60	$^{24,26}Mg$	114.0	1.15	.826	18.8	1.18	.820	25
$^{7}Li \rightarrow {}^{19}F$	21.1	$^{24,26}Mg$	35.4	1.74	1.05	11.5	2.13	.62	26
$^{3}He \rightarrow {}^{60}Ni$	70	$^{58,60}Ni$	126.5	1.12	.837	20.4	1.26	.841	22
$^{7}Li \rightarrow {}^{58}Ni$	12.2	$^{58,60}Ni$	152.0	1.38	.750	5.15	2.38	.58	27
$^{7}Li \rightarrow {}^{12}C$	36	^{16}O	187.8	1.208	.824	12.9	2.17	.770	24

$$j_2 = \ell_2 + s_x = \ell_2 .$$

W denotes a Racah coefficient. S_1 is the α spectroscopic factor for ^{7}Be and is assumed to be 1. S_2 is the α spectroscopic factor for the target nuclide. Contrary to the situation with the zero range approximation, there is no parity requirement to restrict the ℓ transfer. Therefore all ℓ values allowed by angular momentum conservation must be computed and summed according to the formula to arrive at the final answer. For the case of a 0^+ to 0^+ transition, the only possible ℓ transfer is 1 so the sum contains but one term. For a 0^+ to 2^+ transition, ℓ = 1, 2, 3 occur. The spectroscopic factor S_2 is determined by computing the differential cross section without it and then choosing for it a value which best matches the calculated and experimental cross sections.

Reaction calculations have been executed and α spectroscopic factors determined for the first 0^+ and 2^+ levels of ^{8}Be, ^{12}C, ^{20}Ne, ^{22}Ne, ^{54}Fe, and ^{56}Fe, as well as the 11.4 MeV 4^+ of ^{8}Be. Figure 5.1 compares the calculations of the 0^+, 2^+, and 4^+ ^{8}Be levels to the appropriate data. It should be noted that because of the large width of the 2^+ and 4^+ states, primary and secondary peaks due to the excitation of the ^{7}Be ejectile are inseparable. Assuming that the secondary to primary cross sections are in the ratio $2s^*+1/2s+1 = \frac{1}{2}$, s = 3/2 = ^{7}Be spin and s* = 1/2 = ^{7}Be* spin, the calculated cross section is multiplied by 1.5 for comparison to the

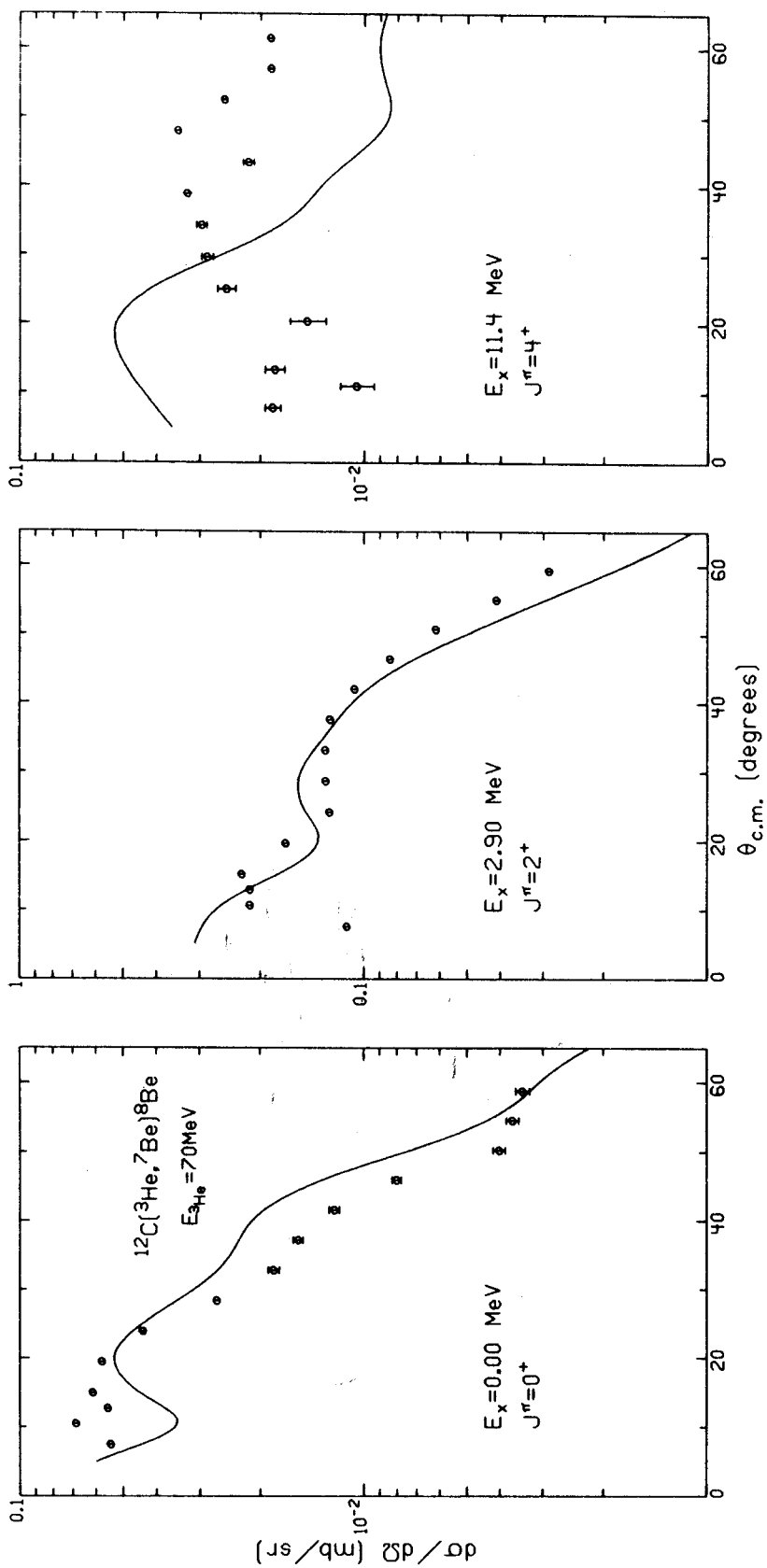

Figure 5.1 DWBA calculations.

measured data. The assumption is probably a poor one in view of the measured ratios for other states. Most ratios are not constant and assume values significantly different from ½. Unfortunately, however, no other alternative is available. The spectroscopic factor values obtained are .042, .120, and .022 respectively for the 0^+, 2^+, and 4^+ levels. The calculations presented in Figure 5.2 for the ^{12}C ground state and 4.44 MeV 2^+ reproduce the foward angle data reasonably well, considering the crudeness of the optical parameters. At angles larger than 30°, however, the data falls much faster than the calculated cross section. The 0^+ and 2^+ spectroscopic factors .75 and 2.27 are inexplicably large because the DWBA calculations are anomalously small for this reaction. Figures 5.3 and 5.4 present calculations for ^{20}Ne and ^{22}Ne respectively. The calculations for the corresponding states in the two isotopes are quite similar, however the data exhibit significant differences. For both ^{20}Ne levels the cross section rises with decreasing angle, as do the calculations, at forward angles. The ^{22}Ne states, however, decline, in sharp contrast to the data, as the scattering angle is reduced from 20°. All four levels have nearly equal spectroscopic factors. For the 0^+ and 2^+ ^{20}Ne levels the values are .022 and .023 while for ^{22}Ne $0^+$and 2^+ they are .038 and .028. As in the case of the neon isotopes, the calculations for ^{54}Fe and ^{56}Fe are almost identical. As can be seen from Figure 5.5, the calculation matches the ^{54}Fe data very well, at least below 20°. On the other hand, Figure

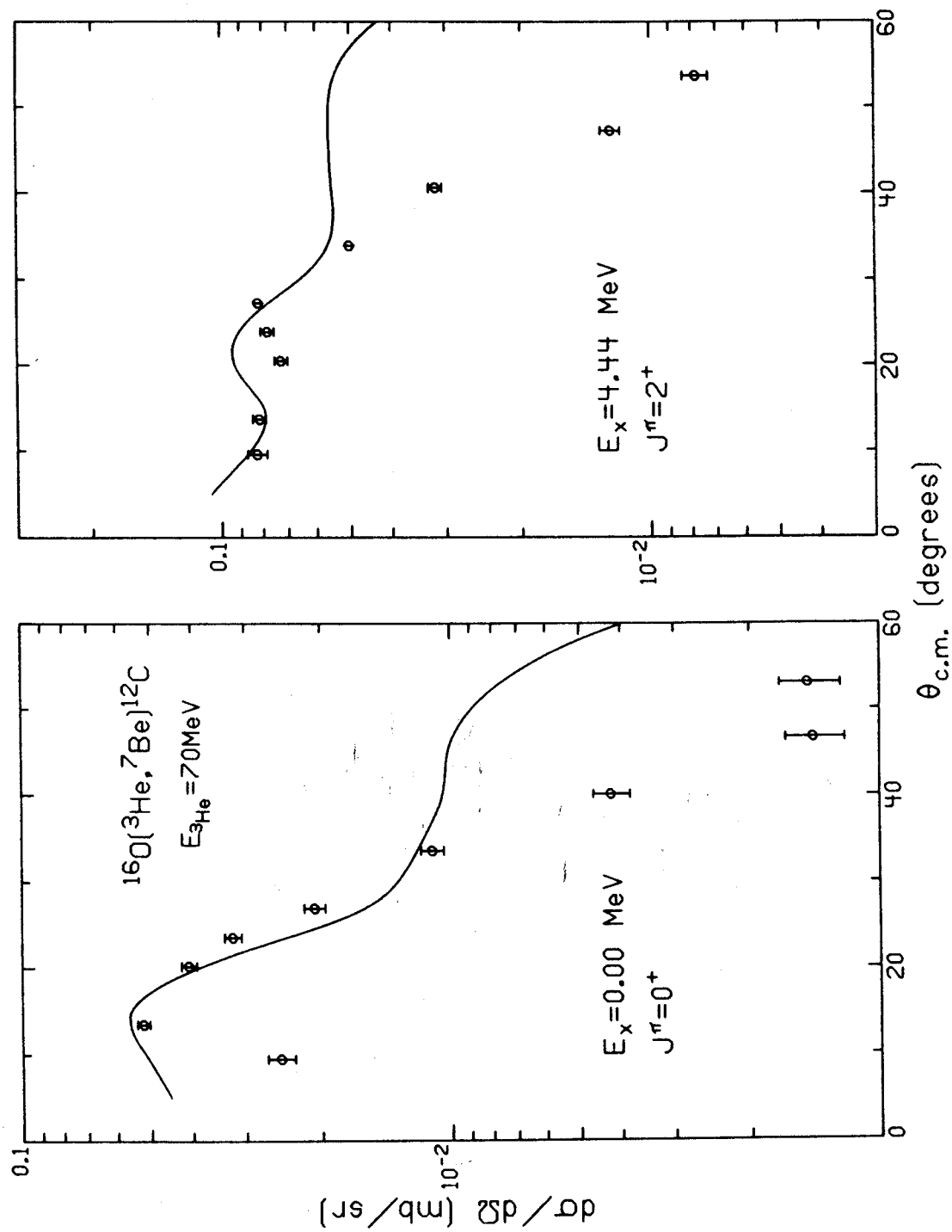

Figure 5.2 As for 5.1.

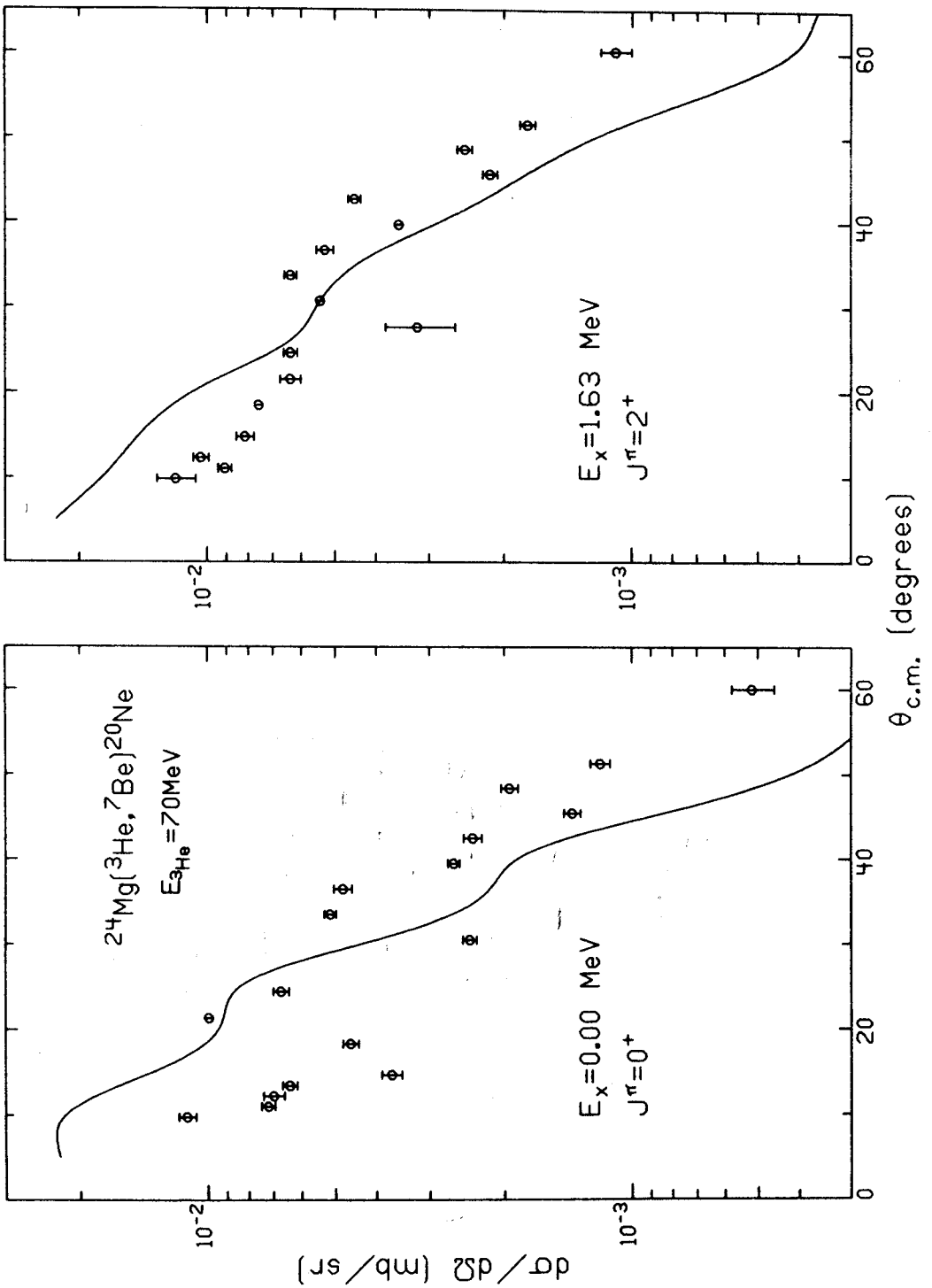

Figure 5.3 As for 5.1.

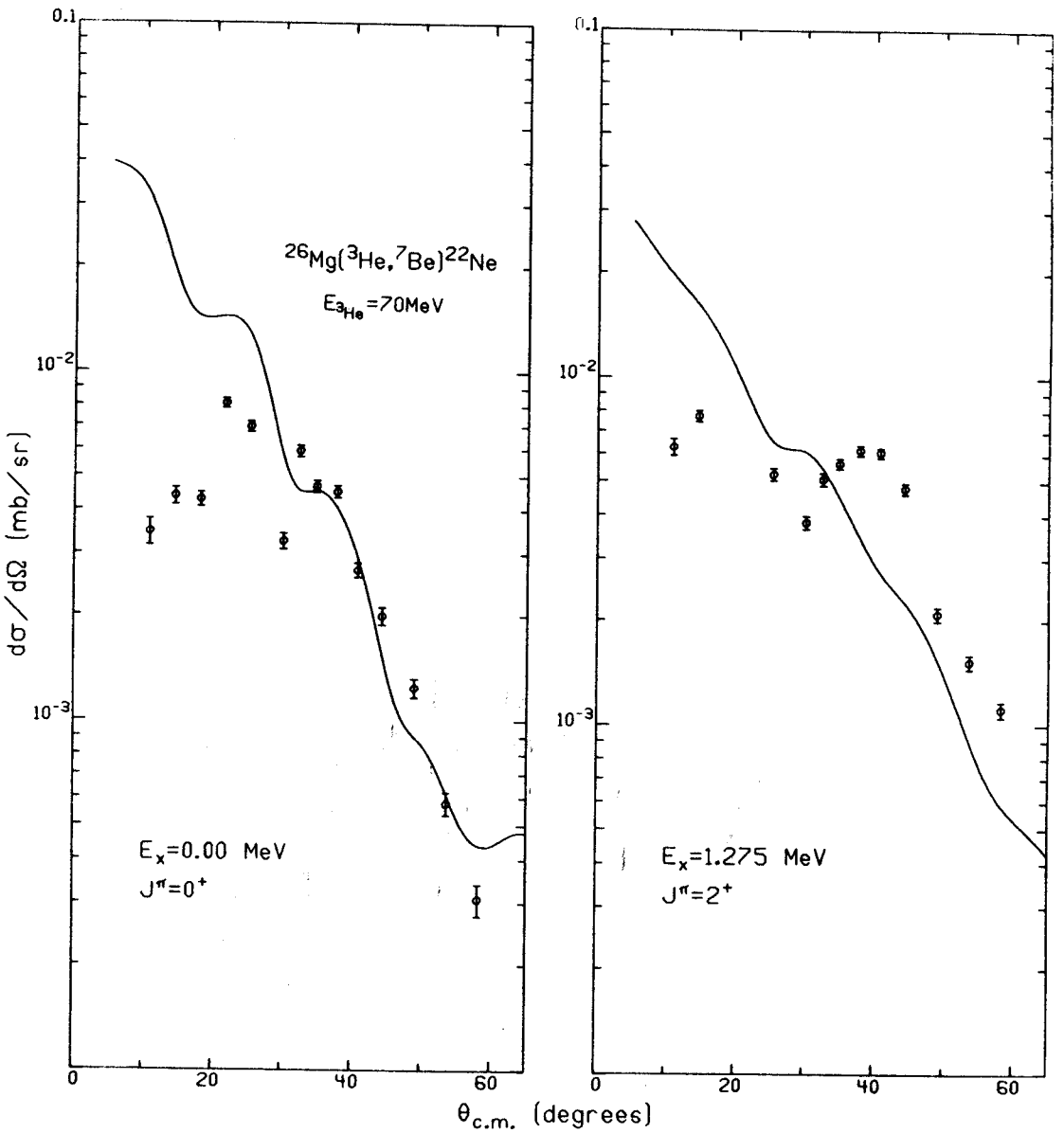

Figure 5.4 As for 5.1.

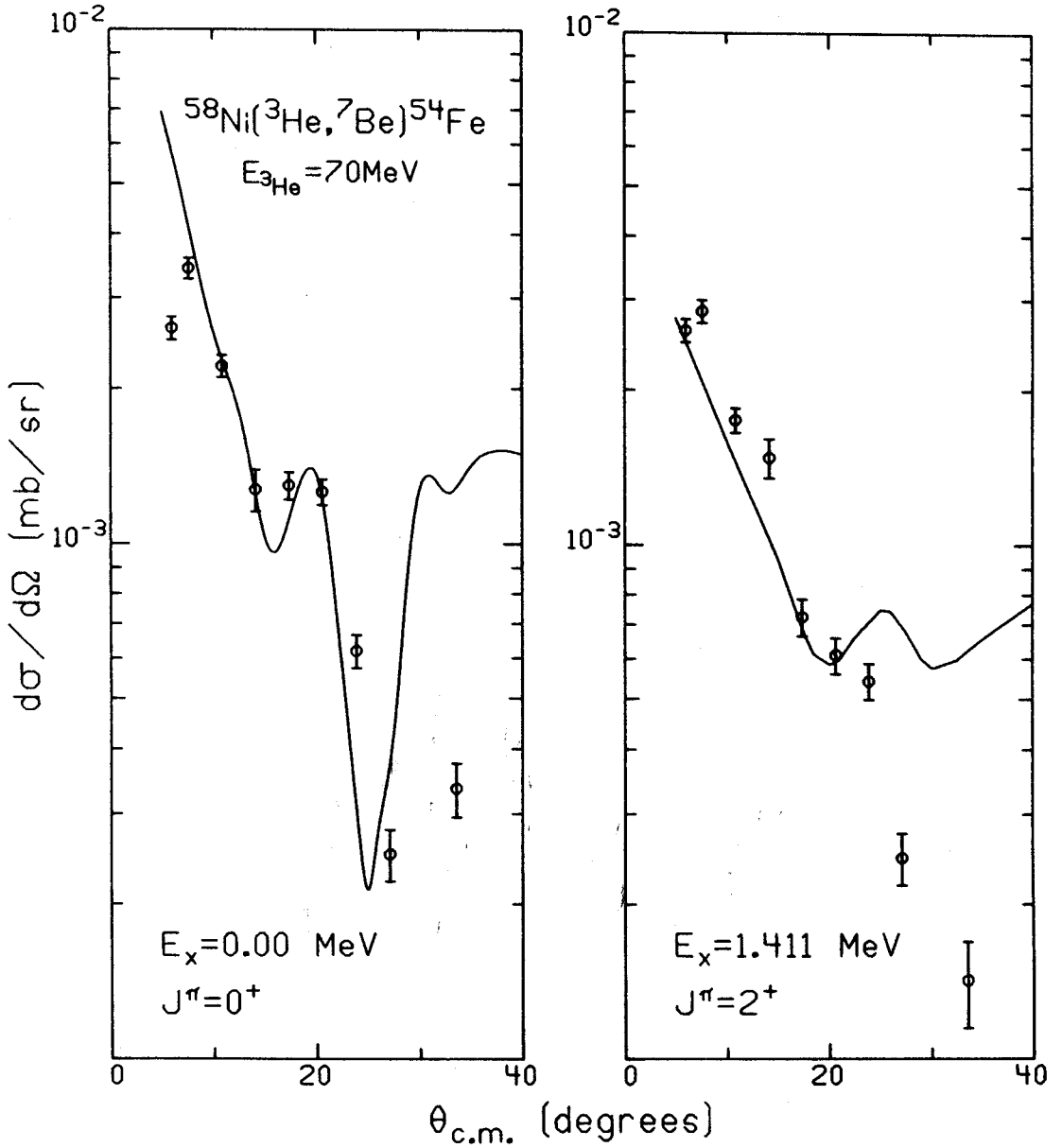

Figure 5.5 As for 5.1.

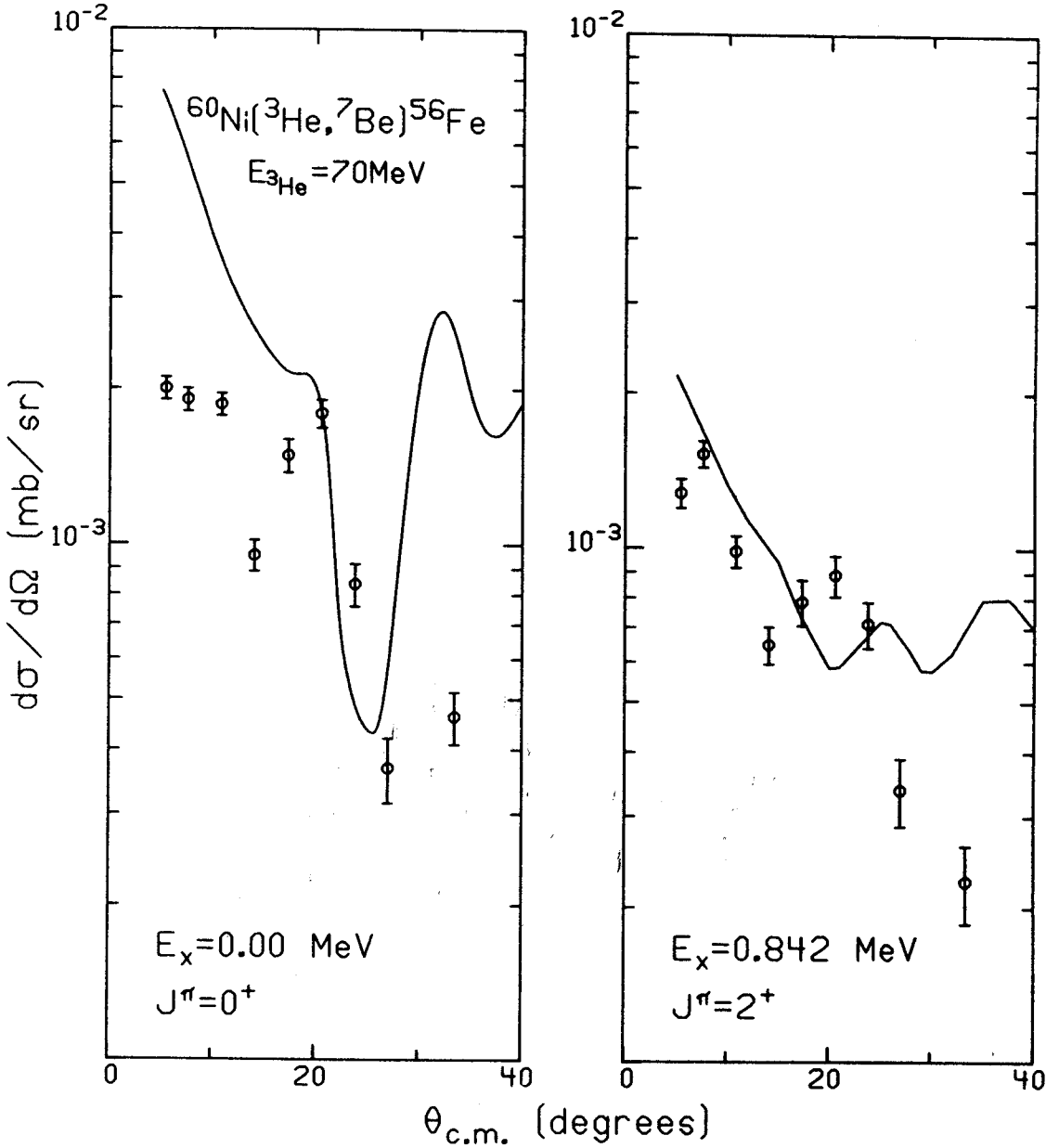

Figure 5.6 As for 5.1.

5.6 displays very little resemblance between the ^{56}Fe calculations and the corresponding data. The extracted spectroscopic factors for ^{54}Fe 0^+, 2^+, and ^{56}Fe 0^+ and 2^+ are respectively .045, .026, .071, and .025.

The actual size of the spectroscopic factors may not be significant because of the assumptions made in obtaining them. Their relative sizes however, indicate the trend of α cluster probability with increasing mass number. The approximate constancy of the α spectroscopic factors agrees with determinations by Martin[3], et. al. with the $(d,^6Li)$ reaction.

VI. CONCLUSIONS

The (^{3}He,^{7}Be) reaction has been studied at a bombarding energy of 70 MeV, somewhat higher than previous work on this reaction. Target nuclides used for the present work include ^{12}C, ^{13}C, ^{16}O, ^{24}Mg, ^{26}Mg, ^{58}Ni, ^{60}Ni, ^{62}Ni, ^{64}Ni, ^{90}Zr, ^{120}Sn, and ^{124}Sn,. A limited amount of additional data has been gathered for the targets ^{48}Ca, ^{144}Sm, and ^{206}Pb. Analysis of the data has proceeded in three directions. An attempt has been made to investigate the extent to which the reaction proceeds by a direct α pickup mechanism. Assuming the reaction to be a direct α pickup, finite range DWBA calculations are used to determine α spectroscopic factors, which are taken as an indication of the extent to which α clusters occur on the nuclear surface. As a third use of the (^{3}He,^{7}Be) reaction, the masses of ^{44}Ar and ^{120}Cd were measured. In addition, some energy levels of ^{44}Ar and ^{60}Fe were determined.

Some stable nuclides, in particular ^{48}Ca, ^{64}Ni, and ^{124}Sn, have such an unusually large neutron excess that the nuclides obtained from them by removal of two proton neutron pairs cannot be produced from a stable target by most standard particle transfer reactions. Since the (^{3}He,^{7}Be) reaction transfers the correct particles, the opportunity was seized to measure new masses and spectra. Although target contamination presented serious problems, the ^{44}Ar mass excess was measured to be -32.27 ± .04 MeV or about 500 keV

greater than the Garvey-Kelson mass formula prediction. The Garvey-Kelson mass excess for ^{120}Cd is closer, only 60 keV above the measured value of -83.98 ± .03 MeV. The first excited state of ^{44}Ar has the anomalously low excitation energy of 700 keV. The lowest first excited state energies of all other even argon isotopes are greater than 1 MeV. Indeed, no even even nuclide of smaller mass has such a low level, most excited states being well above 1.5 MeV. Lawson[28] has reported a calculation indicating a low lying level in ^{44}Ar resulting from core excitation. On the other hand, the first excited state of ^{60}Fe at 835 ± 20 keV continues the pattern of the other iron isotopes: ^{54}Fe 1409 keV, ^{56}Fe 847 keV, and ^{58}Fe 811 keV.

Another problem to which the data have been applied is the question of the reaction mechanism. In contrast to the (d,^{6}Li) reaction, the (^{3}He,^{7}Be) reaction appears to be a direct process. Comfort[4], et. al. have concluded that the (d,^{6}Li) reaction mechanism is largely a complex multistep process, probably at all energies. They find that unnatural parity states, which should not be excited by a purely α transfer mechanism, are as strongly excited as many natural parity states. On the other hand, Détraz, et. al. have found that even at 30 MeV, because of primary and secondary angular distribution similarity and forward peaking, the (^{3}He,^{7}Be) reaction is predominantly a direct α pickup reaction. Further work by Détraz has confirmed the direct nature of the reaction and has established that four nucleons

are transfered predominantly as an α particle fragment. Transfer as an isospin 1 excited α particle was found to be only a negligible component of the reaction mechanism. If the (^{3}He,^{7}Be) reaction at 30 MeV is direct, then it certainly will be at 70 MeV. Indeed, aside from the ^{8}Be (17.64) 1^{+} and ^{20}Ne (4.97) 2^{-} levels, unnatural parity states are not observed; the two exceptions being only weakly excited. The ^{20}Ne (4.97) 2^{-} peak differential cross section, for example, is 5 μb/str whereas the ^{20}Ne (1.63) 2^{+} has a maximum cross section of 20 μb/str. Furthermore, most angular distributions show sharply decreasing differential cross section with increasing scattering angle. Since the reaction calculations, which are based on the assumption that the double proton neutron pair is transfered as an α particle, are able to produce a reasonable description of the experimental angular distributions, the reaction may be regarded to some extent as a direct α transfer process. The secondary to primary cross section ratios, however, show that this view of the reaction mechanism cannot be completely correct. Assuming direct transfer of a monolithic α particle, the secondary to primary ratio should equal $2j_1+1/2j_0+1 = \frac{1}{2}$, j_0 and j_1 denoting respectively the ground and first excited state spins of ^{7}Be. The two ^{7}Be levels differ only in the orientation of the ^{3}He spin relative to the ^{3}He - α orbital angular momentum. Therefore any deviation of the secondary to primary ratio from ½ indicates that either a process more complicated than α transfer occurs, or the differential cross section for

the reaction somehow depends on the internal spin orientation of the ^{7}Be nucleus. In fact the data does exhibit such departures from ½. Although many individual ratio values are near ½, for most angular distributions the ratio behavior with angle is not constant. For many distributions, the ratio varies smoothly with angle and in one case, the ^{20}Ne ground state, the ratio reaches a distinct minimum of 0.2 at a center of mass angle of 13°. The ratios range, for the most part, between 0.2 and 0.8. Only in isolated cases does the ratio exceed 1, i.e. the primary peak is almost always larger than the secondary peak. Although ratio values significantly different from ½ occur, the sensitivity of the transfer hypothesis to these departures is not clear. Therefore, for the purposes of the present work, the α transfer mechanism is assumed to be substantially correct. In fact, ratios for some levels actually have a reasonably constant value near ½; for example ^{9}Be (0.00) $3/2^{-}$, ^{20}Ne (1.63) 2^{+}, and ^{22}Ne (1.28) 2^{+}.

To the extent the direct α particle transfer mechanism is correct, the data, together with the reaction calculations, may be used to obtain an estimate of the probability for occurance of α particle clusters on the nuclear surface. Because ^{3}He particles are strongly absorbed, a ^{3}He penetrating the nuclear surface loses its identity. Thus an α particle picked up by a passing ^{3}He may be assumed to have come from the nuclear surface. As a numerical measure of clustering, α particle spectroscopic factors have been calculated. Peak

differential cross section for the ground state transitions are plotted in Figure 6.1 against target mass number. The cross section drops dramatically from 70 μb/str for ^{12}C to 8 μb/str for ^{24}Mg. The cross section continues to decline, though less rapidly, to less than 0.2 μb/str for ^{206}Pb. From ^{64}Ni to ^{144}Sm the cross section has the nearly constant value of 1.0 μb/str. The cross section decreases smoothly with atomic mass number except for the low ^{13}C point; anomalous perhaps because, in contrast to the other targets, its mass number is odd. In addition to declining with increasing target mass, the peak differential cross section decreases as additional neutrons are added to the target. Figure 6.2 plots peak differential cross section of the ground state transitions against neutron excess. Data for several elements are included on the same plot by normalizing the data for a given atomic number so as to make the normalized value 1 for the nuclide with the smallest neutron number. The abscissa is taken to be the number of neutrons exceeding the number for the lightest isotope of the given element. In all cases measured, the peak cross section declines with neutron excess. The decrease is about the same for all elements so the effect is independent of target mass. It would appear that excess neutrons tend to dilute α particle clusters on the nuclear surface.

The decline of peak cross section with increasing mass number and neutron number would tend to indicate a decrease of surface α cluster probability. That is, α clustering is

Figure 6.1 Peak differential cross section for (^{3}He,^{7}Be) at 70 MeV vs. target mass number.

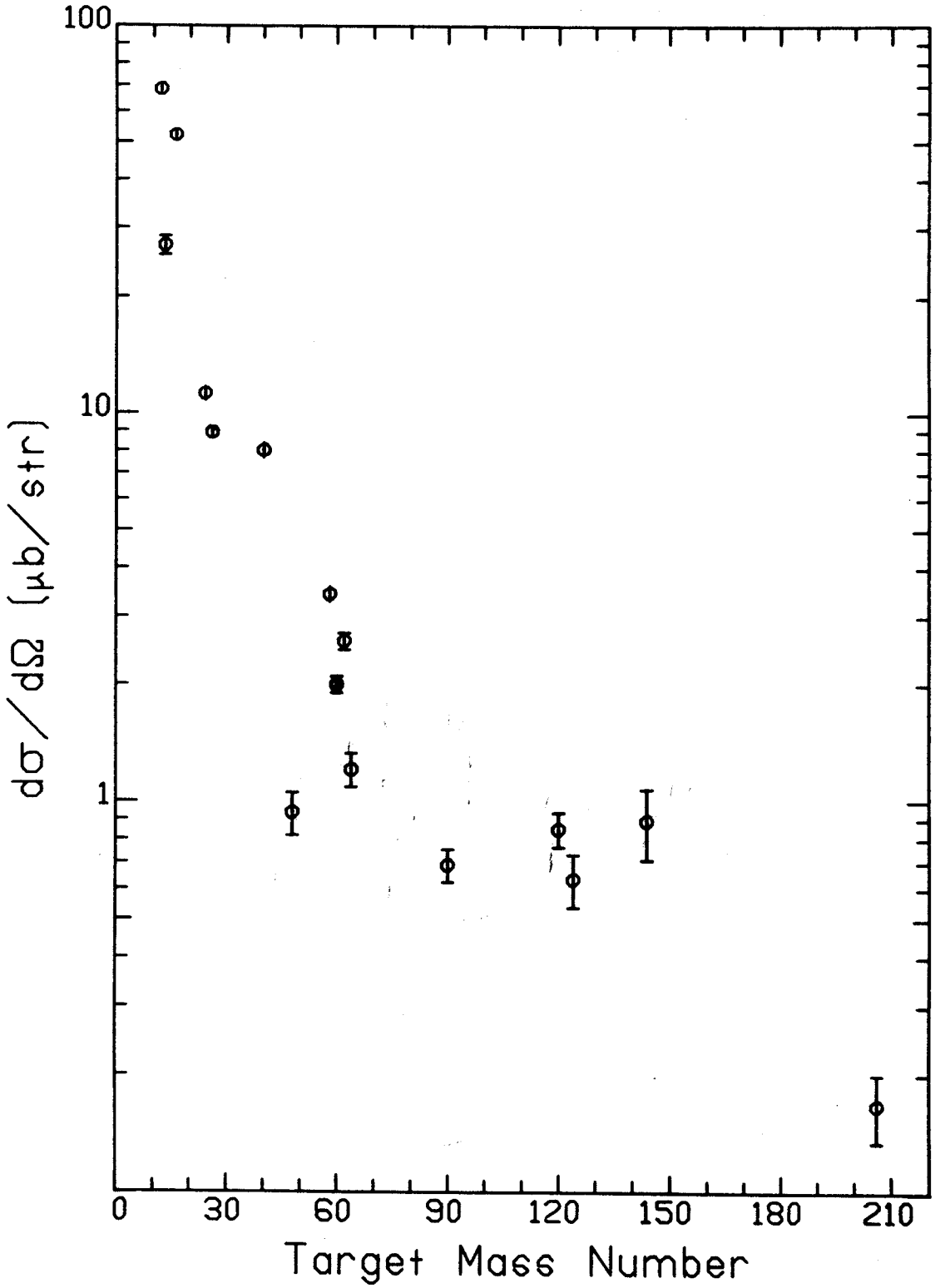
100
10
1
dσ/dΩ (μb/str)
0
30
60
90
120
150
180
210
Target Mass Number

Figure 6.1

Figure 6.2 Peak differential cross section for (^{3}He,^{7}Be) at 70 MeV vs. target neutron excess.

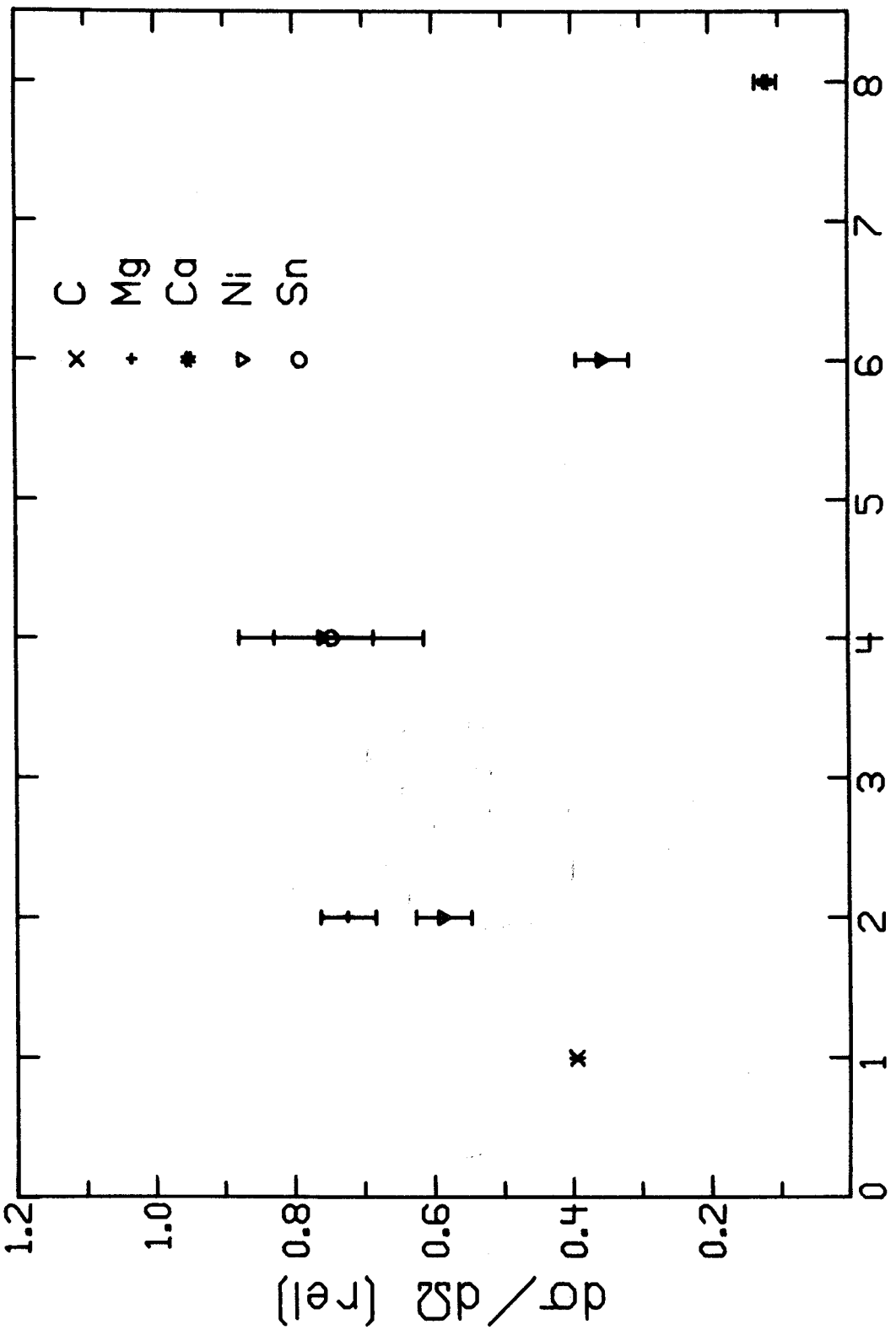
C
Mg
Ca
Ni
Sn
dσ/dΩ (rel)
Neutron Excess
0
1
2
3
4
5
6
7
8
0.2
0.4
0.6
0.8
1.0
1.2

Figure 6.2

Table 6.1 α spectroscopic factors.

Reaction	E_x (MeV)	J^π	S_α
$^{12}C(^3He,^7Be)^8Be$	0.00	0^+	.042
	2.94	2^+	.120
	11.4	4^+	.022
$^{16}O(^3He,^7Be)^{12}C$	0.00	0^+	.75
	4.44	2^+	2.27
$^{24}Mg(^3He,^7Be)^{20}Ne$	0.00	0^+	.022
	1.63	2^+	.023
$^{26}Mg(^3He,^7Be)^{22}Ne$	0.00	0^+	.038
	1.27	2^+	.028
$^{58}Ni(^3He,^7Be)^{54}Fe$	0.00	0^+	.045
	1.41	2^+	.026
$^{60}Ni(^3He,^7Be)^{56}Fe$	0.00	0^+	.071
	0.85	2^+	.025

most likely to occur for light α particle nuclei, those for which neutron and proton number are equal and even. However a more valid conclusion is to be drawn from α spectroscopic factor values. By comparing the data to the DWBA calculations, as the spectroscopic factors do, decreases in cross section not related to α clustering are removed. Table 6.1 lists the α spectroscopic factors determined with the DWBA calculations. In contrast to the peak cross section values, the spectroscopic factors do not decline. Except for the anomalous ^{16}O values, they are nearly constant. Therefore the α clustering phenomenon does not lose importance for heavy nuclides.

APPENDICES

APPENDIX A

KINEMATICAL FORMULAE

The following formulae have been used for the kinematical calculations discussed in Chapter III. They apply to a nuclear reaction of the form $A_1(A_2,A_3)A_4$, where nuclide A_1 is initially at rest. Nuclide A_4 may be left in an excited state, the excitation energy of which is denoted by X_4. The formulae also can be applied to the case where nuclide A_3 is excited, e.g. ^{7}Be (.432), by subtracting the excitation energy X_3 from the Q-value and adding it to the ground state mass. T_i shall denote the kinetic energy of nuclide A_i, p_i its momentum, and m_i its mass. θ is the laboratory scattering angle while ϕ is the scattering angle in the center of mass reference frame. ρ denotes the center of mass to laboratory differential cross section ratio. Let

$$B = \frac{Q(m_1+m_2-m_3-\frac{1}{2}Q) + T_2(m_1-m_3)}{m_1+m_2+T_2}$$

$$\gamma = \frac{m_1+m_2+T_2}{\sqrt{m_2^2+m_1(2(m_2+T_2)+m_1)}}$$

$$\beta = \frac{\sqrt{(2m_2+T_2)T_2}}{m_1+m_2+T_2}$$

$$\delta = \sqrt{B^2+m_3(2B+m_3\beta^2\cos^2\theta)}.$$

Then the kinetic energy of the particle to be detected is given by

$$T_3 = \frac{B+m_3\beta^2\cos^2\theta+\delta\beta\cos\theta}{1-\beta^2\cos^2\theta}$$ and its momentum by

$$p_3 = \sqrt{(2m_3+T_3)T_3}\ .$$

The kinematic broadening is (in energy units per degree)

$$\frac{dT_3}{d\theta} = -.0175 \frac{\beta\sin\theta}{1-\beta^2\cos^2\theta} \{2\beta\cos\theta T_3+m_3\beta\cos\theta(2+\frac{m_3\beta\cos\theta}{\delta})+\delta\}.$$

Given the detected particle's kinetic energy, the excitation energy of the residual nuclide may be computed as follows: Let Q_0 be the Q-value to the ground state of the residual nuclide and let $\alpha = 2T_2(m_1-m_3)-2(T_3-\beta\cos\theta p_3)(m_1+m_2+T_2)$, then

$$X_4 = \frac{Q_0^2+2Q_0m_4+\alpha}{m_4+\sqrt{(m_1+m_2-m_3)^2+\alpha}} .$$ Finally, the center of mass angle and cross section ratio are given by

$$\phi = \tan^{-1}\left\{\frac{p_3\sin\theta}{\gamma(p_3\cos\theta-\beta(T_3+m_3))}\right\} \quad \text{and}$$

$$\rho = \frac{[\gamma^2(p_3\cos\theta-\beta(T_3+m_3))^2+p_3^2\sin^2\theta]^{3/2}}{\gamma p_3^2(p_3-\beta\cos\theta(T_3+m_3))} .$$

APPENDIX B

γ DECAY KINEMATICS

The decay of the 432 keV first excited state of ^{7}Be introduces an additional energy spread into secondary peaks of (^{3}He,^{7}Be) spectra. The mean lifetime of the state is 0.27 ps so most excited ^{7}Be nuclei travel no more than 1 μm before decaying. None enter the spectrometer magnet. In the center of mass reference frame of the excited ^{7}Be nucleus, the recoiling ^{7}Be ground state nucleus has velocity

$$\zeta = \frac{m^{*2}-m^2}{m^{*2}+m^2}$$ where m* is the excited ^{7}Be mass and m is the ground state mass. The velocity of the center of mass system relative to the laboratory is

$$\beta = \frac{\sqrt{2m^*T+T^2}}{T+m^*}$$ where T is the kinetic energy of the excited ^{7}Be nucleus. Let

$$\xi = \frac{1}{\sqrt{1-\zeta^2}} = \frac{m^{*2}+m^2}{2mm^*}$$ and

$$\gamma = \frac{1}{\sqrt{1-\beta^2}} = 1 + \frac{T}{m^*} .$$

If the photon is emitted at a center of mass angle θ relative to the direction of travel, the recoil energy of the ground state ^{7}Be nucleus relative to laboratory coordinates is

$T' = m[\xi\gamma(1-\beta\zeta\cos\theta)-1]$. The difference Δ between the recoil energies for emission in the forward and backward directions provides an upper limit for the contribution to resolution of the ^{7}Be γ decay.

$\Delta = 2m\beta\gamma\zeta\xi$ which has, for several $^7Be^*$ energies, the values listed in Table A.1.

Table A.1

$^7Be^*$ kinetic energy (MeV)	Δ (keV)
50	107
55	112
60	117
65	122
70	127
75	131
80	136

The broadening due to γ decay is smaller than even the best experimental resolution obtained, about 150 keV. Even though some evidence of recoil broadening appears in these cases, for all practical purposes it can be ignored.

LIST OF REFERENCES

LIST OF REFERENCES

1. Wilkinson, Comments on Nucl. and Part. Phys. 1, 1 (1967) 36.

2. G. Igo, L. F. Hansen, and T. J. Gooding, Phys. Rev. 131, 1 (1963) 337.

3. P. Martin, J. B. Viano, J. M. Loiseaux, and Y. LeChalony, Nucl. Phys. A212, (1973) 304.

4. J. R. Comfort, W. J. Braithwaite, J. R. Duray, H. T. Fortune, W. J. Courtney, and H. G. Bingham, Phys. Lett. 40B, 4 (1972) 456.

5. C. Détraz, H. H. Duhm, and H. Hafner, Nucl. Phys. A147, (1970) 488.

6. C. Détraz, C. D. Zafiratos, C. E. Moss, and C. S. Zaidins, Nucl. Phys. A177, (1971) 258.

7. C. D. Zafiratos, C. Détraz, C. E. Moss, and C. S. Zaidins, Phys. Rev. Lett. 27, 7 (1971) 437.

8. C. Détraz, C. D. Zafiratos, H. Rudolf, and C. S. Zaidins, Phys. Rev. Lett. 28, 2 (1971) 117.

9. J. E. Spencer and H. A. Enge, Nucl. Instr. and Meth. 49, (1967) 181.

10. G. F. Trentleman and E. Kashy, Nucl. Instr. and Meth. 82, (1970) 304.

11. W. A. Lanford, W. Benenson, G. M. Crawley, E. Kashy, I. D. Proctor, and W. F. Steele, BAPS 17, (1972) 895.

12. W. A. Lanford, private communication.

13. D. L. Bayer, The Data Acquisition Task TOOTSIE, MSUCL-34 (unpublished).

14. P. R. Bevington, Data Reduction and Error Analysis for the Physical Sciences, McGraw-Hill Book Company, New York, 1969.

15. C. F. Williamson, J. P. Boujot, and J. Picard, Center for Nuclear Studies, Saclay, Report CEA-R 3042 (1966).

16. F. Perey, (unpublished).

17. G. T. Garvey and I. Kelson, Phys. Rev. Lett. 16, 197 (1966). and G. T. Garvey, W. J. Gerace, R. L. Jaffe, I. Talmi, and I. Kelson, Rev. Mod. Phys. 41, S1 (1969).

18. J. Borysowicz, Michigan State University, private communication.

19. A. H. Wapstra and N. B. Gove, Nucl. Data Tables A9, 267 (1971).

20. R. M. DeVries, Phys. Rev. C8, 3 (1973) 951.

21. R. R. Doering, A. I. Galonsky, and R. A. Hinrichs, Jour. of Comp. Phys. 12, 4 (1973) 498.

22. R. R. Doering, Michigan State University, private communication.

23. G. E. Moore, K. W. Kemper, and R. L. White, Proceedings of the International Conference on Reactions Between Complex Nuclei, R. L. Robinson, F. K. McGowan, J. B. Ball, and J. H. Hamilton (ed.), p47, North-Holland Publishing Company, Amsterdam, 1974.

24. P. Schumacher, N. Ueta, H. H. Duhm, K.-I. Kubo, and W. J. Klages, Nucl. Phys. A212, (1973) 573.

25. C. B. Fulmer and J. C. Hafele, Phys Rev. C5, (1972) 1969.

26. K. Bethge, C. M. Fou, and R. W. Zurmühle, Nucl. Phys. A123, (1969) 521.

27. K. O. Pfeiffer, E. Speth, and K. Bethge, Nucl. Phys. A206, (1973) 545.

28. R. D. Lawson, private communication.

29. F. Ajzenberg-Selove and T. Lauritsen, to be published.

30. R. W. Ollerhead, G. F. R. Allen, A. M. Baxter, B. W. J. Gillespie, and J. A. Kuehner, Can. J. Phys. 49, (1971) 594.

31. J. M. Moss, D. L. Hendrie, C. Glashausser, and J. Thirion, Nucl. Phys. A194, (1972) 12.

32. G. S. Mani, Nucl. Phys. A165, (1971) 225.

33. G. S. Mani, Nucl. Phys. A169, (1971) 194.

34. A. V. Ramanya, B. Van Nooijen, J. W. Ford, D. Krmpotić, J. H. Hamilton, J. J. Pinajian, and N. R. Johnson, Phys. Rev. C2, 6 (1970) 2248.

35. P. Neogy, R. Middleton, and W. Scholz, Phys. Rev. C6, 3 (1972) 885.

36. W. Scholz, P. Neogy, K. Bethge, and R. Middleton, Phys. Rev. C6, 3 (1972) 893.

37. M. N. Rao, Nucl. Data Sheets B3, 3 (1970) 4-43.

38. S. Raman, Nucl. Data Sheets B3, 3 (1970) 4-153.

39. J. Rapaport, A. Trier, T. A. Belote, and W. E. Dorenbusch, Nucl. Phys. A187, (1972) 25.

40. R. L. Auble, Nucl. Data Sheets B5-151 (1971).